

EOS-LNG: A Fundamental Equation of State for the Calculation of Thermodynamic Properties of Liquefied Natural Gases

Monika Thol^{a§}, Markus Richter^{a,b,†}, Eric F. May^b, Eric W. Lemmon^c, Roland Span^a

^aRuhr-Universität Bochum, Faculty of Mechanical Engineering, Thermodynamics,
Universitätsstraße 150, 44801 Bochum, Germany

^bThe University of Western Australia, Fluid Science and Resources Division, Crawley,
Western Australia, Australia

^cNational Institute of Standards and Technology, Applied Chemicals and Materials Division,
Boulder, CO, USA

[†]Present address: Chemnitz University of Technology, Department of Mechanical
Engineering, Applied Thermodynamics, Germany

ABSTRACT

A new mixture model (EOS-LNG) for the accurate representation of thermodynamic property data of multicomponent natural gas mixtures in the liquid state is presented. The mathematical approach of the GERG-2008 equation of state of Kunz and Wagner is adopted and new binary-specific functions for methane + *n*-butane, methane + isobutane, methane + *n*-pentane, and methane + isopentane are developed. The representation of all experimental data available in the literature for the corresponding binary systems is carefully analyzed so that these functions can also be applied at fluid states beyond the liquefied natural gas region. The EOS-LNG represents all available binary and multicomponent data in the liquefied natural gas region within their specified experimental uncertainty, which is significantly more accurate than the GERG-2008 model. The main focus was given to the representation of new density data measured between 100 K and 180 K with a maximum pressure of 10 MPa. Deviations from the EOS-LNG presented here do not exceed 0.02% for binary data and 0.05% for multicomponent systems. Deviations of calculated values from experimental data in other fluid regions are similar to or better than those calculated with the GERG-2008 model.

Keywords: density, equation of state, Helmholtz energy, liquefied natural gas, mixture, thermodynamic properties

[§]Corresponding author, m.thol@thermo.ruhr-uni-bochum.de

CONTENTS

1.	Introduction.....	6
2.	The Helmholtz Energy Equation of State for Mixtures	9
2.1	Mathematical approach.....	9
2.2	Fitting mixture equations of state	12
3.	Binary Mixtures	18
3.1	Data assessment	20
3.2	Methane + <i>n</i> -butane (C ₁ C ₄)	25
3.3	Methane + isobutane (C ₁ C _{4i})	33
3.4	Methane + <i>n</i> -pentane (C ₁ C ₅).....	38
3.5	Methane + isopentane (C ₁ C _{5i}).....	44
4.	Representation of Multicomponent Mixtures	47
5.	Conclusion	54
	Acknowledgements.....	51
6.	References.....	56

List of Tables

1.	Binary parameters of the reducing functions for density and temperature	19
2.	Parameters of the departure functions for the systems C_1C_4 , C_1C_{4i} , C_1C_5 , and C_1C_{5i}	20
3.	Average absolute relative deviations calculated with the new equation of state for the binary system C_1C_4	25
4.	Average absolute relative deviations of vapor-liquid equilibrium pressures for the binary system C_1C_4	29
5.	Average absolute relative deviations of density data from values calculated with the new equation of state for the binary system C_1C_{4i}	33
6.	Average absolute relative deviations of vapor-liquid equilibrium pressures for the binary system C_1C_{4i}	37
7.	Average absolute relative deviations for density and excess enthalpy data from values calculated with the new equation of state for the binary system C_1C_5	38
8.	Average absolute relative deviations of vapor-liquid equilibrium pressures for the binary system C_1C_5	41
9.	Average absolute relative deviations calculated with the new equation of state for the binary system C_1C_{5i}	44
10.	Average absolute relative deviations of vapor-liquid equilibrium pressures for the binary system C_1C_{5i}	45
11.	Molar compositions of the three multicomponent mixtures labeled as Libya, Norway, and Oman	47
12.	Molar compositions of the three multicomponent mixtures LNG 2, LNG 5, and LNG 7	48

List of Figures

1.	p,T -diagrams for methane + ethane, carbon dioxide + nitrogen, and methane + chlorine calculated based on the linear and the Lorentz-Berthelot combining rules.....	14
2.	Results obtained from applying typical constraints during the fitting procedure. Top: Residual isochoric heat capacity as a function of temperature along selected Bottom: Residual Grüneisen parameter as a function of temperature along selected isobars	16
3.	Percentage deviations of experimental data measured over the temperature range (293 to 395) K for the systems C_1C_2 of Sage and Lacey ⁵⁷ and C_1C_3 of Sage <i>et al.</i> ⁶⁹ from the GERG-2008 model ¹¹	22
4.	Percentage deviations of experimental data for the binary system C_1C_2 of Sage and Lacey ⁵⁷ and other accurate data from the GERG-2008 model ¹¹	23
5.	Percentage deviations of experimental data of Lentner <i>et al.</i> ^{20,72} for the binary systems C_1C_{4i} and C_1C_5 from the GERG-2008 model ¹¹	24
6.	Percentage deviations of homogeneous density data for the binary system C_1C_4 from the EOS-LNG and the GERG-2008 ¹¹ in selected temperature ranges below 400 K.	27
7.	Percentage deviations of homogeneous density data for the binary system C_1C_4 from the EOS-LNG and the GERG-2008 ¹¹ in selected temperature ranges above 400 K.....	29
8.	Percentage deviations of bubble-point pressure data for the binary system C_1C_4 from the EOS-LNG, the GERG-2008, ¹¹ and the modification of Rowland <i>et al.</i> ⁷³	31
9.	p,x -diagrams representing the vapor-liquid equilibrium data for the binary system C_1C_4	32
10.	Percentage deviations of isobaric heat capacity data of Syed <i>et al.</i> ⁷¹ for the binary system C_1C_4 from EOS-LNG, GERG-2008, ¹¹ and the modification of Rowland <i>et al.</i> ⁷³	32
11.	Percentage deviations of homogeneous density data in the low and medium temperature region from the EOS-LNG for the binary system C_1C_{4i}	34
12.	Percentage deviations of homogeneous density data of Olds <i>et al.</i> ⁵² in the high-temperature region from the EOS-LNG for the binary system C_1C_{4i}	35
13.	Percentage deviations of bubble-point pressure data for the binary system C_1C_{4i} from the EOS-LNG and the GERG-2008 ¹¹	36
14.	Percentage deviations of homogeneous density data from the EOS-LNG for the binary system C_1C_5	39

15.	Percentage deviations of vapor-liquid equilibrium pressure data for the binary system C_1C_5 from the EOS-LNG and the GERG-2008 ¹¹ as a function of the composition x_{C1}	40
16.	p,x -diagrams representing the vapor-liquid equilibrium data of Sage <i>et al.</i> ⁵⁴ for the binary system C_1C_5	41
17.	p,T -diagrams for the binary system C_1C_5 including the critical and cricondenbar lines calculated with EOS-LNG and GERG-2008 ¹¹	43
18.	Percentage deviations of homogeneous density data of Amick <i>et al.</i> ¹⁰⁷ from EOS-LNG for the binary system C_1C_{5i}	44
19.	p,x -diagrams representing the vapor-liquid equilibrium data for the binary system C_1C_{5i}	45
20.	T,x -diagram at $p = 0.1$ MPa for the binary system C_1C_{5i} with the liquid-liquid equilibrium phase boundary calculated with EOS-LNG and GERG-2008 ¹¹	46
21.	Percentage deviations of the density data of three multicomponent LNG mixtures from the EOS-LNG and GERG-2008 ¹¹	48
22.	Percentage deviations of the density data of three multicomponent LNG mixtures from the EOS-LNG and the GERG-2008 ¹¹	49
23.	Percentage deviations of the experimental density data of two multicomponent LNG mixtures from the GERG-2008 ¹¹ and the GERG-2008 model with the Lorentz-Berthelot combining rule for the binary system methane + nitrogen	52
24.	Percentage deviations of the experimental vapor-liquid equilibrium data of Hughes <i>et al.</i> ¹¹² from the EOS-LNG, the GERG-2008, ¹¹ and the modification of Rowland <i>et al.</i> ⁷³	52
25.	Percentage deviations of the experimental isobaric heat capacity data of Syed <i>et al.</i> from the EOS-LNG, the GERG-2008, ¹¹ and the modification of Rowland <i>et al.</i> ⁷³	53

1. Introduction

In this work, an accurate model is presented to calculate thermodynamic properties of natural gas mixtures at liquid states (liquefied natural gas, LNG). Accurate knowledge of these properties is important for safe and efficient designs of any process in the production, storage, distribution, and re-gasification of liquefied natural gas. Accurate thermodynamic property models are required for most custody transfer applications. In particular, the energy equivalent factor E is the central quantity upon which the economic value of the natural gas is determined:

$$E \approx V \rho \Delta h_{cv} \text{ or } \dot{E} \approx \dot{V} \rho \Delta h_{cv} \quad (1)$$

To determine the energy content E with sufficient accuracy for large-scale financial transactions, accurate knowledge of the density ρ is an essential element in addition to the directly measurable volume V or volume flow rate \dot{V} , and the calculated calorific value Δh_{cv} based only on the composition. The density depends on temperature, pressure, and composition of the natural gas mixture. Since no robust and sufficiently accurate apparatus for *in situ* density measurement is available for LNG custody transfer operations, equations of state are currently used to supply this information from measurements of pressure, temperature, and composition.

A variety of equations of state is available in the literature. For example, in most process simulation tools, it is common to apply cubic equations, such as Peng-Robinson^{1,2} or Soave-Redlich-Kwong.^{3,4} These have the advantage that they are rather simple, computationally fast, and easy to extend to new components because only a few substance-specific parameters are needed. Alternatively, the Lee-Kesler-Plöcker^{5,6} equation, which is based on a corresponding-states principle, may be used particularly for single-phase property calculations. However, due to their relative simplicity, none of these equations is very accurate in predicting properties other than saturation pressure for vapor-liquid equilibria. They are certainly not able to reproduce accurate experimental density data within their experimental uncertainty. Several authors, including Klimeck *et al.*,⁷ Dauber and Span,⁸ and George,⁹ have shown that the uncertainties of thermodynamic property data calculated with these simple models are unacceptably high given the accuracy demands of the natural gas industry. Therefore, more accurate equations of state such as the DETAIL characterization method of AGA8 (Part 1)¹⁰ and the GERG-2008¹¹ equation of state have been developed. Due to its moderately simple form (a virial expansion), Part 1 of AGA8¹⁰ is still widely used for the calculation of gaseous properties in the natural gas industry. However, GERG-2008¹¹ is more accurate and covers not only the gaseous region but liquid and supercritical states as well, with uncertainties based on the availability of experimental measurements. It additionally allows for the calculation of bubble-point and dew-point pressures, which is not possible with the DETAIL model.¹⁰ Part 2 of AGA8,¹² which is based on the GERG-2008 model,¹¹ was recently adopted as a U.S. standard. This follows the adoption by ISO of the GERG-2008 model¹¹ in 2015, but contains significantly more information due to research conducted between the time when ISO and AGA

released their standards. In particular, see Lemmon¹³ for information on the revised limits of the DETAIL equation of state. AGA also released computer code in Fortran, C++, and Visual Basic that is highly optimized for both models along with a spreadsheet for quick calculations of properties. This is available at Ref.¹⁴

The GERG-2008¹¹ model is a modern equation of state for multicomponent mixtures expressed in terms of the Helmholtz energy, which includes 21 components taking into account the most common natural gas components such as the normal alkanes (and some isomers), nitrogen, carbon dioxide, and water as well as relevant impurities, *e.g.*, argon, helium, and hydrogen sulfide.

Over the last several years, LNG has become an important commodity. In contrast to compressed natural gas transported in pipelines, LNG can be shipped between continents. This transportation route increases the potential customers for natural gas producers. With increasing trade volume and growing demands on accurate custody transfer, as well as the optimization of the energy-intensive LNG production, accurate calculation of liquid phase properties is a new challenge for the industry. Since most models used for accurate description of natural-gas properties focus mainly on pipeline conditions, other empirical models had to be developed that enable accurate calculation of thermodynamic properties in the subcooled liquid state region: namely at temperatures between approximately 90 K and 180 K with pressures up to 10 MPa. Since the highest demand on accuracy is for density, special equations have been developed for calculating saturated and homogeneous liquid-phase densities over this temperature and pressure range. In the United States, the Costald correlation¹⁵ is often used, whereas Europe follows the guidance of the LNG custody transfer handbook,¹⁶ which recommends the revised Klosek-McKinley equation¹⁷ for densities at saturated liquid states. In the most recent edition,¹⁶ this model was replaced by the enhanced revised Klosek-McKinley equation by Tietz *et al.*,¹⁸ which describes not only saturated states but also homogeneous liquid and supercritical dense states. However, these equations cannot reproduce the most accurate available measurements of LNG densities within their experimental uncertainties.^{18–20} Furthermore, these models cannot be used to calculate thermodynamic properties other than densities.

The GERG-2008 model¹¹ is currently used to accurately calculate properties of LNG, even though it was mainly developed with a focus on calculations at pipeline conditions. As a fundamental equation of state, the GERG-2008 model¹¹ yields consistent results for all thermodynamic properties. However, while the recent density measurements by Lentner *et al.*²⁰ are reproduced within the uncertainty specified for the GERG-2008 model,¹¹ they are not reproduced within their experimental uncertainty. In this work, new correlations are presented for a number of binary mixtures essential for accurately calculating LNG properties. In combination with the correlations given for other binary mixtures by GERG-2008,¹¹ these new models reproduce even the most accurate experimental data within their specified uncertainties.

Furthermore, thermodynamic properties in other regions such as those at pipeline conditions, can be calculated with the same quality as achieved with the GERG-2008 model.¹¹

2. The Helmholtz Energy Equation of State for Mixtures

This section explains the mathematical background of mixture models expressed in terms of the Helmholtz energy. The mixture model in this work can be traced back to the DETAIL model in the 1992 version of AGA8 and also given in the same form in the 2016 version.¹⁰ Although it was originally expressed as an equation of state explicit in pressure, its origin was based on the Helmholtz energy and most of the equations below are valid for this model. The work of Lemmon²¹ followed shortly after the second edition of AGA8 was released in 1994 and presented the original version of the equations given in this work. A revised model was later published in the work of Klimeck *et al.*²² and even later by Kunz *et al.*²³ as GERG-2004. The latter was again revised and published by Kunz and Wagner,¹¹ and labeled as the GERG-2008 equation of state with three additional fluids (21 fluids in total).

2.1 Mathematical approach

The present mixture model is expressed in terms of the molar Helmholtz energy a as a function of temperature T , density ρ , and the composition vector \mathbf{x} . For practical reasons, it is made dimensionless by reducing by the molar gas constant R and the temperature:

$$\alpha(T, \rho, \mathbf{x}) = \frac{a(T, \rho, \mathbf{x})}{RT}. \quad (2)$$

The reduced Helmholtz energy α is commonly separated into an ideal gas contribution α° and a residual part α^r :

$$\alpha(\tau, \delta, \mathbf{x}) = \alpha^\circ(T, \rho, \mathbf{x}) + \alpha^r(\tau, \delta, \mathbf{x}). \quad (3)$$

The ideal part consists of a linear combination of contributions of the ideal-gas fluids in a mixture with N components and an additional composition-dependent term that accounts for the entropy of mixing:

$$\alpha^\circ(T, \rho, \mathbf{x}) = \sum_{i=1}^N x_i \left[\alpha_{o,i}^\circ(\tau_{o,i}, \delta_{o,i}) + \ln x_i \right]. \quad (4)$$

Following the convention used for modern Helmholtz equations of state for pure fluids, the inverse temperature and density are reduced by the critical parameters of the corresponding pure fluids to evaluate the ideal gas contribution

$$\tau_{o,i} = T_{c,i}/T \text{ and } \delta_{o,i} = \rho/\rho_{c,i}. \quad (5)$$

In this work, values of $T_{c,i}$ and $\rho_{c,i}$ from the pure fluid models of GERG-2008¹¹ were adopted.

The residual part is further split into a linear combination of the reduced residual Helmholtz energy of the pure fluids at their corresponding states and a departure term $\Delta\alpha^r$

$$\alpha^r(\tau, \delta, \mathbf{x}) = \sum_{i=1}^N \left[x_i \alpha_{o,i}^r(\tau, \delta) \right] + \Delta\alpha^r(\tau, \delta, \mathbf{x}). \quad (6)$$

The reduced inverse temperature and reduced density of the mixture are used to evaluate α^r both for the pure-fluid contributions and for the departure term:

$$\tau = T_r/T \text{ and } \delta = \rho/\rho_r. \quad (7)$$

The reducing temperature and density are in turn functions of the critical parameters of the pure fluids, the composition \mathbf{x} , and four adjustable parameters $\beta_{T,ij}$, $\gamma_{T,ij}$, $\beta_{v,ij}$, and $\gamma_{v,ij}$ for each binary pair:

$$T_r(\mathbf{x}) = \sum_{i=1}^N x_i^2 T_{c,i} + \sum_{i=1}^{N-1} \sum_{j=i+1}^N 2x_i x_j \beta_{T,ij} \gamma_{T,ij} \frac{x_i + x_j}{\beta_{T,ij}^2 x_i + x_j} \sqrt{T_{c,i} T_{c,j}} \quad (8)$$

and

$$\frac{1}{\rho_r(\mathbf{x})} = \sum_{i=1}^N x_i^2 \frac{1}{\rho_{c,i}} + \sum_{i=1}^{N-1} \sum_{j=i+1}^N 2x_i x_j \beta_{v,ij} \gamma_{v,ij} \frac{x_i + x_j}{\beta_{v,ij}^2 x_i + x_j} \frac{1}{8} \left(\frac{1}{\rho_{c,i}^{1/3}} + \frac{1}{\rho_{c,j}^{1/3}} \right)^3. \quad (9)$$

To ensure that the results do not depend on the order of numbering the components, the following relations have to be maintained:

$$\beta_{T,ij} = \frac{1}{\beta_{T,ji}}, \beta_{v,ij} = \frac{1}{\beta_{v,ji}}, \gamma_{T,ij} = \gamma_{T,ji}, \text{ and } \gamma_{v,ij} = \gamma_{v,ji}. \quad (10)$$

This structure of the reducing functions was introduced by Klimeck²² and differs from other approaches already available in the literature due to several considerations made for highly accurate mixture models that represent not only data for binary mixtures but also multicomponent data. For example, in the limit of pure fluids ($x_i \rightarrow 0$ or 1), the reducing functions have to exhibit a smooth transition to the corresponding pure fluid parameters T_c and ρ_c . Furthermore, the functional form has to be suitable for the description of both symmetric and asymmetric shapes with respect to equimolar compositions. Finally, the adjustable parameters $\beta_{T,ij}$, $\gamma_{T,ij}$, $\beta_{v,ij}$, and $\gamma_{v,ij}$ are binary-specific interaction parameters that can either be adjusted to obtain agreement with available thermodynamic property data for binary mixtures or be defined by a predictive combining rule, *cf.* Bell and Lemmon²⁴ or Lemmon and McLinden.²⁵ Without the departure term in Eq. (6), Eqs. (3) to (10) can be considered as an extended corresponding-states approach – the known features and theoretical limitations of this kind of approach explain both the advantages of the model and its limitations, which occur, for example, for mixtures of components with very different critical temperatures.^{26,27}

The departure term was first introduced by Lemmon and Jacobsen²⁸ and can be considered as a correction to the corresponding-states approach, allowing for higher accuracy in calculated properties that cannot be achieved with the use of the corresponding-states method alone. It consists of a weighing factor F_{ij} and either a binary-specific or a generalized departure function α_{ij}^r :

$$\Delta\alpha^r(\tau, \delta, \mathbf{x}) = \sum_{i=1}^{N-1} \sum_{j=i+1}^N x_i x_j F_{ij} \alpha_{ij}^r(\tau, \delta). \quad (11)$$

In the literature, the departure function is generally constructed from polynomial, exponential, and special exponential terms:

$$\begin{aligned} \alpha_{ij}^r(\tau, \delta) = & \sum_{k=1}^{K_{\text{pol},ij}} n_{ij,k} \delta^{d_{ij,k}} \tau^{t_{ij,k}} + \sum_{k=K_{\text{pol},ij}+1}^{K_{\text{pol},ij}+K_{\text{exp},ij}} n_{ij,k} \delta^{d_{ij,k}} \tau^{t_{ij,k}} \exp(-\beta_{ij,k} \delta^{l_{ij,k}}) \\ & + \sum_{k=K_{\text{pol},ij}+K_{\text{exp},ij}+1}^{K_{\text{pol},ij}+K_{\text{exp},ij}+K_{\text{spec},ij}} n_{ij,k} \delta^{d_{ij,k}} \tau^{t_{ij,k}} \exp\left[-\eta_{ij,k} (\delta - \varepsilon_{ij,k})^2 - \beta_{ij,k} (\delta - \gamma_{ij,k})\right]. \end{aligned} \quad (12)$$

The number of terms in each of these summations varies depending on the quality and quantity of the available experimental data. Typically, not more than ten terms are used. The last summation in Eq. (12) was introduced by Kunz and Wagner;¹¹ however, two of the parameters are unnecessary, and the special terms in the summation can be reduced to

$$n_{ij} \delta^{d_{ij}} \tau^{t_{ij}} \exp\left[-\eta_{ij} \delta^2 + \delta \underbrace{(2\eta_{ij} \varepsilon_{ij} - \beta_{ij})}_{v_{ij}} + \underbrace{\beta_{ij} \gamma_{ij} - \eta_{ij} \varepsilon_{ij}^2}_{\omega_{ij}}\right], \quad (13)$$

where the parameters v_{ij} and ω_{ij} are used for convenience to represent the constants

$$v_{ij} = 2\eta_{ij} \varepsilon_{ij} - \beta_{ij}, \quad (14)$$

and

$$\omega_{ij} = \beta_{ij} \gamma_{ij} - \eta_{ij} \varepsilon_{ij}^2 \quad (15)$$

resulting in the following expression:

$$n_{ij} \exp(\omega_{ij}) \delta^{d_{ij}} \tau^{t_{ij}} \exp[-\eta_{ij} \delta^2 + v_{ij} \delta]. \quad (16)$$

With the addition of the nomenclature

$$\xi_{ij} = \frac{v_{ij}}{2\eta_{ij}} \quad (17)$$

and the modified coefficient

$$n_{ij}^* = n_{ij} \exp(\omega_{ij} + \eta_{ij} \xi_{ij}^2), \quad (18)$$

Eq. (16) results in

$$n_{ij}^* \delta^{d_{ij}} \tau^{t_{ij}} \exp[-\eta_{ij} (\delta - \xi_{ij})^2] \quad (19)$$

Eq. (19) is similar to the density-dependent part of the well-established Gaussian bell-shaped terms for pure fluids.^{29,30} It was further extended to include the temperature-dependent contribution by Bell *et al.*,³¹ and already successfully applied for several binary mixture

models.^{32,33} However, in order to be consistent with the GERG-2008 model,¹¹ the original notation given in Eq. (12) is applied in this work.

Due to the fraction in Eq. (17), an exception is required for the situation when $\eta_{ij} = 0$ to avoid division by zero (*cf.* the binary function of methane + ethane in the GERG-2008 model¹¹). In this case, the special exponential term becomes a simple exponential term, *cf.* Eq. (12):

$$n_{ij} \delta^{d_{ij}} \tau^{t_{ij}} \exp \left[-\eta_{ij} (\delta - \varepsilon_{ij})^2 - \beta_{ij} (\delta - \gamma_{ij}) \right] \quad (20)$$

with $\eta_{ij} = 0$:

$$\begin{aligned} &= n_{ij} \delta^{d_{ij}} \tau^{t_{ij}} \exp \left[-\beta_{ij} \delta + \beta_{ij} \gamma_{ij} \right] \\ &= n_{ij} \exp(\beta_{ij} \gamma_{ij}) \delta^{d_{ij}} \tau^{t_{ij}} \exp \left[-\beta_{ij} \delta \right]. \end{aligned} \quad (21)$$

2.2 Fitting mixture equations of state

The development of equations of state either for pure fluids or mixtures is highly dependent on the underlying experimental database. For pure fluids, only about 15 have been sufficiently well investigated so that a reference equation of state could be developed. These can be used to reproduce all highly-accurate experimental data within their experimental uncertainty. Approximately 135 additional fluids are characterized by equations of state, also formulated in terms of the Helmholtz energy, but are based on less comprehensive and less accurate experimental data.

The properties of other fluids for which Helmholtz equations are not available are often calculated with generalized equations of state such as cubic equations (*e.g.*, Peng-Robinson^{1,2} or Soave-Redlich-Kwong³) or other various extensions, *e.g.*, the CPA equation,³⁴ equations based on statistical associating fluid theory,^{35–38} or corresponding states approaches such as the Lee-Kesler⁵ equation. Since mixture equations require composition as a set of additional independent variables, the experimental databases are even less comprehensive than for pure fluids. Furthermore, the experimental uncertainty of the measured properties for mixtures is generally higher than for pure fluids due to the additional uncertainty in the measurement of the composition. Finally, the determination of phase boundaries is a complex challenge in comparison to the rather simple vapor-liquid equilibrium calculation for pure fluids.

The methods of adjusting binary parameters in Helmholtz models to improve the description of mixtures can generally be separated into four classes depending on the amount and quality of the available experimental data, as discussed in the following subsections.

2.2.1 No experimental data available

If experimental data are not available, it is (obviously) not possible to adjust binary-specific parameters based on measurements. Only predictive combining rules can be applied to determine the parameters for the reducing functions for temperature and density [Eqs. (8) and (9)]. Although there are many different combining rules available in the literature, Kunz and Wagner¹¹ evaluated the Lorentz-Berthelot and linear combining rules and found them to be suitable for natural gases applications:

- Lorentz-Berthelot combining rule:

$$\beta_{T,ij} = \beta_{v,ij} = \gamma_{T,ij} = \gamma_{v,ij} = 1 \quad (22)$$

- Linear combining rule:

$$\gamma_{T,ij} = \frac{1}{2} \frac{(T_{c,i} + T_{c,j})}{(T_{c,i} \cdot T_{c,j})^{0.5}} \quad \text{and} \quad \gamma_{v,ij} = 4 \frac{\left(\frac{1}{\rho_{c,i}} + \frac{1}{\rho_{c,j}} \right)}{\left(\frac{1}{\rho_{c,i}^{1/3}} + \frac{1}{\rho_{c,j}^{1/3}} \right)^3}, \quad (23)$$

$$\beta_{T,ij} = \beta_{v,ij} = 1. \quad (24)$$

However, to date it is still unknown which of these combining rules [Eq. (22) or Eqs. (23) and (24)] should be applied for a given mixture. For asymmetric mixtures (mixtures of pure fluids with significantly different critical parameters) or components with different physical properties (*e.g.*, polar vs. non-polar fluids), different combining rules often yield quantitatively and even qualitatively varying results, particularly for phase-equilibrium calculations. Figure 1 shows that the linear and the Lorentz-Berthelot combining rules yield comparable results for the mixture methane + ethane, which are both hydrocarbons with simple repulsive and attractive intermolecular forces. However, for other mixtures, *e.g.*, carbon dioxide + nitrogen, additional electrostatic interactions occur. For pressures $p > 10$ MPa, the quantitative characterization of the two combining rules differs remarkably. In the case of methane + chlorine, even the qualitative descriptions of the mixture predicted by the two approaches are not similar.

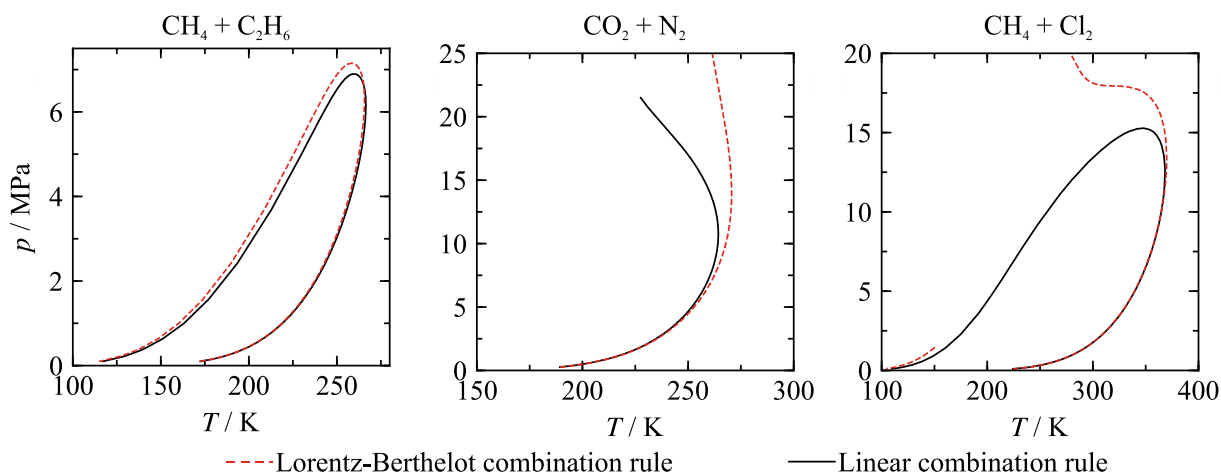


Fig. 1. p, T -diagrams for methane + ethane (left), carbon dioxide + nitrogen (center), and methane + chlorine (right) calculated based on the linear (solid line) and the Lorentz-Berthelot (dashed line) combining rules.

Unfortunately, well-established methods for selecting the correct combining rule based on macroscopic properties (*e.g.*, vapor pressure, virial coefficients, critical properties, *etc.*) or microscopic properties (*e.g.*, dispersive/repulsive forces, electrostatic charges and multipoles, hydrogen bonds, *etc.*) are not yet available. Therefore, the choice of the combining rule for these mixtures should always be critically evaluated before use. For this purpose, more predictive mixture models (*e.g.*, equations based on statistical associating fluid theory) should be analyzed. Other methods for improving the predictive capabilities of multi-fluid mixture models have recently been published by Jäger *et al.*^{39,40}

2.2.2 Few experimental data or only a single type of thermodynamic property available

If some experimental data are available, preferably for vapor-liquid equilibrium pressures and compositions (VLE data), the binary interaction parameters $\beta_{T,ij}$, $\gamma_{T,ij}$, $\beta_{v,ij}$, and $\gamma_{v,ij}$ can be adjusted. The number of fitted parameters depends on the quality, quantity, and range of data available. The mixture model may then be able to represent at least the correct vapor-liquid equilibrium behavior. In theory, these parameters are not subject to any restrictions. However, based on experience, they mostly vary between 0.8 and 1.2 (*cf.* Kunz and Wagner¹¹ or Gernert and Span⁴¹). There are a few exceptions, such as mixtures with hydrogen or water, that exhibit more non-ideal binary-specific parameters that significantly differ from those of the Lorentz-Berthelot or linear combining rules. During the fitting procedure, it can be beneficial to vary the parameters successively instead of simultaneously. Depending on the quality, quantity, and range of the data, it might also be helpful to adjust only certain parameters and set the remaining ones to unity, as is done, *e.g.*, for nitrogen + several hydrocarbons (pentane to octane) or argon + *n*-butane.¹¹

2.2.3 Experimental data of adequate quality and quantity available for similar binary mixtures

This category allows for the use of a departure term through a weighting factor F_{ij} or the full development of a new generalized departure function $\alpha_{ij}^r(\tau, \delta)$. If a departure function is available for physically and chemically similar binary mixtures, the weighing factor F_{ij} can be adjusted in addition to the binary interaction parameters. For the second option, setting up a generalized departure function requires that at least one binary mixture out of a group of “similar” binary mixtures has a comprehensive database with accurate data for different thermodynamic properties, *e.g.*, density, speed of sound, and vapor-liquid equilibrium data. This database serves as the basis for the optimization of the generalized departure function. If available, reliable datasets from similar binary mixtures can be considered concurrently during a simultaneous optimization process.⁴² This approach enables a more accurate reproduction of the experimental measurements while ensuring better representation of mixture properties for all similar binary mixtures that only have a restricted database. The functional form of the generalized function is not restricted to certain term types or numbers of terms. Lemmon and Jacobsen²⁸ first used this method for mixtures of methane through butane. It was later improved in the GERG-2008 model,¹¹ where this approach was applied for mixtures of, *e.g.*, (methane or ethane) + (*n*-butane or isobutane).

2.2.4 Comprehensive database available that includes many state points for different thermodynamic properties and with known experimental uncertainties

If a comprehensive and accurate database is available, it is possible to develop a binary-specific departure function. This function may consist of polynomial terms and exponential functions [see Eq. (12)], each with an arbitrary number of terms, which leads to a very flexible functional form. The adjustment of its parameters requires substantial knowledge of their impact to ensure that the physical behavior of the mixture equation is not compromised in regions where data are not available. Therefore, only selected binary systems have dedicated departure functions in the literature (*e.g.*, 7 out of 221 binary mixtures in the GERG-2008 model¹¹). However, fitting algorithms and computing power have significantly improved over the last decade, so that both experimental measurements and constraints on the thermodynamic properties can be utilized in the optimization process. Several of the key binary systems, which are investigated here, still have not been comprehensively measured; and, thus, the development of departure functions for these binaries may not be considered advisable. However, since the aim of this work is to represent new accurate density measurements in the subcooled liquid state within their experimental uncertainty, departure functions were necessary. Based on extensive studies of pure fluids,^{43–47} several constraints, which are also valid for binary mixtures, were devised and applied to the fitting procedure. Two examples are illustrated in Fig. 2.

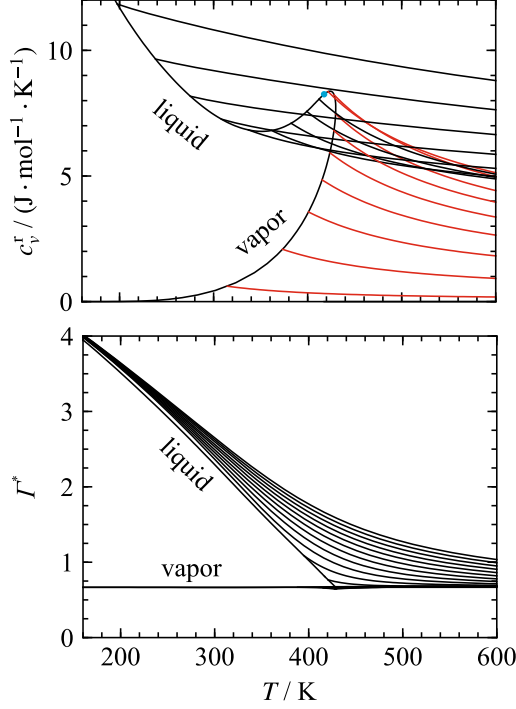


Fig. 2. Results obtained from applying typical constraints during the fitting procedure. Top: Residual isochoric heat capacity as a function of temperature along selected isochores (illustrated density range: $0.1 \text{ mol} \cdot \text{dm}^{-3}$ - $2.5 \text{ mol} \cdot \text{dm}^{-3}$). Isochores in the gaseous state are colored red. The location of the critical point is indicted with a blue circle. Bottom: Residual Grüneisen parameter as a function of temperature along selected isobars (illustrated pressure range: 0.1 MPa - 30 MPa). The new equation of state for methane + *n*-pentane developed in this work was used at equimolar composition for the calculations shown in the two diagrams.

In the top panel, the residual isochoric heat capacity as a function of temperature along selected isochores is shown. Characteristic features of this property include values on the saturated vapor line, where both the slope and curvature should be positive up to the vicinity of the critical point. The corresponding isochores in the vapor phase should have a negative slope and positive curvature. To transition correctly to the ideal gas limit, the residual isochoric heat capacity has to diminish at high temperatures. In contrast, the saturated liquid c_v^r has to retain positive curvature to the critical point. The slope has to be negative at low temperatures and must change sign after passing through the minimum.

In the bottom panel of Fig. 2, the residual Grüneisen parameter⁴⁸ [with $\Gamma = (\partial p / \partial T)_\rho / (\rho c_v)$] along selected isobars is depicted as a function of temperature. The saturated vapor line exhibits negative slope and curvature up to the vicinity of the critical point. The saturated liquid line and the corresponding isobars have negative slopes and positive curvatures throughout.

Any departure function for the systems investigated in this work must satisfy each of the constraints shown in Fig. 2. There might be exceptions, *e.g.*, for water or hydrogen mixtures, but these are not part of the present study. By applying these constraints with the fitting procedure, the new models developed exhibited physically reasonable behavior despite the limited data available in some cases. The flexibility of the functional form of the departure

function then allows for the development of a correlation that achieves the required accuracy while ensuring the correct reproduction of the mixture thermodynamic behavior.

3. Binary Mixtures

The new equations of state for four binary mixtures are presented in this section, which are designated collectively as EOS-LNG. Special focus was given to the accurate representation of the liquefied natural gas (LNG) region. The reproduction of all other available data was simultaneously monitored so that the uncertainty of EOS-LNG is smaller than or at least similar to the uncertainty of the GERG-2008 model¹¹ over the whole temperature and pressure range for which the models are valid. To accurately calculate mixture LNG properties with the models in this work, the models must be used simultaneously with the models of GERG-2008¹¹ for the other binary subsystems. Otherwise, uncertainties can be larger than 0.1% in terms of density and 0.5% in terms of speed of sound.

Statistical analyses were generally carried out by evaluating relative deviations according to

$$\Delta X = 100 \frac{X_{\text{DATA}} - X_{\text{EOS}}}{X_{\text{DATA}}} \quad (25)$$

and the average absolute relative deviation

$$\text{AARD} = \frac{1}{N} \sum_{i=1}^N |\Delta X_i|. \quad (26)$$

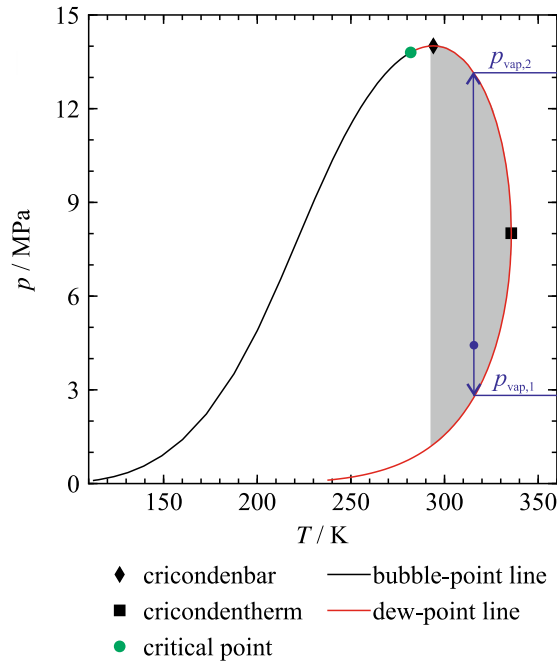


Fig. 3. Pressure as function of temperature for the binary system C_1C_4 at $x_{\text{C}_1} = 0.8$ calculated with the EOS-LNG. Two solutions ($p_{\text{vap},1}$ and $p_{\text{vap},2}$) are present in the shaded area between the temperature at the cricondenbar and cricondentherm when calculating deviations in terms of dew-point pressures.

Dew-point data are treated differently because the steep slope of the dew-point line in the vicinity of the cricondenbar (*cf.* Fig. 3) causes significant deviations in terms of dew-point pressures when only slightly changing the temperature. Furthermore, above the temperature at

the cricondenbar, two solutions are present when calculating deviations between an experimental state point (blue solid circle in Fig. 3) and calculated values ($p_{\text{vap},1}$ and $p_{\text{vap},2}$). In the vicinity of the cricondentherm, it is especially difficult to determine which solution is correct. Therefore, the dew-point line is statistically evaluated in terms of absolute deviations with respect to mole fraction of methane according to

$$\Delta y_{\text{C}_1} = 100(y_{\text{C}_1,\text{DATA}} - y_{\text{C}_1,\text{EOS}}) \quad (27)$$

and an average absolute deviation

$$\text{AAD} = \frac{1}{N} \sum_{i=1}^N |\Delta y_{\text{C}_1,i}|. \quad (28)$$

The evaluation of the experimental density data measured for six typical multicomponent natural gas mixtures^{19,49} with the GERG-2008 model¹¹ showed that four binary systems needed refinement to represent the multicomponent data within their experimental uncertainty: methane + *n*-butane (C_1C_4), methane + isobutane (C_1C_{4i}), methane + *n*-pentane (C_1C_5), and methane + isopentane (C_1C_{5i}). The new models were made consistent with the GERG-2008¹¹ through the use of the same pure fluid equations and the same mathematical structure as for the mixture models described in Sec. 2.1. Due to the data situation prevalent at the time of its formulation, no binary-specific departure functions were developed for these four mixtures in GERG-2008.¹¹ A generalized departure function was fitted for the methane + butane mixtures (C_1C_4 and C_1C_{4i}), whereas only the reducing functions were adjusted for the methane + pentane mixtures (C_1C_5 and C_1C_{5i}). Modern fitting techniques and experimental data published over the last decade now allow for the development of binary-specific departure functions for these four binary mixtures. The corresponding parameters of each binary-specific function of the new EOS-LNG model are given in Tables 1 and 2. The departure functions only include polynomial and special exponential terms as per Eq. (12).

Table 1. Binary parameters of the reducing functions for density and temperature, *cf.* Eqs. (8) and (9). Component *i* refers to methane (C_1).

Component <i>j</i>	$\beta_{T,ij}$	$\gamma_{T,ij}$	$\beta_{v,ij}$	$\gamma_{v,ij}$
<i>n</i> -butane (C_4)	0.9421	1.0307	1.035	1.118
isobutane (C_{4i})	0.9405	0.9917	1.0434	1.143
<i>n</i> -pentane (C_5)	0.9082	1.03884	1.02874	1.13209
isopentane (C_{5i})	0.886	0.993	1.023	1.076

Table 2. Parameters of the departure functions for the systems C_1C_4 , C_1C_{4i} , C_1C_5 , and C_1C_{5i} , *cf.* Eq. (12).

k	$n_{ij,k}$	$t_{ij,k}$	$d_{ij,k}$	$\eta_{ij,k}$	$\varepsilon_{ij,k}$	$\beta_{ij,k}$	$\gamma_{ij,k}$
C_1C_4							
1	0.7588	1.02	1				
2	-0.4386	0.71	2				
3	-0.02273	1.57	3				
4	45.05	3.41	1	1.34	0.59	1.07	0
5	-2.291	2.12	1	1.45	1.90	1.06	0
6	-62.51	3.28	1	0.96	0.87	1.11	0
7	33.32	3.37	2	1.33	1.12	1.20	0
8	-12.14	3.40	1	1.90	1.43	1.23	0
C_1C_{4i}							
1	0.9396	1.43	1				
2	-0.1439	0.30	2				
3	-0.1413	1.20	3				
4	35.32	3.10	1	1.87	1.73	1.67	0
5	-4.216	1.78	1	1.05	0.78	1.76	0
6	59.17	3.36	1	1.78	1.75	1.02	0
7	-76.68	2.70	2	1.19	1.84	1.76	0
8	-41.39	3.70	1	2.0	1.71	1.06	0
C_1C_5							
1	0.03711	1.54	2				
2	-0.12154	0.95	3				
3	27.086	0.47	1	0.6	0.7	0.916	0.5
4	-13.614	0.9	1	0.43	0.61	0.87	0.5
5	-14.45	0.22	1	0.7	0.7	0.86	0.5
6	-0.46867	2.65	2	1.40	0.46	2.8	0.5
C_1C_{5i}							
1	0.051	0.2	2				
2	-0.1580	0.53	3				
3	-67.49	1.79	1	0.64	0.5	1.56	0
4	-88.27	2.1	1	0.39	0.5	1.33	0
5	154.9	2.0	1	0.48	0.5	1.46	0
6	3.725	0.2	2	1.00	0.5	2.7	0

3.1 Data assessment

The new mixture models are mainly based on homogeneous density and vapor-liquid equilibrium data. Thorough assessment of the quality of the datasets available for developing the mixture models was an essential step in the tuning process. For three systems (C_1C_4 , C_1C_{4i} , and C_1C_5), the largest number of datasets for both properties were provided by the same research group: over the course of several API (American Petroleum Institute) research projects

between 1930 and 1960, more than 30 papers presenting measurements on natural gas mixtures were published by Sage, Lacey, Olds, Reamer, and other authors.

The apparatus used for these measurements was described in detail by Sage and Lacey,⁵⁰ with refinements and mixture-specific modifications occurring as the experimental campaign proceeded. The apparatus was basically a U-tube with mercury used as a confining fluid, the pressure of which was varied to change the volume of a known mass of the sample. The effective volume of the chamber filled with the sample was obtained by measuring the elevation of the mercury, which was determined by a moveable electrical contact. The temperature was controlled by a temperature bath and the pressure was measured with a Bordon tube gauge connected to the part of the U-tube filled with air. The authors state that this apparatus could be used to measure pure fluids, simple mixtures, and complex mixtures at homogeneous (gaseous and liquid) conditions as well as at vapor-liquid equilibrium states over a broad temperature and pressure range (approximately 290 K to 590 K with pressures up to 70 MPa). They report an overall uncertainty of 0.2% in density for all measurements, although recent mixture modelling has demonstrated that this claim is too optimistic. Sage and Lacey were very thoughtful in setting up their apparatus as they were aiming at a low uncertainty in measurement; however, the estimate of 0.2% is questionable based on comparisons with other data. There are many subtle details reported about the construction of the experimental apparatus (*e.g.*, even a home-made “pressure balance” was developed) as well as in conducting the measurements. When analyzing their paper, no obvious source of error becomes apparent; nevertheless, it is well-known that volumetric measurement techniques typically have issues with accurate volume and sample mass determination. It can thus be stated that the complexity of the apparatus makes it prone to errors. Since no reliable estimate of the actual experimental uncertainty is available, the data for methane + ethane (C_1C_2) and methane + propane (C_1C_3) measured with this apparatus were compared to the GERG-2008¹¹ as shown in Fig. 4. Deviations of up to 3% in the case of C_1C_2 and more than 5% for C_1C_3 are observed. Comparisons to other binaries such as C_1C_4 (Sage *et al.*⁵¹), C_1C_{4i} (Olds *et al.*⁵²), C_1C_5 (Sage *et al.*^{53,54}), C_2C_5 (Reamer *et al.*⁵⁵), and C_3C_5 (Sage and Lacey⁵⁶) show similar results.

To eliminate the equation of state as the source of the deviations, the binary C_1C_2 was investigated in further detail. In addition to the data of Sage and Lacey⁵⁷ (red symbols), Fig. 5 shows a comparison of the GERG-2008¹¹ to more recent experimental data with small, well-characterized uncertainties from several authors^{58–63} covering the same temperature, pressure, and composition ranges. These other data are consistent and are represented far more accurately than the data of Sage and Lacey.⁵⁷ Similar results were demonstrated for the binary C_1C_3 by Karimi *et al.*⁶⁴ who showed that the data of Reamer *et al.*⁶⁵ (as well as those of Huang *et al.*⁶⁶ and Arai and Kobayashi⁶⁷) were significantly lower in quality than other more modern data available in the literature and should be given low weights when developing improved equations of state. All the data from the Sage and Lacey group were thus assumed to be less

accurate than claimed in their publications. While no clear indication of errors in their measurement procedure could be found, it is known from literature⁶⁸ and our own critical data analysis that variable-volume devices do not enable uncertainties in density significantly smaller than 1% for pure substances. Considering possible inconsistencies in temperature and pressure measurement, and particularly in the determination of the mixture composition, an experimental uncertainty of approximately 4% was assigned to these data in the model development, based on comparisons with the GERG-2008 model¹¹ averaged across each of the binary systems.

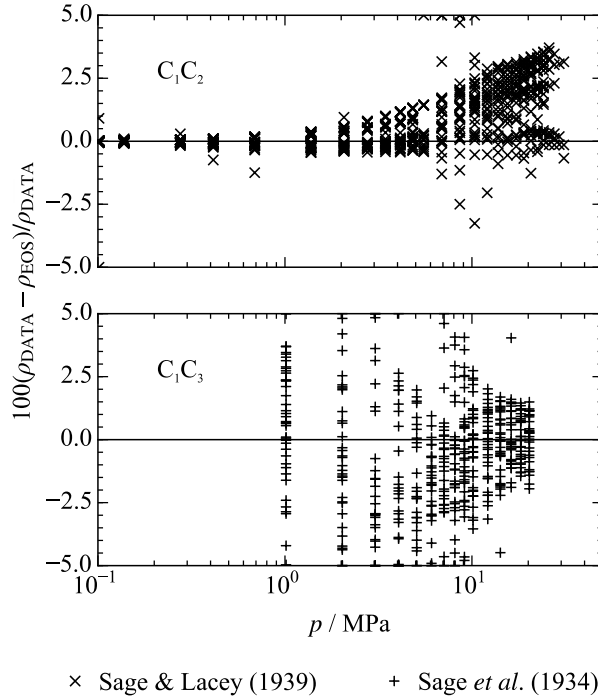


Fig. 4. Percentage deviations of experimental data measured over the temperature range (293 to 395) K for the systems C_1C_2 of Sage and Lacey⁵⁷ and C_1C_3 of Sage *et al.*⁶⁹ from the GERG-2008 model.¹¹

In contrast, the development of the EOS-LNG was strongly influenced by recent, accurate measurements of key binaries published after the development of GERG-2008.¹¹ These include the VLE data of May *et al.*⁷⁰ for C_1C_{4i} and C_1C_4 , the heat capacity data of Syed *et al.*⁷¹ for C_1C_4 , and the liquid mixture density datasets recently published by Lentner *et al.*^{20,72} To illustrate this point, we consider the case of Lentner *et al.*^{20,72} in further detail: during their measurements, special focus was given to the temperature, pressure, and composition ranges that are important for LNG transport, storage, and custody transfer. They measured one mixture composition of C_1C_{4i} and one of C_1C_5 . Comparisons to the GERG-2008¹¹ show negative deviations that increase with increasing temperatures and decreasing pressures for C_1C_{4i} as shown in Fig. 6. The maximum deviation is -0.58% . A systematic offset of approximately 0.5% can be observed for the system C_1C_5 . The relative combined expanded uncertainty ($k = 2$) in experimental density was specified to be 0.02% by Lentner *et al.*,^{20,72} which indicates the need to improve the equation of state for these binaries.

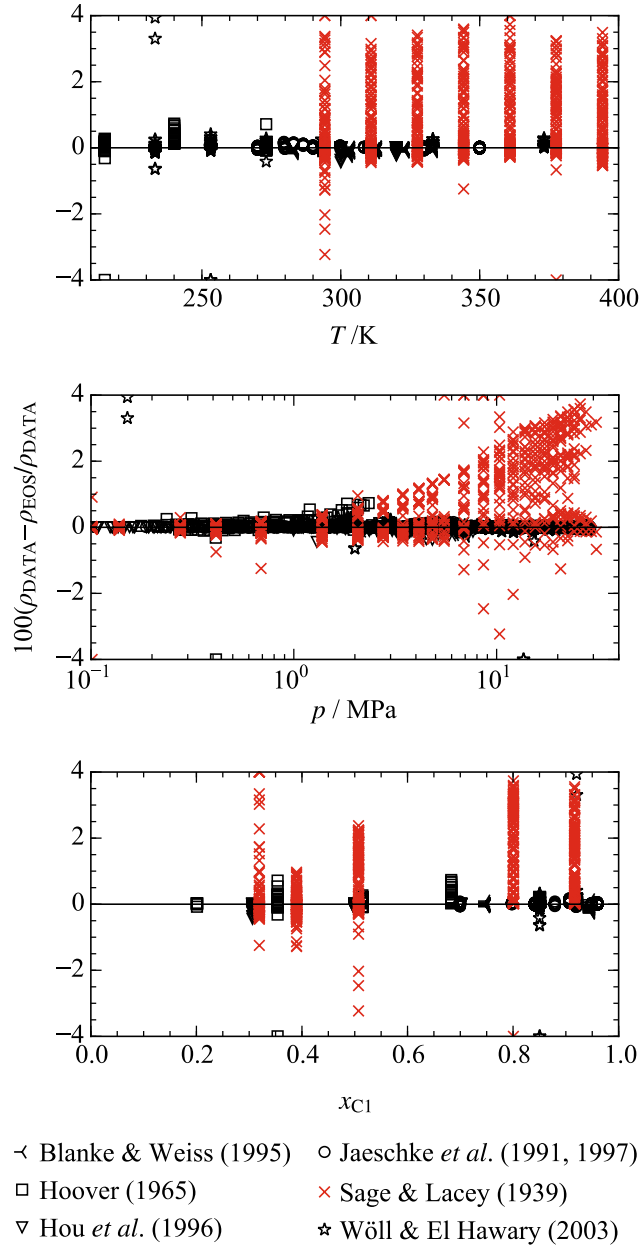


Fig. 5. Percentage deviations of experimental data for the binary system C_1C_2 of Sage and Lacey⁵⁷ and other accurate data⁵⁸⁻⁶³ from the GERG-2008 model.¹¹

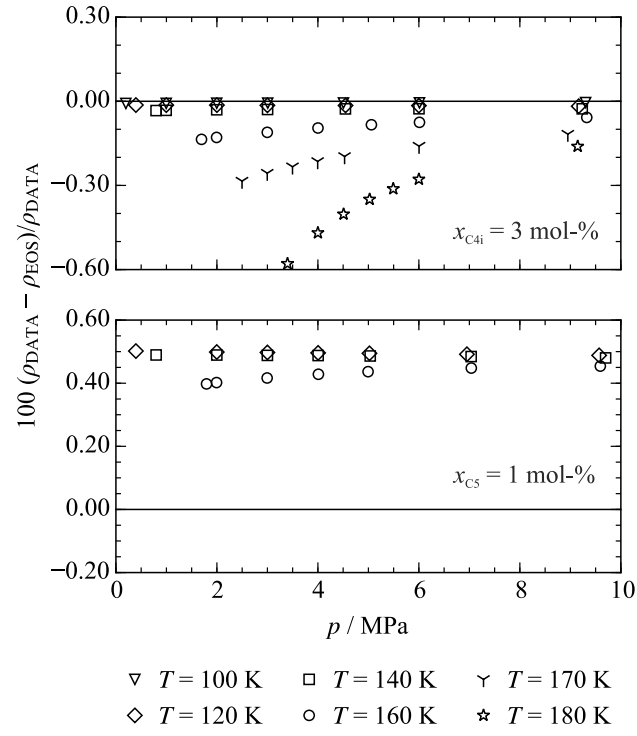


Fig. 6. Percentage deviations of experimental data of Lentner *et al.*^{20,72} for the binary systems C_1C_{4i} (top) and C_1C_5 (bottom) from the GERG-2008 model.¹¹

3.2 Methane + *n*-butane (C₁C₄)

The most comprehensively investigated binary system considered in this work is methane + *n*-butane. Summaries of the available data are given in Tables 3 and 4. Rowland *et al.*⁷³ published a modification of the GERG-2008 equation of state¹¹ that improved the description of this binary. They carried out investigations on the generalized departure function used for this binary in GERG-2008¹¹ and found that the term with high temperature and density exponents often made the representation of caloric data worse, in particular the representation of isobaric heat capacities measured for butane-rich binaries by Syed *et al.*⁷¹ They also improved the representation of the VLE at lower temperatures. However, the overall representation of density data by GERG-2008¹¹ and by the modification of Rowland *et al.*⁷³ does not differ significantly. Therefore, this modification is not shown for comparisons with the available homogeneous density data presented here.

Table 3. Average absolute relative deviations (AARD / %) calculated with the new equation of state for the binary system C₁C₄. For a better overview, comprehensive datasets are separated into different composition ranges and the overall AARD is given. Comparisons with available VLE data for this binary are listed in Table 4.

Author	<i>N</i>	$T_{\min} - T_{\max}$ / K	$p_{\min} - p_{\max}$ / MPa	$x_{C1,\min} - x_{C1,\max}$	AARD (EOS-LNG)	AARD (GERG-2008)
Density $\rho\rho T_x$						
Beattie <i>et al.</i> (1941) ⁷⁴	83	398 - 574	3.0 - 33.7	0.2507	1.4	0.75
	94	373 - 574	3.1 - 35.7	0.5044	1.2	0.82
	125	348 - 574	3.2 - 35.7	0.749	1.4	1.1
Overall	302	348 - 574	3.0 - 35.7	0.250 - 0.749	1.3	0.94
Ellington (1986) ⁷⁵	27	278 - 300	0.7 - 6.3	0.9576	0.03	0.06
Fenghour <i>et al.</i> (1999) ⁷⁶	15	366 - 478	8.7 - 31.1	0.3458	1.3	1.0
	8	362 - 415	8.8 - 19.5	0.3522	1.2	0.34
	11	381 - 479	8.7 - 21.0	0.3724	2.1	0.36
	16	336 - 480	10.0 - 48.2	0.4396	0.70	0.39
	9	316 - 405	12.0 - 40.9	0.5034	0.71	0.48
	12	339 - 479	11.5 - 38.7	0.5333	0.83	0.23
Overall	71	316 - 480	8.7 - 48.2	0.345 - 0.533	1.1	0.47
Haynes (1983) ⁷⁷	19	115 - 141	p_{liq}	0.777 - 0.928	0.10	0.44
Hiza <i>et al.</i> (1977) ⁷⁸	4	120 - 131	p_{liq}	0.5883	0.048	0.26
Jaeschke & Humphreys (1991) ⁶² and	268	270 - 354	0.3 - 28.2	0.985	0.017	0.014
Jaeschke <i>et al.</i> (1997) ⁶¹	285	280 - 350	0.4 - 27.9	0.9492	0.029	0.030
Overall	553	270 - 354	0.3 - 28.2	0.949 - 0.985	0.023	0.023
Kestin & Yata (1968) ⁷⁹	34	293 - 304	0.1 - 0.7	0.355 - 0.844	0.47	0.44
Pan <i>et al.</i> (1975) ⁸⁰	2	108 - 116	0.1 - 0.2	0.9499	0.098	0.38
Reamer <i>et al.</i> (1947) ⁸¹	120	310 - 511	1.3 - 69.0	0.1879	0.71	0.75
	131	310 - 511	1.3 - 69.0	0.396	3.5	3.6
	126	310 - 511	1.3 - 69.0	0.6002	0.57	0.53
	135	310 - 511	1.3 - 69.0	0.7997	0.57	0.47
Overall	512	310 - 511	1.3 - 69.0	0.187 - 0.800	1.4	1.4

Author	N	$T_{\min} - T_{\max}$ / K	$p_{\min} - p_{\max}$ / MPa	$x_{C1,\min} - x_{C1,\max}$	AARD (EOS-LNG)	AARD (GERG-2008)
Sage <i>et al.</i> (1940) ⁵¹	138	294 - 395	0.2 - 10.4	0.002 - 0.921	3.8	2.6
Tomlinson (1985) ⁸²	21	279 - 323	2.6 - 24.3	0.0242	10.0	10.0
Speed of sound w						
Plantier <i>et al.</i> (2005) ⁸³	9	311	3.9 - 13.8	0.158	1.5	1.0
	11	311	13.1 - 17.3	0.724	17.0	14.0
	23	311	2.0 - 17.3	0.894	1.6	1.1
Overall	43	311	2.0 - 17.3	0.158 - 0.894	5.6	4.4
Isobaric heat capacity c_p						
Syed <i>et al.</i> (2014) ⁷¹	4	148 - 179	5.05	0.95	2.3	2.0
	6	118 - 169	5.15	0.88	2.6	3.2
	6	118 - 169	5.15	0.6	0.62	20.0
Overall	16	118 - 179	5.0 - 5.2	0.600 - 0.950	1.8	9.1
Excess enthalpy h^E						
Hutchings <i>et al.</i> (1978) ⁸⁴	97	277 - 395	0.1	0.209 - 0.898	20.0	10.9

Reamer *et al.*⁸¹ published approximately 500 state points in the homogeneous state region at temperatures between 310 K and 511 K with pressures up to 69 MPa over a wide composition range. This publication was part of the comprehensive API research project on natural gases discussed above. Deviations are mostly within 2% except for the mixture with $x_{C1} = 0.396$. For this composition, the data scatter around the equation of state within 10%, which causes the comparably high AARD of 3.5%. For the remaining binary mixtures (AARD = 0.57% - 0.71%), the data are more consistent and more accurate as shown in Figures 7 and 8. In most regions, the data of Reamer *et al.*⁸¹ are reproduced more accurately by the EOS-LNG than with the GERG-2008.¹¹ However, the deviations between the data of Reamer *et al.*⁸¹ and the EOS-LNG increase at higher temperatures more than they do for GERG-2008.¹¹ This is caused by the different representation of the vapor-liquid equilibrium of the two models (see Fig. 9). The EOS-LNG was adjusted to the phase-equilibrium data of Sage *et al.*,⁸⁵ which caused a shift in the equilibrium curves predicted at higher temperatures, as shown in Fig. 10. This shift has a significant influence on the slope and curvature of the isotherms in a pressure-density plane. Therefore, the representation of homogeneous density data near the phase boundary, where the data of Reamer *et al.*⁸¹ are located, is different for both models; consequently, the comparison of the AARD statistics of the EOS-LNG and the GERG-2008¹¹ models in Table 3 does not give a complete representation of the model performance with a temperature-dependent analysis being preferable for this dataset. Older density measurements by Beattie *et al.*⁷⁴ and Sage *et al.*⁵¹ exhibit even larger deviations from both models and were, therefore, not considered in the fitting procedure.

Jaeschke and Humphreys⁶² and Jaeschke *et al.*⁶¹ published more than 550 accurate density data between 270 K and 354 K with a maximum pressure of 28 MPa. Because they focused on

hydrocarbon mixtures with typical natural gas compositions, they only considered two binary mixtures with high methane contents. However, due to the very low reported uncertainties of less than 0.05%, these data had a larger influence while developing both the GERG-2008¹¹ and the EOS-LNG model. The data are similarly reproduced by both models and are mostly represented within the experimental uncertainty.

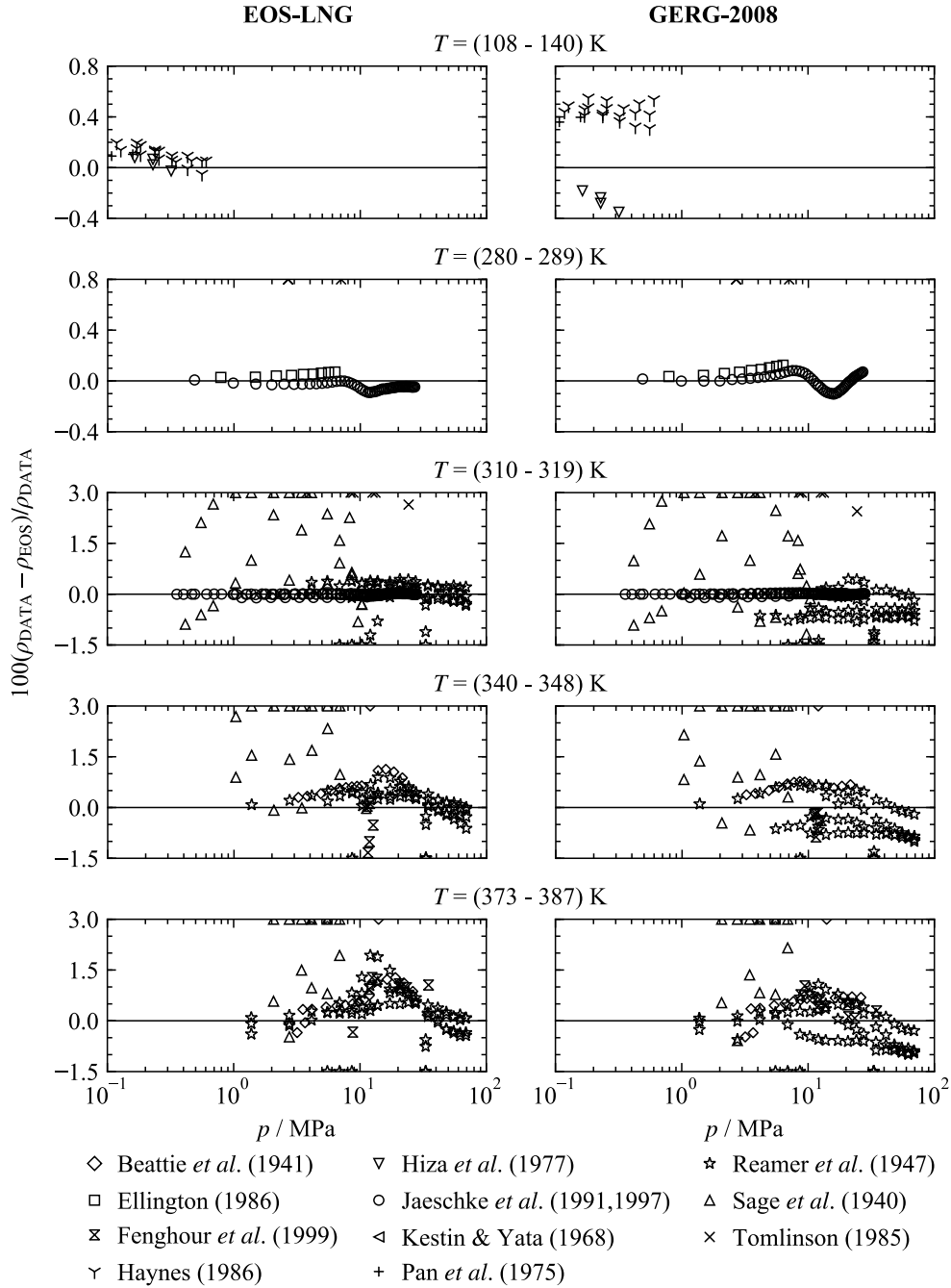


Fig. 7. Percentage deviations of homogeneous density data for the binary system C_1C_4 from the EOS-LNG (left) and the GERG-2008 (right) in selected temperature ranges below 400 K.

Ellington⁷⁵ made similar measurements, which were carried out in a restricted temperature range. They agree very well with the data of Jaeschke and Humphreys⁶² and Jaeschke *et al.*,⁶¹ as well as with the equations of state. The most recent density dataset of Fenghour *et al.*⁷⁶

comprises 71 data points between 316 K and 480 K with pressures up to 48 MPa and methane concentration of approximately $x_{C1} = 0.4$. Although a very detailed and careful description of the experiment is provided and the overall uncertainty in density is reported to be less than 0.05%, the overall AARD from the EOS-LNG is 1.1% while for the GERG-2008 model¹¹ the AARD is 0.47%. The difference in the performance of the two models in representing this dataset is most likely caused by the choice of data favored while fitting the two models. As explained earlier, the representation of the vapor-liquid equilibrium data of Sage *et al.*⁸⁵ was significantly improved by EOS-LNG in comparison to the GERG-2008 model.¹¹ Neither model can accurately represent both the VLE data and the density data measured at similar temperatures, and EOS-LNG prioritized the VLE data over the density data of Fenghour *et al.*⁷⁶ For future work, accurate measurements overlapping with the T_{px} ranges of Reamer *et al.*⁸¹ and more accurate vapor-liquid equilibrium data would be valuable to clarify this situation.

In the low-temperature region for which the fluid compositions are more similar to liquefied natural gases, only two state points of Pan *et al.*⁸⁰ are available for the compressed liquid density. They are represented within 0.1% by the EOS-LNG. In addition, two datasets of Hiza *et al.*⁷⁸ and Haynes⁷⁷ are available for the saturated liquid density. Both were measured with the same magnetic-suspension densimeter, which is known to be an accurate apparatus for this purpose. [Note: The “magnetic-suspension densimeter” of William (Mickey) Haynes and colleagues at NBS (today NIST) differs significantly from more modern magnetic-suspension densimeters, which is in particular a densimeter incorporating a magnetic-suspension coupling^{86,87} as, *e.g.*, used by McLinden,⁸⁸ Richter *et al.*,⁴⁹ and Lentner *et al.*^{19,20,72} for recent LNG density measurements.] For the measurements at NBS, the mixtures were prepared gravimetrically. According to a very detailed analysis of the experimental uncertainties, the authors state an overall uncertainty of 0.13% and 0.12% ($k = 2$), respectively. Comparisons of their data for well-known binary mixtures such as C_1C_2 or C_1C_3 show that they do not deviate by more than 0.1% from values calculated with GERG-2008.¹¹ In the case of C_1C_{4i} , Hiza *et al.*⁷⁸ suspected problems during the filling process or dew-point related errors in the mixture preparation so that the experimental uncertainty might be slightly higher. They assumed that similar problems occurred for the system C_1C_4 . However, these data can be reproduced within 0.08% (AARD = 0.048%), which is consistent with the representation of the data of Haynes⁷⁷ (AARD = 0.10%). Due to the high methane concentrations of these mixtures, the correct representation of these saturated liquid density data is crucial to the model’s performance in describing liquefied natural gases.

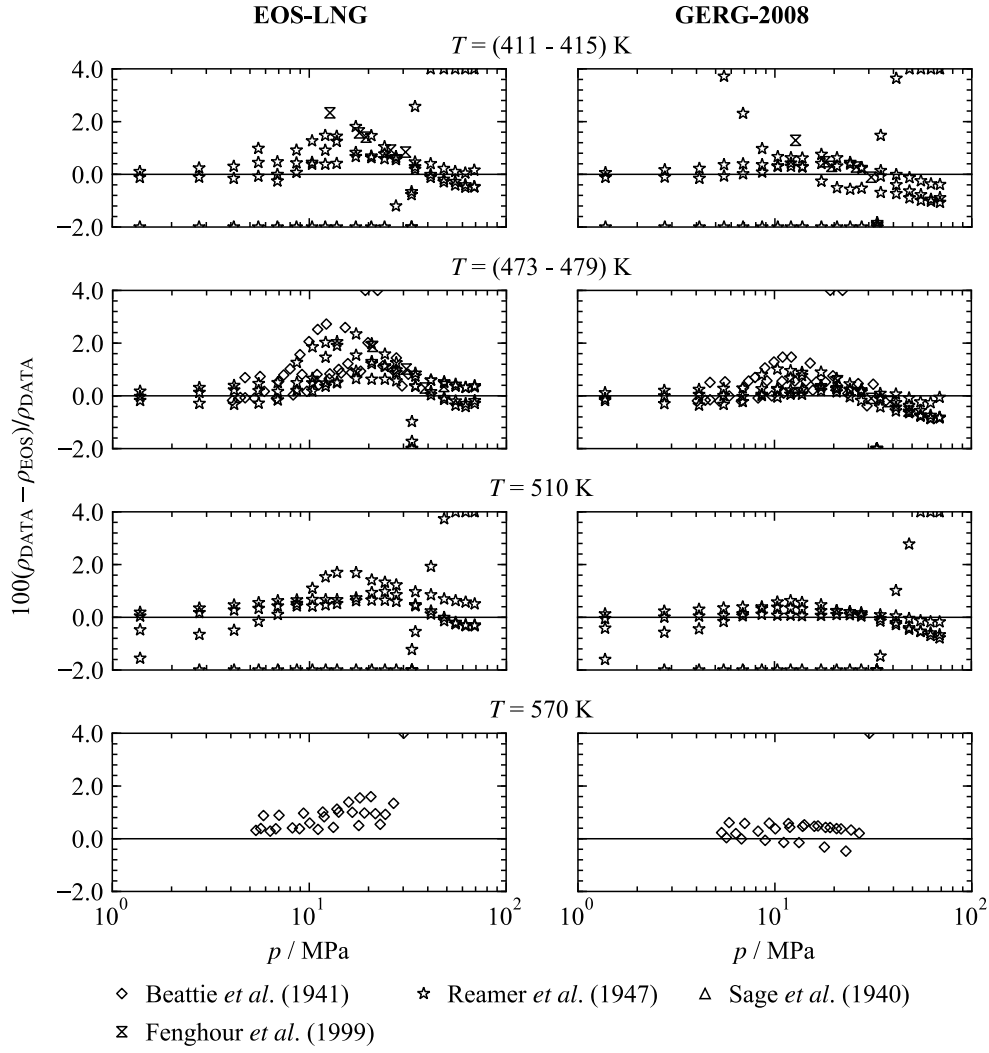


Fig. 8. Percentage deviations of homogeneous density data for the binary system C_1C_4 from the EOS-LNG (left) and the GERG-2008 (right) in selected temperature ranges above 400 K.

Table 4. Average absolute relative deviations of bubble-point pressure data ($\text{AARD}_{\text{pliq}} / \%$) and average absolute deviations in terms of percentage mole fraction of methane in the saturated vapor phase ($\text{AAD}_{\text{yC}_1} / \%$) for the binary system C_1C_4 . N denotes the total number of points in each publication except for pure-fluid measurements, whereas N_x and N_y indicate the number of bubble-point (index “x”) and dew-point (index “y”) pressure data. If N_x or N_y differ from N , state points were deleted from the numerical analysis for both models due to flash calculation errors or because they are outliers, which would distort the AARD or AAD.

Author	N	N_x	N_y	$T_{\min} - T_{\max} /$ K	$p_{\min} - p_{\max} /$ MPa	$\text{AARD}_{\text{pliq}}$ (EOS-LNG)	AAD_{yC_1} (EOS-LNG)	$\text{AARD}_{\text{pliq}}$ (GERG-2008)	AAD_{yC_1} (GERG-2008)
Chen <i>et al.</i> (1974) ⁸⁹	167	- ^a	167	144 - 278	0.1 - 12.9	-	0.30	-	0.34
Elliot <i>et al.</i> (1974) ⁹⁰	102	102	102	144 - 278	0.1 - 12.6	8.7	0.74	7.9	0.78
Fenghour <i>et al.</i> (1999) ⁷⁶	5	5	-	336 - 382	8.7 - 11.6	3.8	-	1.7	-
Haynes (1983) ⁷⁷	19	19	-	115 - 141	0.1 - 0.6	1.3	-	1.8	-
Kahre (1974) ⁹¹	70	70	70	166 - 284	0.1 - 11.1	7.2	0.15	6.4	0.13
May <i>et al.</i> (2015) ⁷⁰	20	20	20	203 - 274	1.3 - 10.2	4.3	0.20	9.1	0.22
Nederbragt (1938) ⁹²	9	9	9	252 - 317	1.0 - 3.1	4.1	1.2	6.4	1.4
Rigas <i>et al.</i> (1958) ⁹³	7	7	7	310 - 311	6.6 - 12.9	4.3	1.1	5.9	2.0

Author	N	N_x	N_y	$T_{\min} - T_{\max} /$ K	$p_{\min} - p_{\max} /$ MPa	AARD _{pliq} (EOS-LNG)	AAD _{yCl} (EOS-LNG)	AARD _{pliq} (GERG-2008)	AAD _{yCl} (GERG-2008)
Roberts <i>et al.</i> (1962) ⁹⁴	75	75	72	210 - 411	0.1 - 13.2	10.0	2.0	7.5	3.1
Sage <i>et al.</i> (1940) ⁸⁵	117	116	105 ^b	294 - 395	0.2 - 13.4	1.7	2.7	2.5	3.1
Wang & McKetta (1964) ⁹⁵	24	24	23	177 - 311	0.5 - 11.8	9.1	0.70	8.7	0.71
Wiese <i>et al.</i> (1970) ⁹⁶	25	25	24	277 - 378	1.3 - 13.3	2.6	2.7	1.7	2.3

^a Only dew-point pressures were measured.

^b Most of the state points, which are not included in the statistics, are measured at high pressures, which are significantly underestimated by the GERG-2008, *cf.* Fig. 10.

Table 4 lists a summary of the literature datasets for VLE compared with EOS-LNG and GERG-2008.¹¹ Percentage deviations of these data from saturation-pressure values calculated with EOS-LNG, GERG-2008,¹¹ and with the modification of Rowland *et al.*⁷³ are presented in Fig. 9. For this system, the most comprehensive vapor-liquid equilibrium dataset was provided by Sage *et al.*⁸⁵ Their data cover a temperature range from 294 K to 395 K with a maximum pressure of 13.4 MPa. Since the data were measured together with the homogeneous density data, they were used in this work to determine the location of the vapor-liquid equilibrium boundary. The overall AARD in terms of bubble-point pressures of EOS-LNG is 1.7% for this dataset, whereas GERG-2008¹¹ represents the dataset with an AARD of 2.5%. This difference is mainly caused by the choice of the dataset that was fitted.

For the development of GERG-2008,¹¹ the VLE data of Roberts *et al.*⁹⁴ were favored. They state an uncertainty in their pressure measurements of 0.014 MPa, which is between 1% and more than 10% depending on the saturation pressure. Furthermore, it was found that the data of Roberts *et al.*⁹⁴ and Wang and McKetta,⁹⁵ which were measured with the same apparatus, significantly differ from other experiments, *e.g.*, of Sage *et al.*,⁸⁵ Elliot *et al.*,⁹⁰ and May *et al.*⁷⁰ (*cf.* Fig. 10, $T = 244.3$ K, Elliot *et al.*⁹⁰ and May *et al.*⁷⁰). Because the data of those three sources agree very well, the data of Elliot *et al.*⁹⁰ (AARD = 8.7%) and May *et al.*⁷⁰ (AARD = 4.3%) were used to model the vapor-liquid equilibrium of EOS-LNG at low temperatures down to 210 K. The comparably high AARD for the data of Elliot *et al.*⁹⁰ is mainly caused by the low pressure region. The most significant improvement was achieved in the high temperature region. Because GERG-2008¹¹ was fitted to the data of Roberts *et al.*⁹⁴ up to 411 K, the data of Sage *et al.*⁸⁵ are considerably underestimated in this region. Deviations of up to -2 MPa can be observed for GERG-2008¹¹ at $T = 394.2$ K, which is far more accurately represented by EOS-LNG (*cf.* Fig. 10).

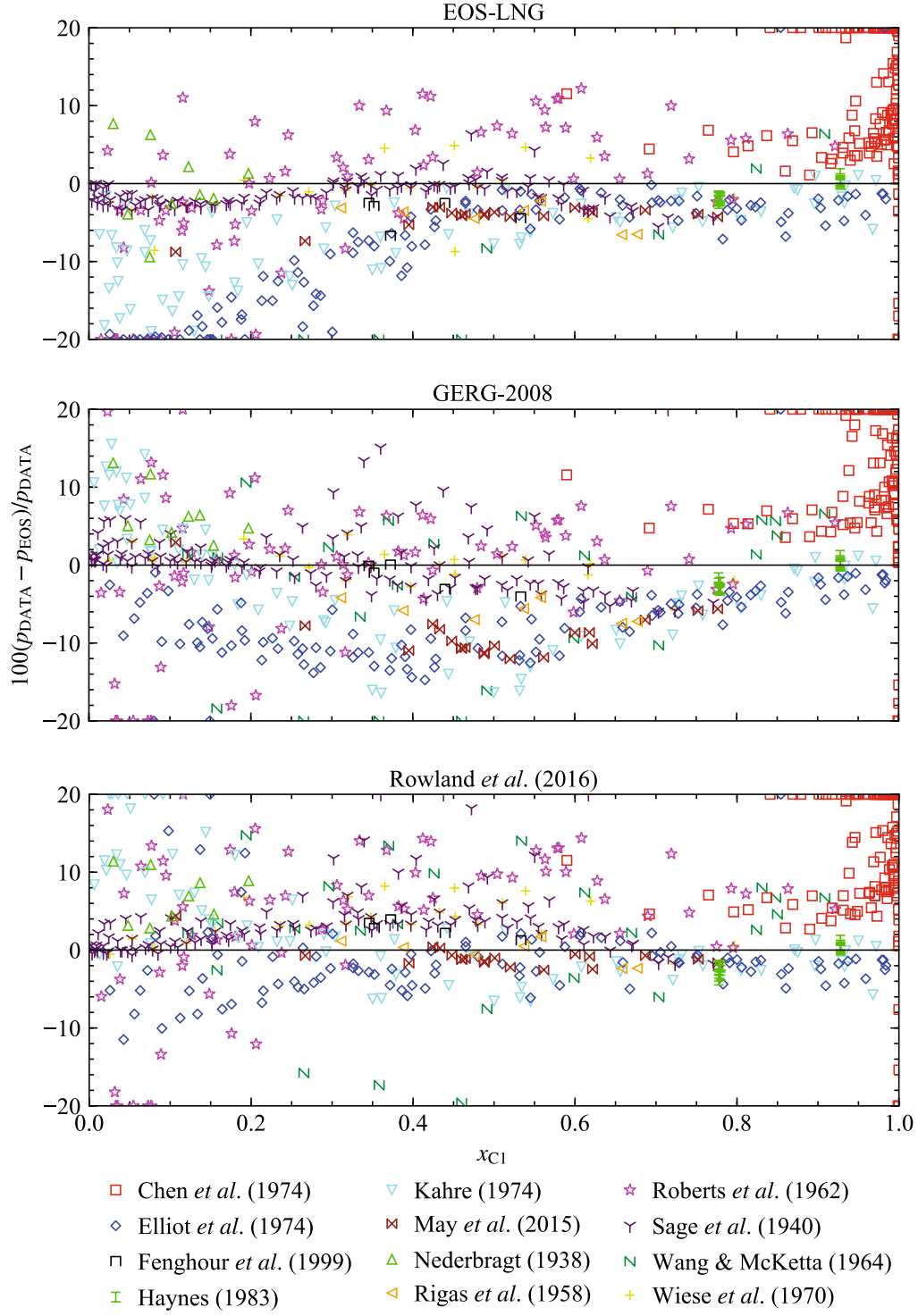


Fig. 9. Percentage deviations of bubble-point pressure data for the binary system C_1C_4 from the EOS-LNG (top), the GERG-2008¹¹ (center), and the modification of Rowland *et al.*⁷³ as a function of the composition x_{C1} .

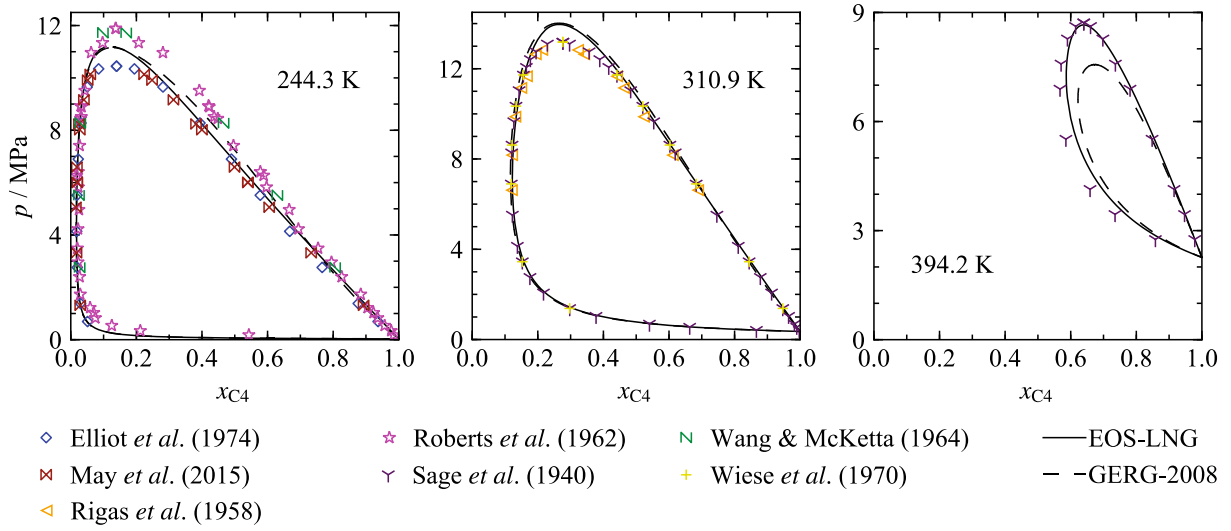


Fig. 10. p, x -diagrams representing the vapor-liquid equilibrium data for the binary system C_1C_4 .

With respect to caloric data, only one dataset each is available for speed of sound, for isobaric heat capacity, and for excess enthalpy. The speed of sound data of Plantier *et al.*⁸³ are mostly scattered around the EOS-LNG and the other two models^{11,73} within 10%. Excess enthalpies of Hutchings *et al.*⁸⁴ deviate by up to 40%, which is again similar for all three models. Significant differences among the three equations can only be observed for the isobaric heat capacities, *cf.* Fig. 11. The objective of Rowland *et al.*⁷³ was to better represent the recent measurements of Syed *et al.*,⁷¹ which are reproduced within 5% (AARD = 2.8%), whereas GERG-2008¹¹ deviates by more than 10% (AARD = 9.1%). With the new fitted parameters and departure function of the EOS-LNG, deviations are reduced to 3% (AARD = 1.8%).

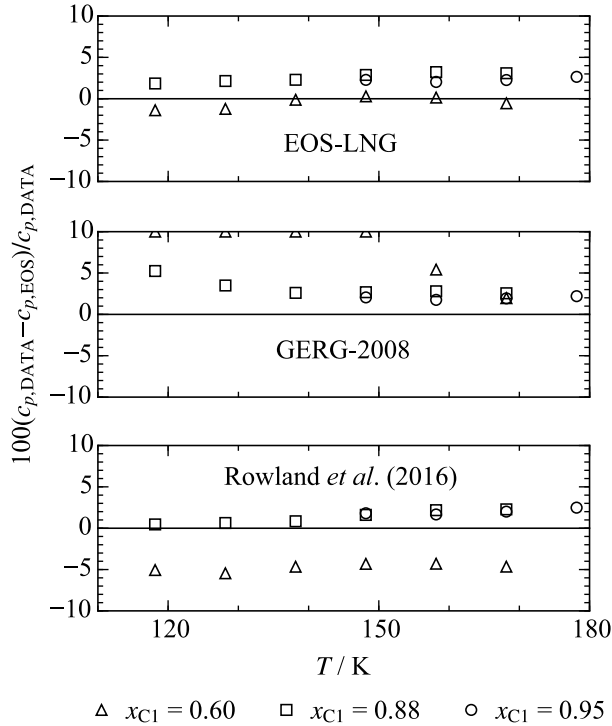


Fig. 11. Percentage deviations of isobaric heat capacity data of Syed *et al.*⁷¹ for the binary system C_1C_4 from EOS-LNG (top), GERG-2008¹¹ (center), and the modification of Rowland *et al.*⁷³

3.3 Methane + isobutane (C₁C_{4i})

The available database for the binary system methane + isobutane is more restricted than for methane + *n*-butane. There are four datasets available for the homogeneous density and five datasets containing vapor-liquid equilibrium data. Except for new homogeneous liquid densities measured by Lentner *et al.*^{20,72}, the density data were also available for the development of the GERG-2008.¹¹ An overview of the performance of EOS-LNG and GERG-2008¹¹ in representing these data is given in Table 5 and shown in Figs. 12 and 13.

Table 5. Average absolute relative deviations (AARD / %) of density data from values calculated with the new equation of state for the binary system C₁C_{4i}. For a better overview, comprehensive density (*ppTx*) datasets are separated into different composition ranges for the data of Olds *et al.*⁵²

Author	<i>N</i>	$T_{\min} - T_{\max}$ / K	$p_{\min} - p_{\max}$ / MPa	$x_{C1,\min} -$ $x_{C1,\max}$	AARD (EOS-LNG)	AARD (GERG-2008)
Density <i>ppTx</i>						
Lentner <i>et al.</i> (2018) ^{20,72}	47	100 - 180	0.2 - 9.31 and p_{liq}	0.9701	0.010	0.12
Ellington (1986) ⁷⁵	27	278 - 300	0.7 - 6.30	0.9576	0.16	0.17
Rodosevich & Miller (1973) ⁹⁷	7	95 - 115	p_{liq}	0.915 - 0.947	0.030	0.023
Olds <i>et al.</i> (1942) ⁵²	142	310 - 511	1.3 - 34.5	0.16	0.57	0.66
	137	310 - 511	1.3 - 34.5	0.277	0.36	0.35
	136	310 - 511	1.3 - 34.5	0.4681	0.28	0.16
	140	310 - 511	1.3 - 34.5	0.7101	0.26	0.42
Overall	555	310 - 511	1.3 - 34.5	0.160 - 0.711	0.37	0.40
Haynes (1983) ⁷⁷	13	110 - 140	p_{liq}	0.783 - 0.921	0.057	0.049
Hiza <i>et al.</i> (1977) ⁷⁸	4	115 - 130	p_{liq}	0.4869	0.068	0.96

Figure 12 shows the low-temperature region covered by homogeneous density data. Lentner *et al.*^{20,72} published data for six isotherms in the LNG region between 100 K and 180 K. Modeling these data was challenging because the isotherms at higher temperatures approach the phase boundary in their low-pressure limit. If the available vapor-liquid equilibrium data are not consistent with the homogeneous density data, this offset has the largest effect near the phase boundary and it is only possible to accurately reproduce either the VLE or the homogeneous density data. The new density measurements were not available when the GERG-2008¹¹ was developed. Therefore, the model was mainly fitted to represent the VLE and homogeneous density data of Olds *et al.*⁵² This gives rise to increasing deviations at increasing temperatures between the new density data⁷² and the GERG-2008¹¹ (*cf.* Fig. 6, top panel), which leads to the assumption that the homogeneous density data of Olds *et al.*⁵² were overfitted in the development of GERG-2008.¹¹ However, because no other data are available, EOS-LNG was fitted to ensure that the new data were represented as well as possible and that the accuracy of GERG-2008¹¹ for all other regions and properties was retained. Consequently, the density data by Lentner *et al.*^{20,72} are reproduced within their experimental uncertainty, except for three state points at the lower pressures of the isotherm $T = 180$ K, *cf.* Fig. 12. The AARD was reduced from 0.12% (GERG-2008¹¹) to 0.01% (EOS-LNG).

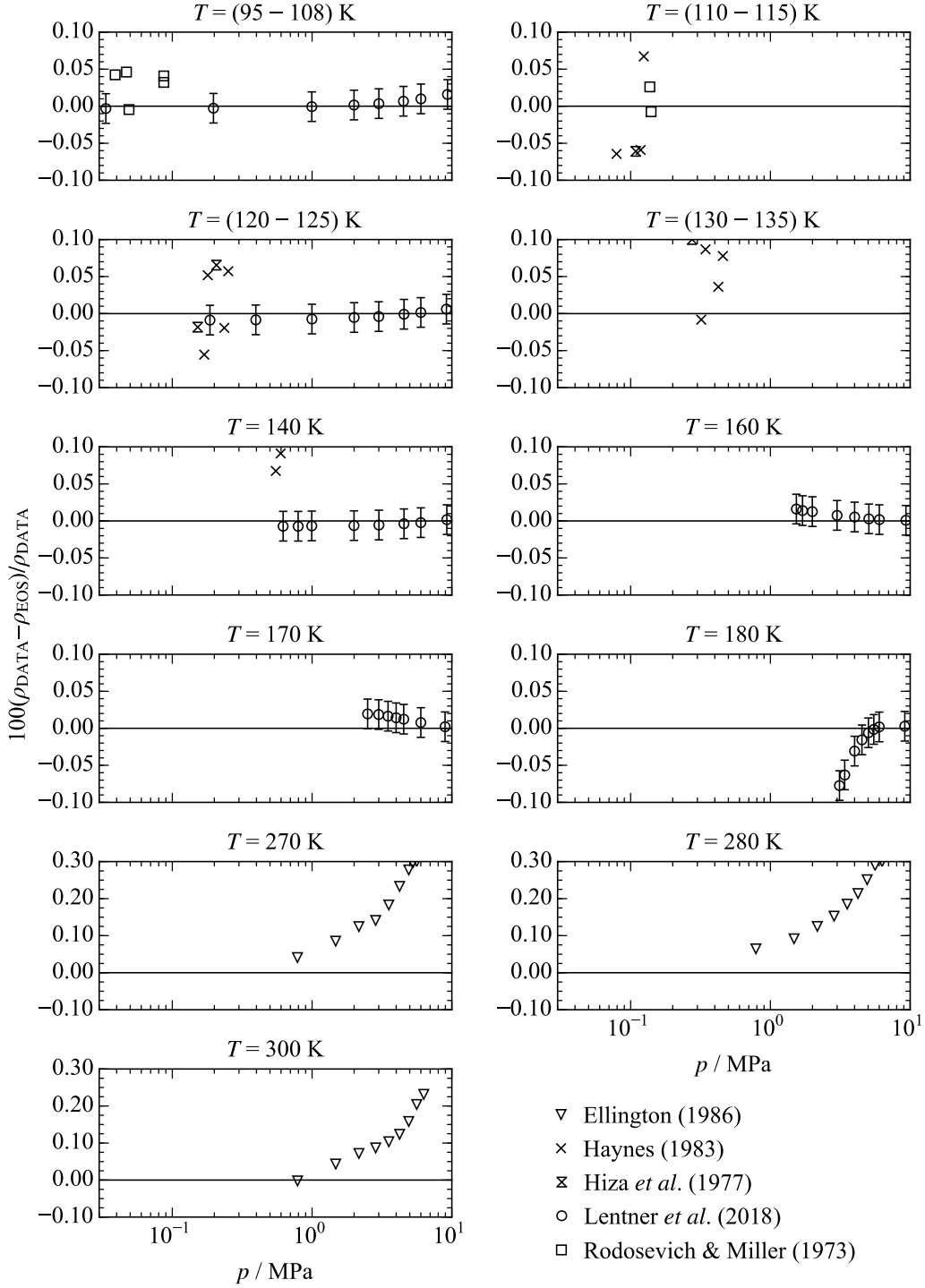


Fig. 12. Percentage deviations of homogeneous density data in the low and medium temperature region from the EOS-LNG for the binary system C_1C_{4i} . The uncertainties of the data of Lentner *et al.*^{20,72} are also shown. The scale of the y-axis changes at 270 K.

This improvement in the homogeneous liquid state at low temperatures resulted in an AARD of 0.057% ($AARD_{GERG-2008} = 0.049\%$) for the saturated liquid density data of Haynes⁷⁷ and 0.068% ($AARD_{GERG-2008} = 0.96\%$) for the measurements of Hiza *et al.*⁷⁸ As with C_1C_4 , the experimental uncertainty of these datasets is approximately 0.12%, and EOS-LNG reproduces all data within this value. For comparison, only one data point deviates by more than 0.1% for the systems C_1C_2 and C_1C_3 . The dataset of Lentner *et al.*^{20,72} also includes saturated liquid

density data at each measured temperature, which overlap the data of Haynes⁷⁷ and Hiza *et al.*⁷⁸ The data of Lentner *et al.*^{20,72} are represented within their experimental uncertainty (less than 0.017%) except for the state point at $T = 180$ K, which deviates by 0.076%. In the same temperature range, seven saturated liquid density data points were published by Rodosevich and Miller.⁹⁷ Measurements were carried out with a special gas expansion system in a narrow temperature range for several binary mixtures including hydrocarbons and nitrogen. Deviations of these data with respect to EOS-LNG are less than 0.05%, which is well within the experimental uncertainty of 0.1%.

In the medium-temperature range, only three isotherms from one author are available. Because the data were disclosed as private communication from Ellington⁷⁵ to Jaeschke and were later published in the supplementary material of a GERG report,⁶¹ no information on the measurement procedure or the accuracy is available. With increasing pressure, the data show increasing deviations of up to 0.3% (AARD = 0.16%). This matches the representation of the experimental data by the GERG-2008¹¹ (AARD = 0.17%).

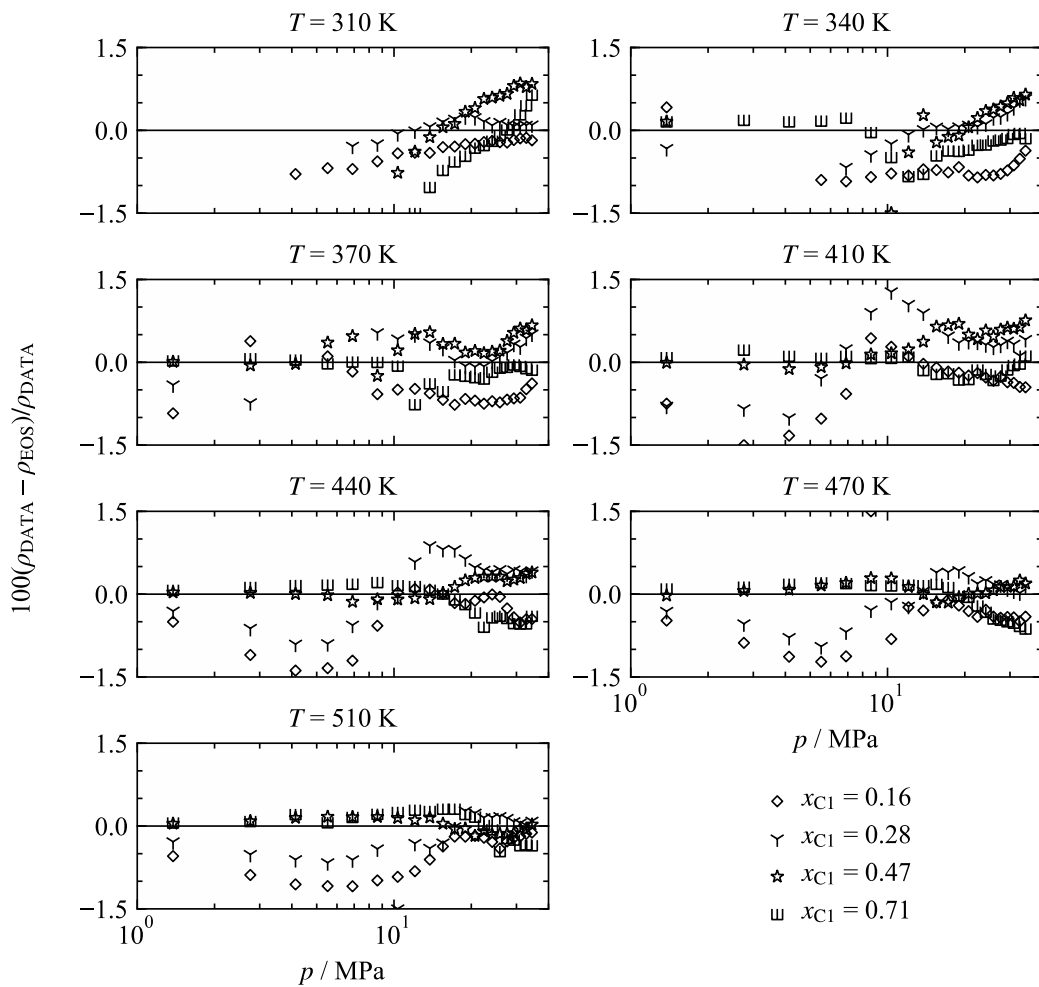


Fig. 13. Percentage deviations of homogeneous density data of Olds *et al.*⁵² in the high-temperature region from the EOS-LNG for the binary system C_1C_{4i} .

The high-temperature region (310 K to 511 K) was comprehensively investigated over a wide composition range by Olds *et al.*⁵² with data extending to a maximum pressure of 34.5 MPa. As illustrated in Fig. 13, deviations up to 1.5% are obtained for the EOS-LNG, which is comparable to that for GERG-2008.¹¹ The overall AARD is 0.37%, whereas it is 0.40% for GERG-2008.¹¹ As discussed in the introduction of Sec. 3, reliable experimental uncertainties of these data are not available. New measurements in this state region are desirable to accurately assess the data.

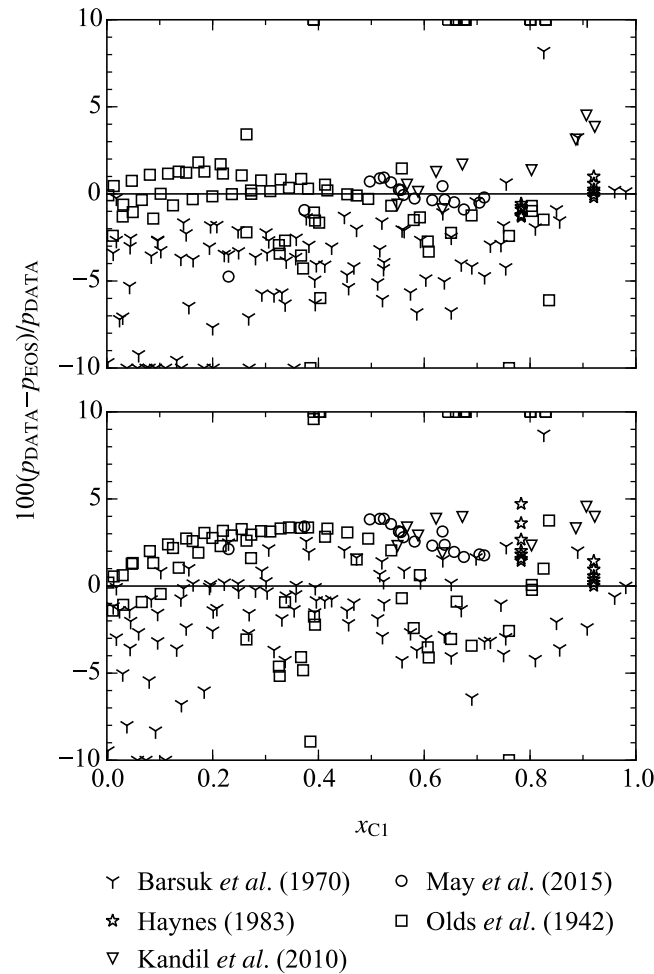


Fig. 14. Percentage deviations of bubble-point pressure data for the binary system C_1C_{4i} from the EOS-LNG (top) and the GERG-2008¹¹ (bottom) as a function of the composition x_{C1} .

Figure 14 gives an overview of the percentage deviations of each VLE dataset from values calculated with EOS-LNG and GERG-2008,¹¹ where the different choice of datasets used to develop the two models becomes apparent. The most extensive vapor-liquid equilibrium datasets available for this binary system are those of Barsuk *et al.*⁹⁸ and Olds *et al.*⁵² The dew-point pressure data of those two publications agree quite well, whereas the bubble-point pressure data of Barsuk *et al.*⁹⁸ are systematically lower than the data of Olds *et al.*⁵² No reliable information on the uncertainty of the data were provided by the authors. Since the density data of Olds *et al.*⁵² were used to model the homogenous region, this dataset was also prioritized for

the description of VLE data in this work. In this way, an inconsistency between the two properties is avoided. Furthermore, recent VLE measurements of May *et al.*⁷⁰ confirm this approach. When fitting the VLE data of Olds *et al.*,⁵² it is possible to reproduce the bubble-point pressure data of May *et al.*⁷⁰ within 0.9% (AARD = 0.73%) except for one state point measured at the lowest methane mole fraction, *cf.* Fig. 14. For the development of the GERG-2008,¹¹ the data of Barsuk *et al.*⁹⁸ were chosen as the reference dataset since the data of May *et al.*⁷⁰ were unavailable at the time of fitting. Consequently, the data of May *et al.*⁷⁰ are systematically underpredicted by GERG-2008¹¹ and can only be reproduced with an AARD of 2.8%. Additionally, 13 bubble-point pressure data measured by Haynes⁷⁷ and 10 saturation pressure data measured by Kandil *et al.*⁹⁹ are available. The data of Haynes⁷⁷ are reproduced within 1.4% by the EOS-LNG (4.8% by the GERG-2008¹¹), whereas the data of Kandil *et al.*⁹⁹ exhibit positive deviations of up to 4.5% (4.6% by the GERG-2008¹¹). However, the data of Kandil *et al.*⁹⁹ were measured with an earlier version of the apparatus used subsequently by May *et al.*⁷⁰ with poorer temperature control, and the experimental uncertainties estimated by Kandil *et al.*⁹⁹ are much larger than those of May *et al.*⁷⁰

Table 6. Average absolute relative deviations of bubble-point pressure data (AARD_{pliq} / %) and average absolute deviations in terms of percentage mole fraction of methane in the saturated vapor phase (AAD_{yC1} / %) for the binary system C₁C_{4i}. *N* denotes the total number of points in each publication except for pure-fluid measurements, whereas *N_x* and *N_y* indicate the number of bubble-point (index “x”) and dew-point (index “y”) pressure data. If *N_x* or *N_y* differ from *N*, state points were deleted from the numerical analysis for both models due to flash calculation errors or because they are outliers, which would distort the AARD or AAD.

Author	<i>N</i>	<i>N_x</i>	<i>N_y</i>	$T_{\min} - T_{\max} /$ K	$p_{\min} - p_{\max} /$ MPa	AARD _{pliq} (EOS-LNG)	AAD _{yC1} (EOS-LNG)	AARD _{pliq} (GERG-2008)	AAD _{yC1} (GERG-2008)
Barsuk <i>et al.</i> (1970) ⁹⁸	96	96	94	198 - 378	0.4 - 12	6.0	2.6	2.5	2.9
Haynes (1983) ⁷⁷	13	13	-	110 - 141	0.08 - 0.59	0.70	-	1.7	-
Kandil <i>et al.</i> (2010) ⁹⁹	10	10	7 ^b	151 - 252	1.0 - 8.4	1.8	0.09	3.2	0.13
May <i>et al.</i> (2015) ⁷⁰	18	18	18	203 - 274	2.6 - 8.7	0.73	0.15	2.8	0.32
Olds <i>et al.</i> (1942) ⁵²	75	41 ^a	75	310 - 378	0.5 - 12	0.83	1.3	2.2	1.7

^aFor 34 state points out of 75, no liquid-phase composition was measured.

^bFor 3 state points out of 10, no vapor-phase composition was measured.

3.4 Methane + *n*-pentane (C₁C₅)

For the binary system methane + *n*-pentane, only a few data sources are available. Overviews are given in Tables 7 and 8.

Table 7. Average absolute relative deviations (AARD / %) for density and excess enthalpy data from values calculated with the new equation of state for the binary system C₁C₅. For a better overview, comprehensive density (*ppTx*) datasets are separated into different composition ranges and the overall AARD is given.

Author	<i>N</i>	$T_{\min} - T_{\max}$ / K	$p_{\min} - p_{\max}$ / MPa	$x_{C1,\min} - x_{C1,\max}$	AARD (EOS-LNG)	AARD (GERG-2008)
Density <i>ppTx</i>						
Jaeschke & Humphreys (1991) ⁶² and Jaeschke <i>et al.</i> (1997) ⁶¹	21	292 - 309	3.7 - 6.4	0.9973	0.030	0.034
Lentner <i>et al.</i> (2018) ^{20,72}	32	110 - 160 and p_{liq}	0.4 - 9.7	0.9901	0.010	0.48
Sage <i>et al.</i> (1936) ⁵³	39	310 - 378	2.7 - 20.7	0.2572	0.79	1.1
	31	310 - 378	4.1 - 20.7	0.5341	2.2	2.6
	28	310 - 378	5.5 - 20.7	0.6253	2.7	3.2
Overall	100	310 - 511	2.7 - 34.5	0.257 - 0.983	1.8	2.2
Sage <i>et al.</i> (1942) ⁵⁴	135	310 - 511	1.3 - 34.5	0.1263	0.57	0.45
	145	310 - 511	1.3 - 34.5	0.2933	0.95	1.2
	146	310 - 511	1.3 - 34.5	0.4636	0.76	1.3
	145	310 - 511	1.3 - 34.5	0.7385	1.0	1.0
	147	310 - 511	1.3 - 34.5	0.9404	0.40	0.20
	147	310 - 511	1.3 - 34.5	0.9822	0.36	0.24
Overall	987	310 - 511	0.1 - 34.5	0.001 - 0.983	0.82	0.74
Zhang <i>et al.</i> (2002) ¹⁰⁰	14	476.60	3.0 - 4.9	0.0093	11.0	11.0
Excess enthalpy h^E						
Hutchings <i>et al.</i> (1978) ⁸⁴	84	318 - 404	0.10	0.255 - 0.708	5.7	30.0

In Fig. 15, deviations of all available experimental density data from EOS-LNG are illustrated. Since the main focus of this work was the more accurate description of the LNG region, the new density data of Lentner *et al.*^{20,72} were prioritized during the fit. The experimental uncertainty of the data is specified to be 0.02%, which is reproduced by the EOS-LNG.

As for the other binaries, the most comprehensive dataset for C₁C₅ was published by Sage *et al.*^{53,54} They cover temperatures from 310 K to 511 K with a maximum pressure of 34.5 MPa over the full composition range. The deviations of the data from Sage *et al.*⁵³ from 1936 to both models are slightly higher than to those from 1942.⁵⁴ For the EOS-LNG, the overall AARD amounts to 1.8%, whereas the dataset of Sage *et al.*⁵⁴ exhibits an AARD of 0.82%. No temperature, pressure, or composition dependency could be observed, except for higher deviations in the vicinity of the critical points of each mixture.

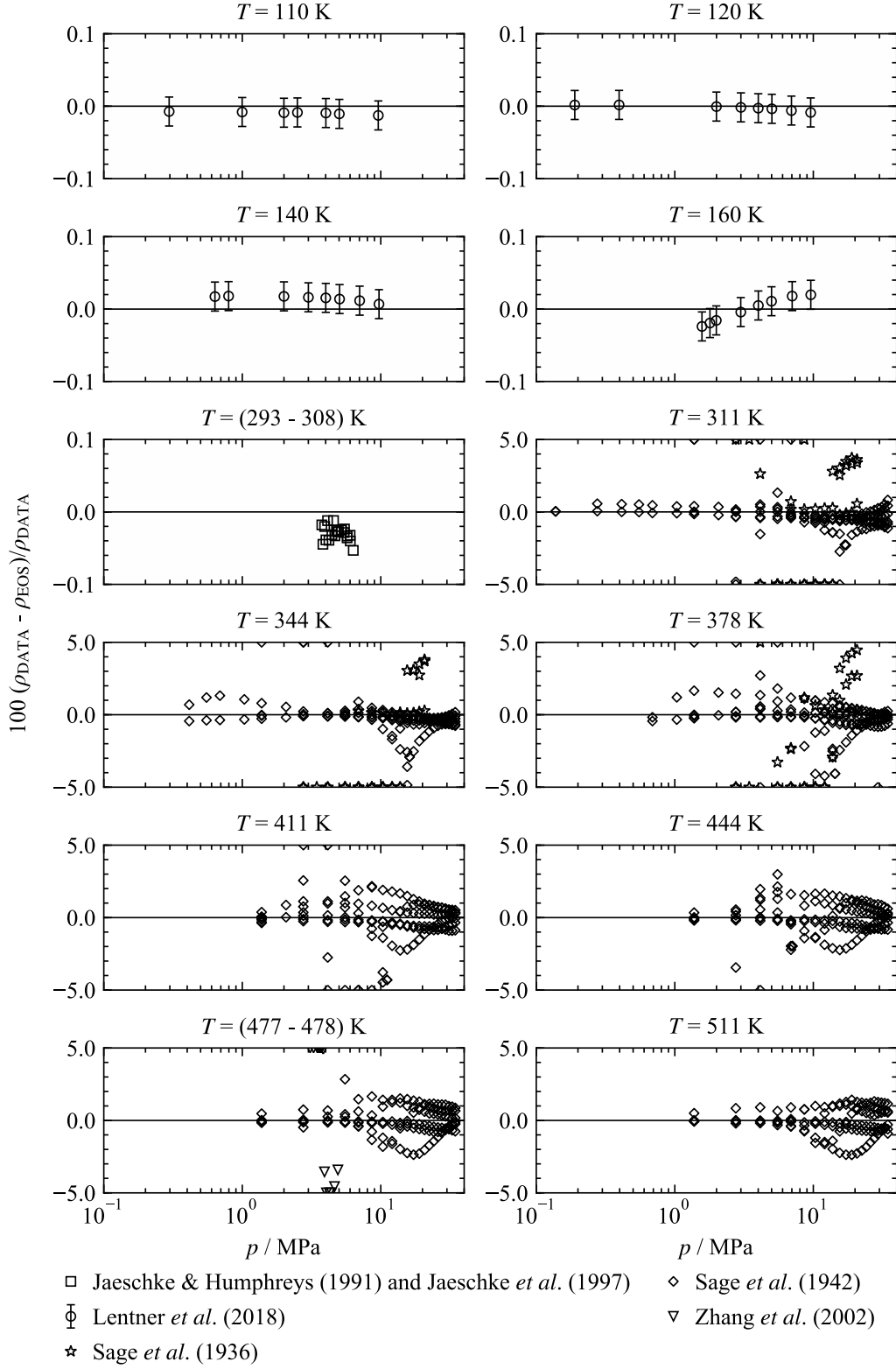


Fig. 15. Percentage deviations of homogeneous density data from the EOS-LNG for the binary system C_1C_5 . The scale of the y-axis changes at 311 K.

The most recent gas-phase density data for this binary were published by Jaeschke and Humphreys⁶² (and also Jaeschke *et al.*⁶¹) as part of a comprehensive measurement campaign of the GERG in the 1990s. Their reported uncertainty is less than 0.05%, which agrees with the

representation of the data by EOS-LNG. Only one data point deviates by 0.053%, whereas all other state points differ by approximately -0.03% .

There is one dataset of Zhang *et al.*¹⁰⁰ for a mixture with 99.07 mole percent pentane at $T = 476.6$ K. These data exhibit large deviations with respect to the new equation of state as well as with respect to GERG-2008.¹¹ Since the pure fluid experiments by Zhang *et al.*¹⁰⁰ on *n*-pentane already deviate by up to 12%, the measurement procedure may have been faulty, and their data were not considered further in this work.

In Table 8, comparisons of experimental vapor-liquid equilibrium data with values calculated from the EOS-LNG are listed. Separate comparisons are presented for states at the dew-point and bubble-point lines. Percentage deviations in terms of bubble-point pressure as a function of composition are depicted in Fig. 16.

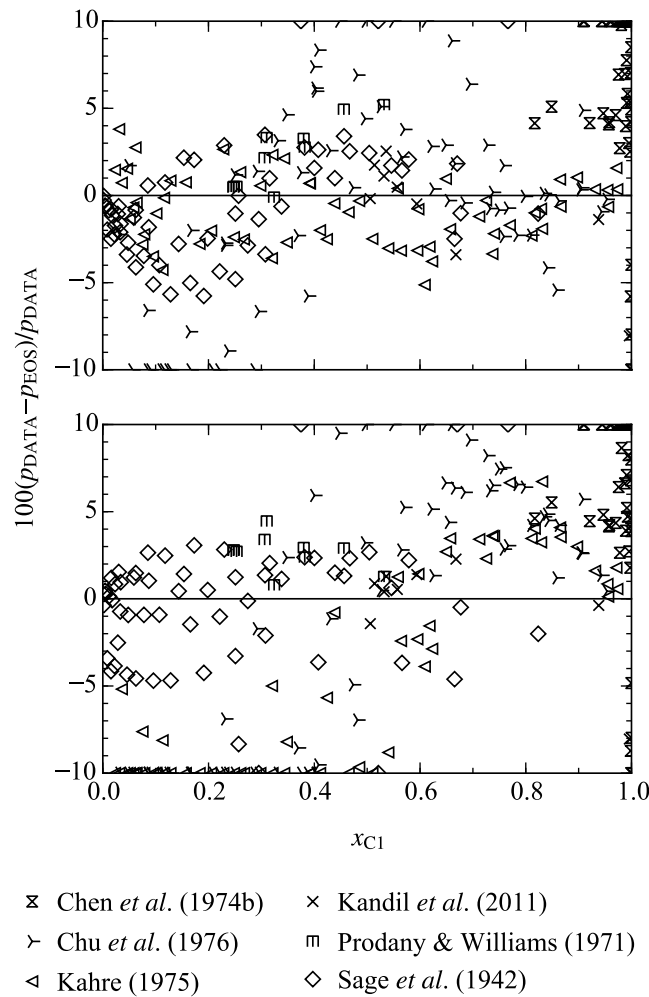


Fig. 16. Percentage deviations of vapor-liquid equilibrium pressure data for the binary system C_1C_5 from the EOS-LNG (top) and the GERG-2008¹¹ (bottom) as a function of the composition x_{C1} .

Table 8. Average absolute relative deviations of bubble-point pressure data ($AARD_{pliq} / \%$) and average absolute deviations in terms of percentage mole fraction of methane in the saturated vapor phase ($AAD_{yC1} / \%$) for the binary system C_1C_5 . N denotes the total number of points in each publication except for pure-fluid measurements, whereas N_x and N_y indicate the number of bubble-point (index “x”) and dew-point (index “y”) pressure data. If N_x or N_y differ from N , state points were deleted from the numerical analysis for both models due to flash calculation errors or because they are outliers, which would distort the AARD or AAD.

Author	N	N_x	N_y	$T_{min} - T_{max}$ / K	$p_{min} - p_{max}$ / MPa	$AARD_{pliq}$ (EOS-LNG)	AAD_{yC1} (EOS-LNG)	$AARD_{pliq}$ (GERG-2008)	AAD_{yC1} (GERG-2008)
Chen <i>et al.</i> (1974) ¹⁰¹	118	-	112	173 - 274	0.1 - 16	-	3.9	-	10.0
Chu <i>et al.</i> (1976) ¹⁰²	70	70	47 ^a	176 - 274	0.1 - 16	5.8	0.06	18.0	0.10
Kahre (1975) ¹⁰³	64	62	55	177 - 284	0.3 - 16	1.8	0.14	15.0	0.09
Kandil <i>et al.</i> (2011) ¹⁰⁴	9	9	9	173 - 244	2.4 - 8.0	2.2	0.11	1.9	0.08
Prodany & Williams (1971) ¹⁰⁵	10	10	10	377.57	6.9 - 14	2.3	0.12	2.6	0.10
Sage <i>et al.</i> (1942) ⁵⁴	61	61	60	310 - 445	0.1 - 17	2.2	0.93	2.4	2.9

^aFor 23 state points out of 70, no vapor-phase composition was measured.

Because the most comprehensive part of the homogeneous region was mainly fitted to the data of Sage *et al.*,⁵⁴ these data were also prioritized when fitting the vapor-liquid equilibrium. Moreover, these are the only data in the high-temperature region. The bubble-point pressure were fitted with an $AARD_{pliq}$ of 2.2% and the dew-point line exhibits an AAD_{yC1} of 0.93% in terms of mole fraction of methane. In comparison to the GERG-2008,¹¹ a significant improvement was achieved in the high-pressure region for both the dew-point and bubble-point lines.

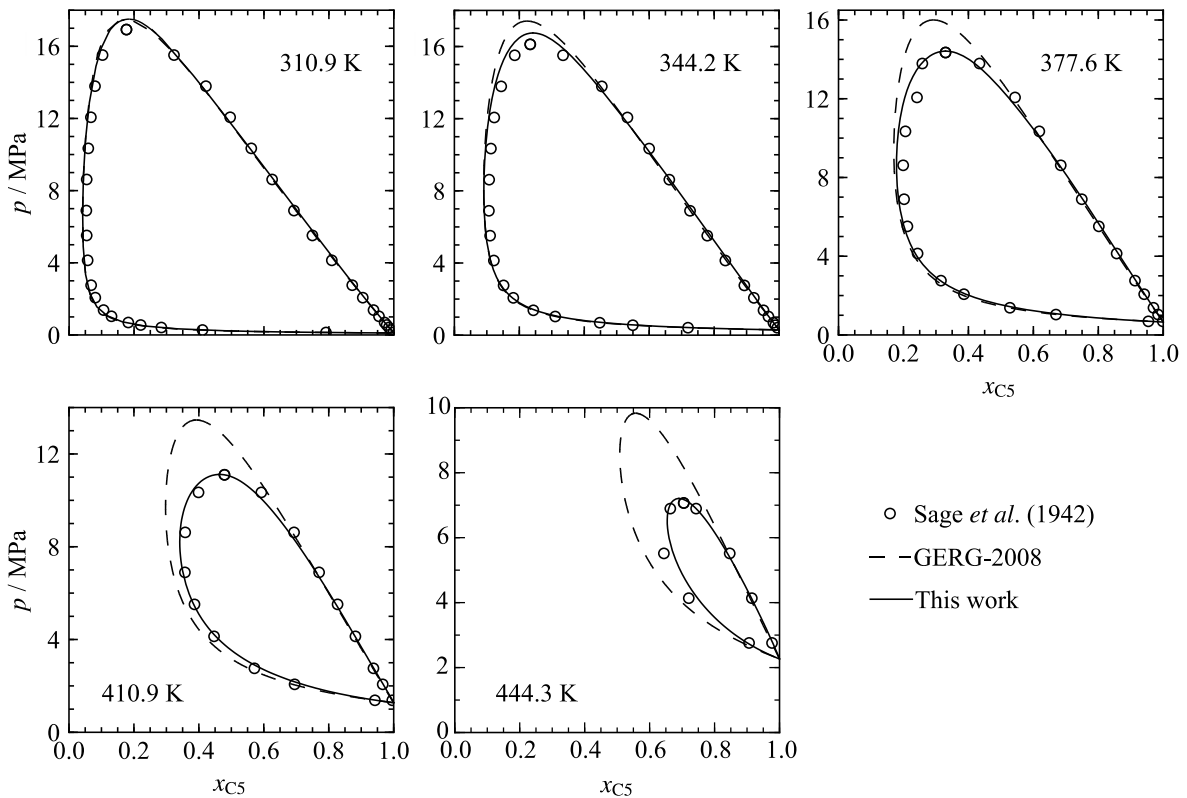


Fig. 17. p, x_{C5} -diagrams representing the vapor-liquid equilibrium data of Sage *et al.*⁵⁴ for the binary system C_1C_5 .

The p,x -diagrams shown in Fig. 17 exemplify this more accurate representation by EOS-LNG. The GERG-2008 model¹¹ overpredicts the VLE pressures. Deviations from the available experimental data of up to 3 MPa are eliminated by the new equation of state. Similar to the preceding binary systems, the dew-point line passes through an infinite slope at higher pressures, which gives rise to large pressure deviations. However, Fig. 17 illustrates that the trend of the new equation of state matches the experimental data very well. In the low-temperature region, significant improvement was achieved with respect to the representation of the bubble-point pressure data of Kahre¹⁰³ ($\text{AARD}_{p_{\text{liq}},\text{EOS-LNG}} = 1.8\%$ vs. $\text{AARD}_{p_{\text{liq}},\text{GERG-2008}} = 15\%$) and Chu *et al.*¹⁰² ($\text{AARD}_{p_{\text{liq}},\text{EOS-LNG}} = 5.8\%$ vs. $\text{AARD}_{p_{\text{liq}},\text{GERG-2008}} = 18\%$). The bubble-point pressure data of Prodany and Williams¹⁰⁵ at $T = 377.6$ K are reproduced with an AARD of 2.3% by EOS-LNG, which is a slight improvement over GERG-2008.¹¹ Both models represent the bubble-point pressure data of Kandil *et al.*¹⁰⁴ well within their experimental uncertainty.

The experimental critical-point data measured by Sage *et al.*⁵⁴ for this binary system present an opportunity to evaluate the predictions of the critical and cricondenbar lines by both models. In the upper panels of Fig. 18, p,T -phase diagrams calculated with EOS-LNG and GERG-2008¹¹ are presented. The methane + n -pentane system can be classified as a type I mixture with a pressure maximum on the critical line according to Deiters and Kraska.¹⁰⁶ In their work, a comprehensive analysis of the critical line behavior is presented. However, no such analysis of the behavior of the cricondenbar line is available in the literature. Therefore, the new binary-specific function, which agrees well with the experimental critical points of Sage *et al.*,⁵⁴ is evaluated for that purpose. At first glance, the trend of the cricondenbar line appears to be suspicious due to the inflection point at approximately 8 MPa. Starting from the critical point of the more volatile component (methane), it follows the trend of the critical line with lower pressures until both lines meet at the same maximum. After passing this maximum and while approaching the less volatile component (n -pentane), the cricondenbar line exhibits a steep negative slope resulting in a distinct change in curvature, which is more pronounced than for GERG-2008.¹¹ Since there are no measurements available in the literature, it is not possible here to conclude if this behavior is correct. On the bottom of Fig. 18, three p,x -diagrams, which also contain the VLE data of Sage *et al.*,⁵⁴ are shown. The corresponding critical point of each isotherm is depicted as a solid, inverted triangle in the p,T -diagrams in the same color. The experimental critical points of Sage *et al.*⁵⁴ are reproduced better by EOS-LNG than by GERG-2008.¹¹ For each of the critical points, the overall composition of the binary mixture was determined and the corresponding phase envelope is plotted as a dashed-dotted line. The calculated cricondenbar of each phase envelope is marked as a solid diamond and the calculated cricondentherm is illustrated with solid stars. For type I mixtures, the critical pressure is generally located between the pressure of the cricondenbar and the pressure of the cricondentherm. This is correctly modeled with both the EOS-LNG and the GERG-2008,¹¹

except for the critical point at 444.3 K. The phase envelope of the GERG-2008¹¹ would have to be shifted to lower pressures ($p_c(T_c = 444.3 \text{ K}) \approx 7.5 \text{ MPa}$ instead of $\approx 10 \text{ MPa}$) to match this criterion as it was done for the EOS-LNG (*cf.* Fig. 18, top left and bottom right panels). Since both models show the same behavior and the new model matches the VLE data of Sage *et al.*,⁵⁴ it appears that at least the qualitative behavior is correct for the cricondenbar line. Furthermore, additional investigations on methane + (propane to hexane) yielded the same results. However, additional measurements would be needed to provide a more reliable statement on the quantitative performance of the model.

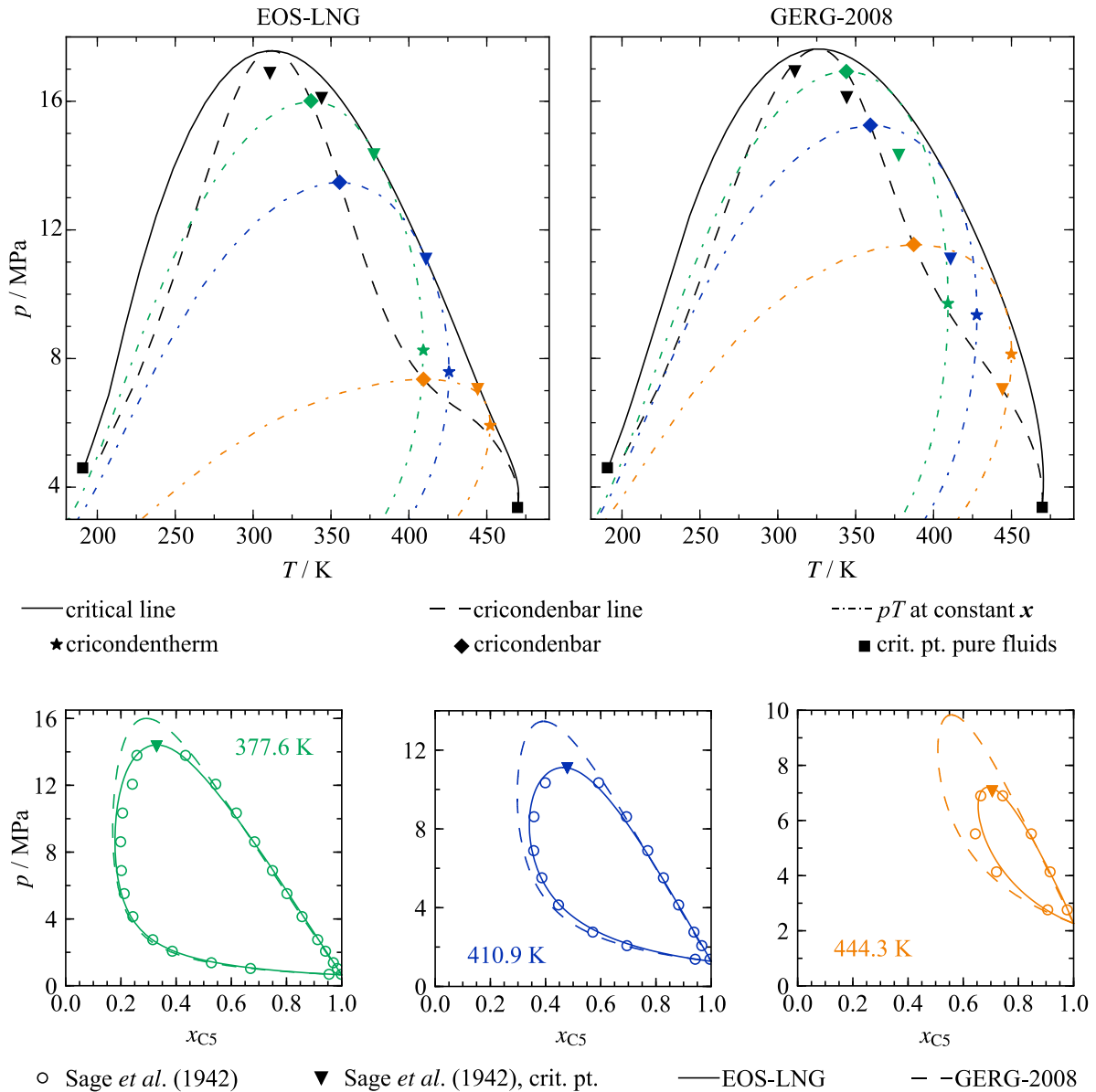


Fig. 18. p, T -diagrams for the binary system C_1C_5 including the critical and cricondenbar lines calculated with EOS-LNG and GERG-2008¹¹ (top). The critical points of Sage *et al.*,⁵⁴ which are shown in the bottom panel, are included as solid, inverted triangles. The phase envelopes for the compositions of the critical points are shown as dashed-dotted lines in the same colors as in the bottom panel (green, blue, and orange), along with the cricondenbars and the cricondentherms.

3.5 Methane + isopentane (C₁C_{5i})

For the methane-isopentane binary system, only the two datasets of Amick *et al.*¹⁰⁷ (homogeneous density and VLE) and Prodany and Williams¹⁰⁵ (VLE) are available as shown in Tables 9 and 10.

Table 9. Average absolute relative deviations (AARD / %) calculated with the new equation of state for the binary system C₁C_{5i}. For a better overview, the dataset is separated into different composition ranges and the overall AARD is given.

Author	N	$T_{\min} - T_{\max}$ / K	$p_{\min} - p_{\max}$ / MPa	$x_{C1,\min} - x_{C1,\max}$	AARD (EOS-LNG)	AARD (GERG-2008)
Amick <i>et al.</i> (1952) ¹⁰⁷	20	460 - 478	3.4 - 5.52	0.15	2.8	5.9
	37	449 - 478	2.0 - 9.05	0.3339	2.2	2.4
	78	377 - 478	1.3 - 10.4	0.4976	1.0	1.0
	92	360 - 478	1.3 - 10.4	0.6175	0.76	0.36
	102	344 - 478	1.3 - 8.96	0.7949	0.46	0.21
Overall	329	344 - 478	1.3 - 10.4	0.15 - 0.795	1.0	1.0

For the determination of the homogeneous density data, Amick *et al.*¹⁰⁷ used an apparatus similar to the one modified by Kay.¹⁰⁸ A known mass of a mixture was loaded into a glass bulb sealed at one end. At the other end, mercury was used to change the volume and pressure of the sample, which was kept at constant temperature. The samples that were used (99.7 mole percent pure methane and 99.7 mole percent pure isopentane) were further refined, but no information is available on the final sample purity. The measured densities were then graphically smoothed. On average, the smoothed data can be reproduced within 1.5% by EOS-LNG as illustrated in Fig. 19. The deviations are similar to those calculated for GERG-2008.¹¹

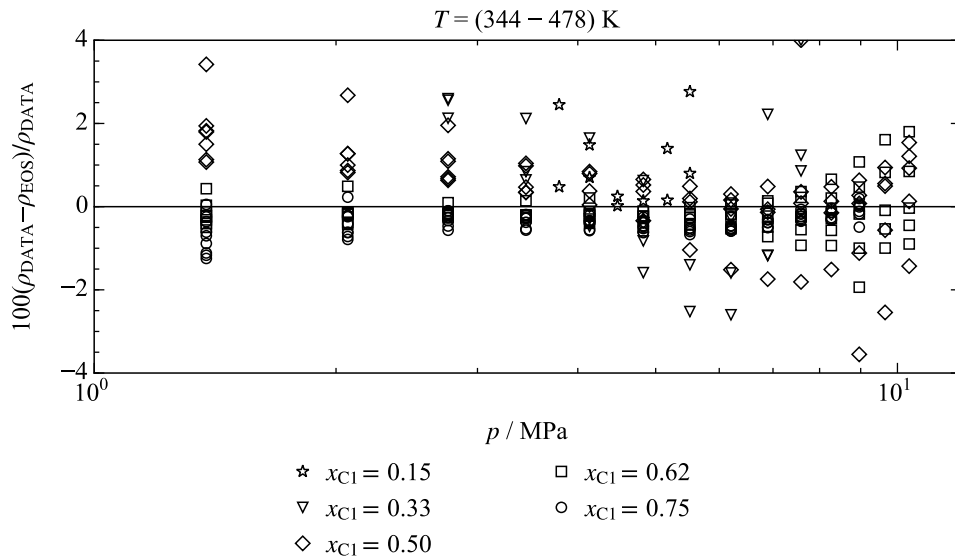


Fig. 19. Percentage deviations of homogeneous density data of Amick *et al.*¹⁰⁷ from EOS-LNG for the binary system C₁C_{5i}.

Table 10. Average absolute relative deviations of bubble-point pressure data ($AARD_{pliq} / \%$) and average absolute deviations in terms of percentage mole fraction of methane in the saturated vapor phase ($AAD_{yC1} / \%$) for the binary system C_1C_{5i} . N denotes the total number of points in each publication except for pure-fluid measurements, whereas N_x and N_y indicate the number of bubble-point (index “x”) and dew-point (index “y”) pressure data. If N_x or N_y differ from N , state points were deleted from the numerical analysis for both models due to flash calculation errors or because they are outliers, which would distort the AARD or AAD.

Author	N	N_x	N_y	$T_{min} - T_{max} / K$	$p_{min} - p_{max} / MPa$	$AARD_{pliq}$ (EOS-LNG)	AAD_{yC1} (EOS-LNG)	$AARD_{pliq}$ (GERG-2008)	AAD_{yC1} (GERG-2008)
Amick <i>et al.</i> (1952) ¹⁰⁷	29	29	29	344 - 450	2.7 - 6.9	14.5	5.8	11.0	3.2
Prodany & Williams (1971) ¹⁰⁵	21	20	21	344 - 411	3.4 - 15.2	1.8	2.6	6.5	3.1

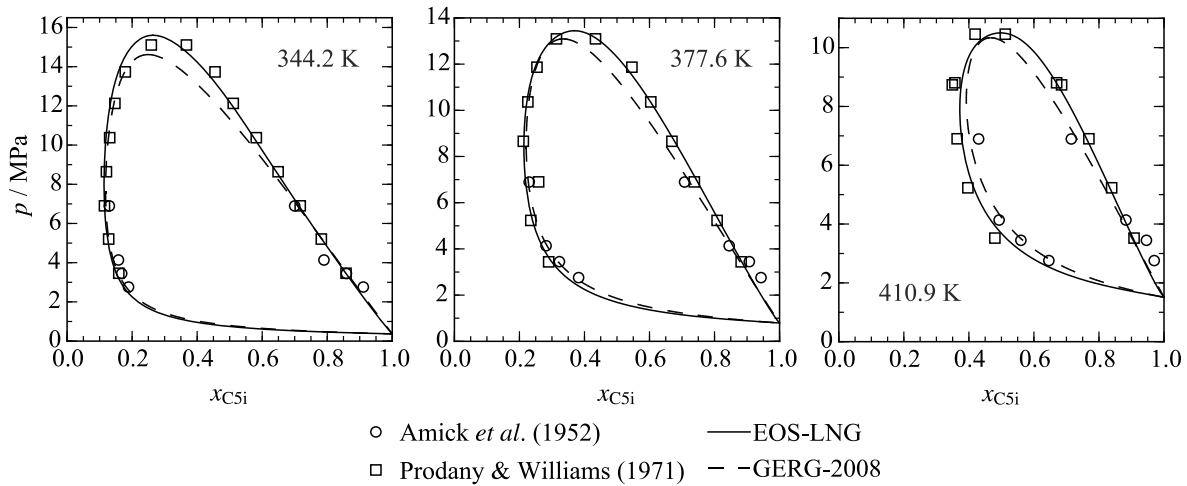


Fig. 20. p, x -diagrams representing the vapor-liquid equilibrium data for the binary system C_1C_{5i} .

Improvements were made in the representation of the vapor-liquid equilibrium measurements. The bubble-point pressure data of Prodany and Williams,¹⁰⁵ whose measurements for the system C_1C_5 are in good agreement with the data of Sage *et al.*,⁵⁴ are represented with an $AARD = 1.8\%$ ($AARD_{x,GERG-2008} = 6.5\%$). The three isotherms investigated by Prodany and Williams¹⁰⁵ are depicted in Fig. 20. For all temperatures, the bubble-point lines calculated with EOS-LNG match the data better than those calculated with GERG-2008.¹¹ The dew-point lines were already accurately represented by GERG-2008¹¹ except those at the highest isotherm. At this temperature, the deviations with respect to the data of Prodany and Williams¹⁰⁵ were also reduced by EOS-LNG as compared with those from GERG-2008.¹¹ These plots show that the vapor-liquid equilibrium data of Amick *et al.*¹⁰⁷ deviate significantly from the data of Prodany and Williams¹⁰⁵ and, thus, they were not utilized in the development of the new equation of state.

Since the only two available datasets for this binary are rather old and inconsistent, it would be valuable to further investigate this system experimentally. Accurate density data are needed over the entire fluid surface. In particular, the possible existence of liquid-liquid equilibrium for C_1C_{5i} should be investigated given that it does exist for methane + n -heptane (C_1C_7),¹⁰⁹ and it was also suspected during the experiments on C_1C_5 by Lentner *et al.*^{20,72} and Kandil *et al.*¹⁰⁴

Figure 21 shows the locus of the liquid-liquid equilibrium on a T,x -plane as can be traced with modern phase-equilibrium algorithms such as proposed by Bell and Deiters.¹¹⁰ This binary system can be categorized as a type II mixture according to Deiters and Kraska,¹⁰⁶ therefore, the LLE temperature at a given overall composition is nearly independent of the pressure. The GERG-2008¹¹ equation of state illustrates that even for typical methane-rich LNG mixtures (more than 90 mole percent methane), liquid-liquid equilibrium might occur in the low-temperature region. New measurements must take this into account because such a phase equilibrium can perturb the stability of the signal observed with densimeters, as might have happened during the LNG measurements for the binary systems C_1C_{4i} and C_1C_5 .^{20,72} The EOS-LNG also predicts the occurrence of liquid-liquid phase equilibrium, but the shape and equilibrium temperature are completely different from those predicted with GERG-2008.¹¹ Simpler equations such as the Peng-Robinson^{1,2} ($k_{ij} = 0$) or Soave-Redlich-Kwong^{3,4} ($k_{ij} = 0.007$)¹¹¹ equations do not indicate liquid-liquid phase equilibrium. Since there is no conclusive experimental information available, it is not possible to state here which model is correct.

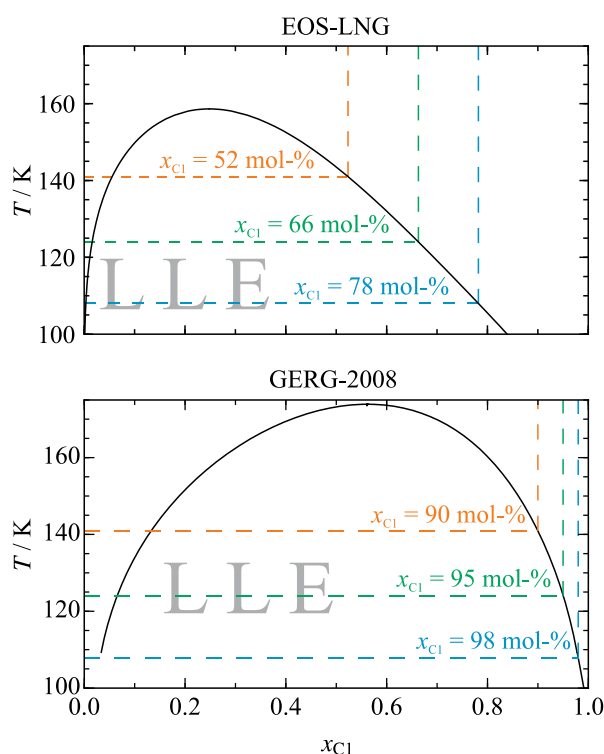


Fig. 21. T,x -diagram at $p = 0.1$ MPa for the binary system C_1C_{5i} with the liquid-liquid equilibrium phase boundary calculated with EOS-LNG (top) and GERG-2008¹¹ (bottom). The indicated equilibrium temperatures are the same in both plots and the compositions shown are those for the lower-density (methane rich) liquid phase at the temperatures 141 K (orange), 124 K (green), and 108 K (blue).

4. Representation of Multicomponent Mixtures

After fitting the parameters of EOS-LNG to represent the available experimental data for the four binary mixtures described previously, while ensuring no degradation in performance relative to GERG-2008,¹¹ the new model's performance was tested with the use of data for multicomponent mixtures for LNG-like systems available in the literature. The functions for the binary mixtures other than the four binaries discussed in Sec. 3 are taken from the GERG-2008 model.¹¹ In Fig. 22, deviations of density data for three multicomponent mixtures^{19,49} from values calculated with GERG-2008¹¹ and EOS-LNG are presented. Each of these synthetic mixtures, which are representative of three commercial LNGs from three different regions, mainly consists of methane and ethane with small quantities of propane, *n*-butane, and nitrogen, *cf.* Table 11.

Table 11. Molar compositions of the three multicomponent mixtures labeled as Libya, Norway, and Oman.^{19,49}

	Libya	Norway	Oman
x_{C1} / mol-%	81.5626	91.798	87.8854
x_{C2} / mol-%	13.3744	5.698	7.2738
x_{C3} / mol-%	3.6793	1.303	2.9257
x_{C4} / mol-%	0.6884	0.396	1.5647
x_{N2} / mol-%	0.6953	0.805	0.3504

In comparison to the GERG-2008 model,¹¹ only the new departure function developed for C_1C_4 has changed for the representation of these three multicomponent mixtures. This emphasizes the importance of this binary system for the representation of multicomponent LNG mixtures. For Libya and Norway, the amount of *n*-butane in the system is rather low. Therefore, deviations from GERG-2008¹¹ are less than 0.06%, which is almost within the range of the accuracy targeted in this work. The new departure function for C_1C_4 reduces these deviations to approximately 0.03% in the case of LNG Libya and even to 0.02% for LNG Norway. In contrast, the *n*-butane content of the LNG Oman mixture is more than twice that of the other two mixtures. The deviations with respect to the GERG-2008¹¹ are 0.13%, which is much larger than the experimental uncertainty of the data. The new binary mixture model for C_1C_4 used in EOS-LNG reduces these deviations to less than 0.04%, achieving the target accuracy of 0.05% with respect to the representation of the multicomponent data. These results show that the binary system C_1C_4 has a significant influence on the representation of multicomponent density data. Since there were no experimental data available in the homogeneous LNG region for the development of the new binary-specific function, additional measurements of density in the LNG region for this system would help to improve the representation of multicomponent mixtures in future work.

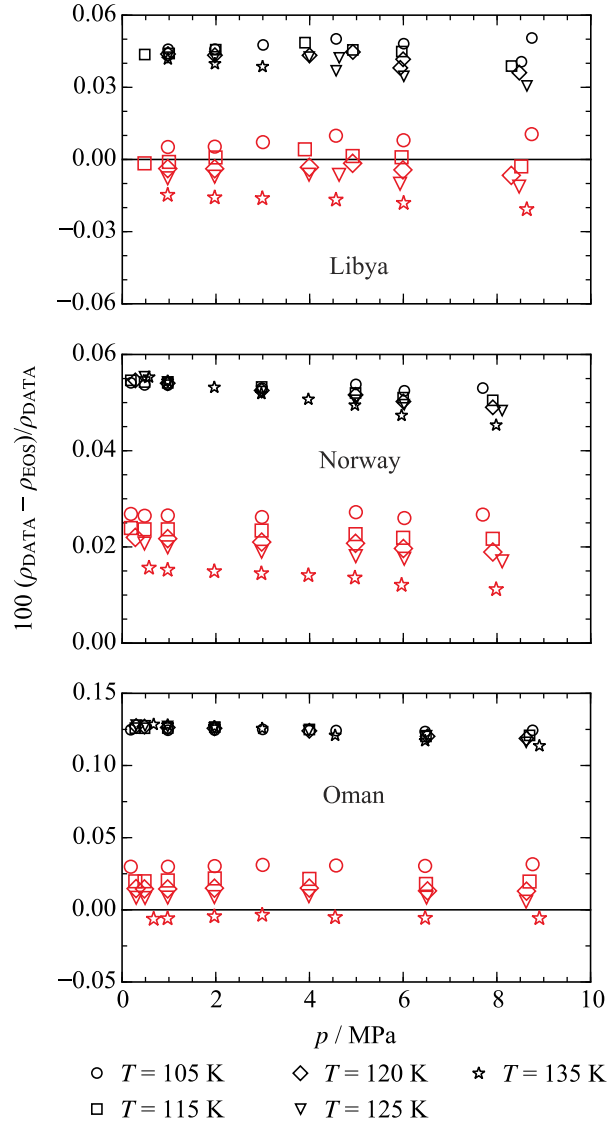


Fig. 22. Percentage deviations of the density data of three multicomponent LNG mixtures^{19,49} from the EOS-LNG (red symbols) and the GERG-2008¹¹ (black symbols).

Table 12. Molar compositions of the three multicomponent mixtures LNG 2, LNG 5, and LNG 7.¹⁹

	LNG 2	LNG 5	LNG 7
$x_{\text{C1}} / \text{mol-}\%$	84.6362	87.9716	97.8898
$x_{\text{C2}} / \text{mol-}\%$	12.8000	7.24000	0.99900
$x_{\text{C3}} / \text{mol-}\%$	1.49900	2.90000	0.49710
$x_{\text{C4}} / \text{mol-}\%$	0.20930	0.69170	0.20920
$x_{\text{C4i}} / \text{mol-}\%$	0.21990	0.64280	0.17710
$x_{\text{C5}} / \text{mol-}\%$	0.03010	0.10040	0.01617
$x_{\text{C5i}} / \text{mol-}\%$	0.02010	0.11000	0.01833
$x_{\text{N2}} / \text{mol-}\%$	0.58540	0.34350	0.19330

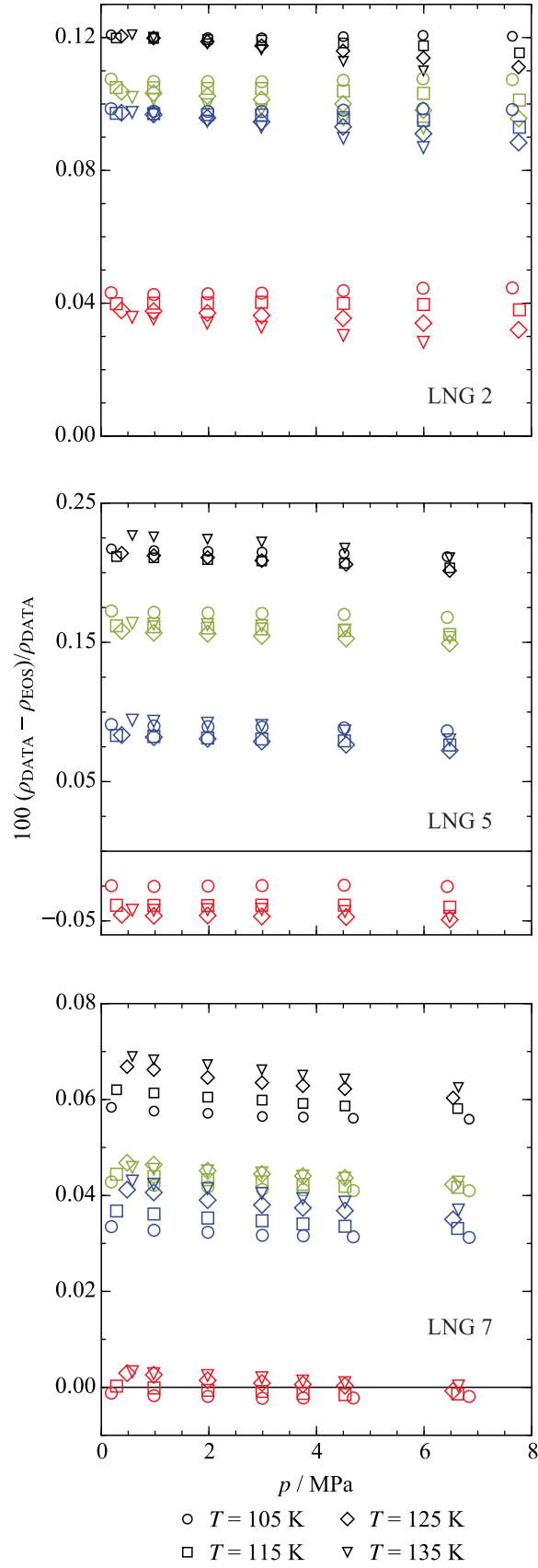


Fig. 23. Percentage deviations of the density data of three multicomponent LNG mixtures¹⁹ from the EOS-LNG (red symbols) and the GERG-2008¹¹ (black symbols). The green symbols show deviations calculated with the GERG-2008¹¹ and the adjusted binary function only for C₁C₄, whereas the blue symbols depict the deviations calculated with the GERG-2008¹¹ and the adjusted binary function only for C₁C_{5i}.

Lentner *et al.*¹⁹ also published measurements for multicomponent LNG mixtures including *n*-butane, isobutane, *n*-pentane, and isopentane as shown in Table 12. Figure 23 shows that deviations of these density data from predictions calculated with GERG-2008¹¹ (black symbols) are within 0.22%, whereas the EOS-LNG (red symbols) is able to represent all of the mixture data within 0.05%. The green symbols in Fig. 23 show only the contribution of the new departure function for C₁C₄ to the improved performance of EOS-LNG. For these three multicomponent LNGs, the C₁C₄ departure function is responsible for 10% to 35% of the change in the deviations between the GERG-2008¹¹ and EOS-LNG models. Figure 23 also shows the contribution in the improvement (blue symbols) due to the new version of the C₁C_{5i} departure function, which accounts for 20% to 65% of the change for these multicomponent mixtures. The biggest impact of the C₁C_{5i} departure function occurs for LNG 5, which has more than five times the isopentane content of the other two LNG mixtures. Tests on the other two binary functions showed that their influence is not as significant as those of C₁C₄ and C₁C_{5i}.

Clearly, the improvement of the two departure functions for C₁C₄ and C₁C_{5i} has a significant impact on the ability of EOS-LNG to represent the data of Lentner *et al.*¹⁹ within 0.05%. However, as shown in Sec. 3.5, the departure function for C₁C_{5i} and the binary parameters in the new EOS-LNG are tuned to a very limited database with no binary data available at conditions directly relevant to LNG. Therefore, new measurements of homogeneous densities and vapor-liquid (maybe also liquid-liquid) equilibrium data are needed to further improve the C₁C_{5i} binary function.

During the analysis of the multicomponent data of Lentner *et al.*¹⁹ and Richter *et al.*,⁴⁹ an interesting observation was made. In Fig. 24, deviations of the experimental data^{19,49} are illustrated for the original GERG-2008 equation of state¹¹ (black symbols) and for a modified version of the GERG-2008¹¹ that used the Lorentz-Berthelot combining rule (no departure function) for the system methane + nitrogen (C₁N₂) instead of the original adjusted interaction parameters combined with the departure function. Although the binary-specific function for C₁N₂ of the GERG-2008¹¹ is one of the most accurate mixture models in the literature, density deviations of the investigated multicomponent LNG mixtures (see Tables 12 and 13) are lower when applying the Lorentz-Berthelot combining rule. In the case of the LNG Norway and LNG Libya mixtures (the mixtures with higher nitrogen contents), the deviations decreased from 0.05% to 0.02%. This effect is related to the parameters of the reducing functions in Eqs. (8) and (9). Because the amount of nitrogen is rather low in the multicomponent systems investigated here, the correct modeling of the transition from the binary mixture to the pure fluids ($x_{C1} \rightarrow 0$ or 1), in particular at the methane pure-fluid limit, is very important. The influence of the departure function vanishes in this region. Therefore, the departure function is not needed here and the mixture behavior seems to be mainly related to the reducing parameters. During the development of binary mixture functions, it is common practice to simultaneously adjust the reducing parameters and the departure function. This can result in models where the

interaction parameters can be set to anything if the departure function is developed to account for any change resulting from the interaction parameters. This can result in models where the interaction parameters are not optimal if the departure function is developed to account for deficiencies of the interaction parameters. Therefore, it is most likely that for C_1N_2 the reducing parameters were fitted so that they joined in a way with the departure function to meet the uncertainties in the data over the entire composition range but do not necessarily behave correctly in the pure-fluid limits in multicomponent systems. When fitting departure functions, it might be favorable to first adjust the reducing parameters to experimental data where $x_{C1} \rightarrow 0$ or 1, and then adjust the departure function to experimental data with concentrations between those limits. Conversely, measurements at LNG conditions for the binary system C_1N_2 with very high methane contents ($x_{C1} = 0.97$ and 0.99)⁷² are accurately reproduced within 0.02% (0.25% with the Lorentz Berthelot combining rule), which leads to the assumption that the choice of the reducing parameters is less important for the binary systems but crucial for the interaction of binary functions in a multicomponent system.

Several tests not only on C_1N_2 but also on the four binary systems adjusted for the EOS-LNG showed that β_v and γ_v are the most sensitive parameters when modeling densities. However, this has to be investigated in more detail in future work.

Since there is no conclusive answer to the correct choice of reducing parameters, the binary-specific function for C_1N_2 of the GERG-2008 model,¹¹ which is the most accurate model available for that system, should still be applied for the calculation of natural gas properties.

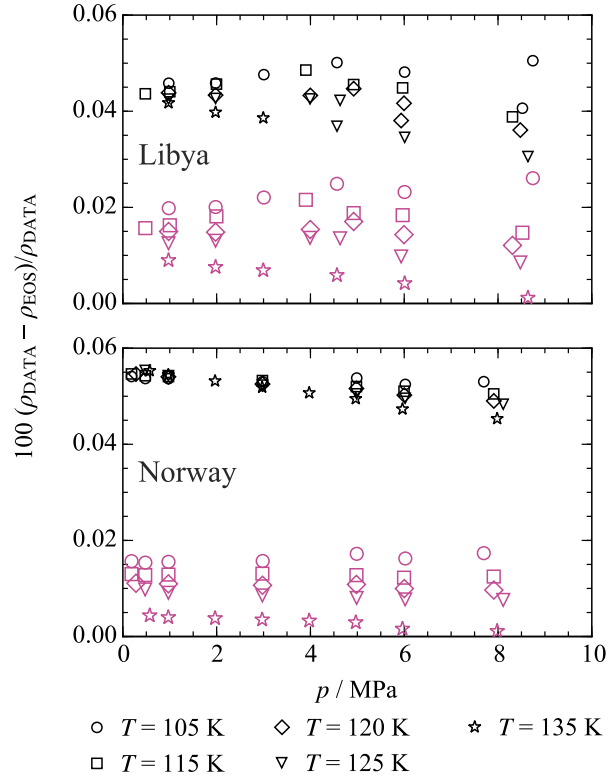


Fig. 24. Percentage deviations of the experimental density data of two multicomponent LNG mixtures^{19,49} from the GERG-2008¹¹ (black symbols) and the GERG-2008 model¹¹ with the Lorentz-Berthelot combining rule for the binary system methane + nitrogen (magenta symbols).

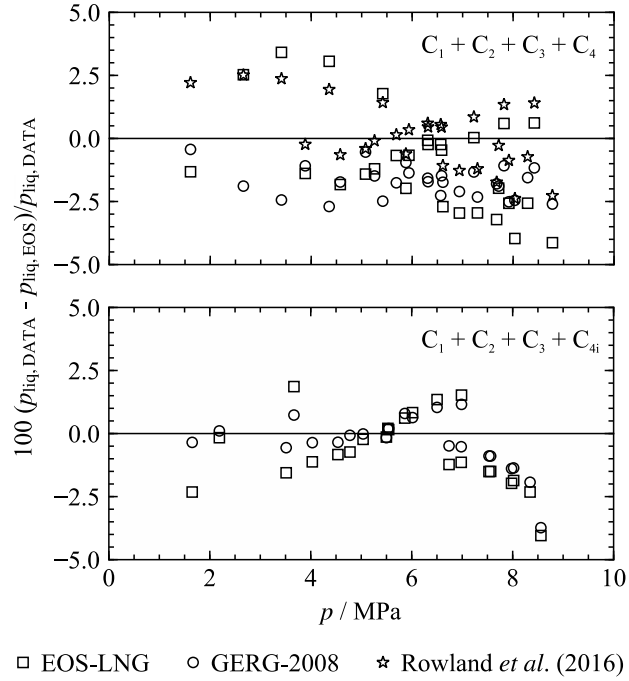


Fig. 25. Percentage deviations of the experimental vapor-liquid equilibrium data of Hughes *et al.*¹¹² from the EOS-LNG (C_1C_4 and C_1C_{4i}), the GERG-2008¹¹ (C_1C_4 and C_1C_{4i}), and the modification of Rowland *et al.*⁷³ (C_1C_4). Temperatures range from 200 K to 275 K.

Comparison with the multi-component VLE data reported by Hughes *et al.*¹¹² for mixtures containing *n*-butane and isobutane are shown in Fig. 25. The representation of these data is similar for the EOS-LNG, GERG-2008,¹¹ and the modification of Rowland *et al.*⁷³

Significant improvements are observed for the representation of the heat capacity data (multicomponent mixture of methane, ethane, propane, *n*-butane, and nitrogen) measured by Syed *et al.*⁷¹ While the GERG-2008 model¹¹ exhibits deviations of up to 14.6%, the EOS-LNG and the modification of Rowland *et al.*⁷³ deviate by not more than 6.5%, *cf.* Fig. 26.

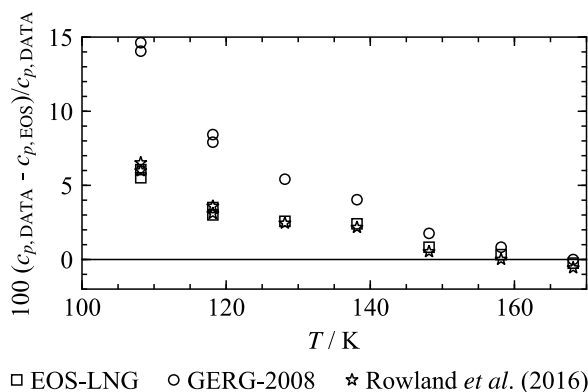


Fig. 26. Percentage deviations of the experimental isobaric heat capacity data of Syed *et al.*⁷¹ from the EOS-LNG, the GERG-2008,¹¹ and the modification of Rowland *et al.*⁷³ at pressures of 1 MPa and 5 MPa.

Although the main focus was given to the accurate representation of the subcooled liquid state, the gaseous and supercritical regions, which are important for the calculation of natural gas properties at pipeline conditions, were monitored to ensure that properties predicted in this region with the EOS-LNG are of comparable quality to predictions made with the GERG-2008.¹¹ In contrast to the liquid state, there is a significant amount of data available in this region, which were carefully evaluated and analyzed in the GERG Technical Monograph No. 15.²³ Based on these datasets, comparisons between the EOS-LNG and GERG-2008¹¹ were carried out. The results are presented in Tables A1 and A2 in Appendix A. Due to the number of data, graphical evaluation of the results is not presented here. Since the mole fractions of the four components investigated in this work are generally rather small in the systems listed in Tables A1 and A2, no significant differences between the representation of the data by the two equations of state are observed. Only the datasets of Jaeschke and Schley¹¹³ and of Watson and Millington¹¹⁴ (RNG1 to RNG7 in the table) contain a significant amount of butanes or pentanes and can, therefore, be used as a baseline for comparisons with the EOS-LNG. In general, these data are now reproduced more accurately than with the GERG-2008.¹¹ One remarkable result, which is in line with the analysis of the corresponding binary mixtures, is the improved representation of the saturated liquid density data of Hiza and Haynes¹¹⁵ (M7 to M10 in the table) and Haynes¹¹⁶ (M1 to M17 in the table). For example, the deviations of samples containing more than 4 mol% *n*-butane (M8 - Hiza and Haynes,¹¹⁵ M1 and M2 - Haynes¹¹⁶) are reduced by a factor of approximately five.

5. Conclusion

In this paper, a new fundamental equation of state in terms of the Helmholtz energy is presented for accurately representing properties of multicomponent natural gas mixtures in the liquid state region (EOS-LNG). The general mathematical form and most of the binary functions are adopted from GERG-2008,¹¹ which is the reference model for natural gases in the literature. Based on new experimental data and new fitting techniques, binary-specific functions for methane + *n*-butane, methane + isobutane, methane + *n*-pentane, and methane + isopentane were developed. In comparison to GERG-2008,¹¹ different density data were chosen for the fitting procedure and new data in the liquefied natural gas region were applied. This results in a significantly better representation of the homogeneous density data in the LNG region and for vapor-liquid equilibrium states. The representation of caloric properties (*e.g.*, heat capacities and excess enthalpies) was also improved.

By combining the four new binary-specific functions developed in this work with the remaining functions of GERG-2008,¹¹ deviations with respect to density data of six exemplary multicomponent mixtures could be reduced from 0.22% calculated with GERG-2008¹¹ to 0.05% with EOS-LNG. For further improvements, new experimental data (*e.g.*, density, speed of sound, and vapor-liquid equilibrium) are required, in particular for the systems methane + *n*-butane and methane + isopentane. The representation of multicomponent vapor-liquid equilibrium data with the EOS-LNG is similar to GERG-2008,¹¹ whereas deviations from heat capacity data are reduced by a factor of approximately 2.5.

Although the main focus was given to the temperature, pressure, and composition range of liquefied natural gases, the representation of all other binary mixture data that were available for the four adjusted systems is better or at least similar to GERG-2008.¹¹ Therefore, the new model is not only valid in the liquefied-natural-gas region but also in any other fluid state and is available in common software packages such as TREND,¹¹⁷ REFPROP,¹¹⁸ and CoolProp.¹¹⁹ Test values for computer implementation are given in Appendix B.

Acknowledgments

We gratefully acknowledge helpful discussions with Ian H. Bell and Jadran Vrabec throughout the development of the models. Furthermore, we thank Sven Pohl for his assistance during data evaluation and Robin Fingerhut for providing the figures of the molecular models in the graphical abstract.

Funding: This work was part of the Joint Research Project “Metrological support for LNG custody transfer and transport fuel applications” (JRP: ENG60 LNGII) and was carried out as part of the European Metrology Research Program (EMRP), which was jointly funded under the researcher grant contract no. ENG60-REG3 by the EMRP participating countries within the European Association of National Metrology Institutes (EURAMET). The authors thank the German Academic Exchange Service (DAAD) for funding the international collaboration between the groups at Ruhr-Universität Bochum and The University of Western Australia. Eric F. May is grateful for the support of the Ruhr-University Research School PLUS, funded by Germany’s Excellence Initiative [DFG GSC 98/3]. EFM also acknowledges the support of the Australian Research Council Industrial Transformation Training Centre for LNG Futures (IC150100019).

6. References

- ¹ D.-Y. Peng and D. B. Robinson, *Ind. Eng. Chem. Fundam.* **15**, 59 (1976).
- ² D. B. Robinson and D.-Y. Peng, *The Characterization of the Heptanes and Heavier Fractions for the GPA Peng-Robinson Programs* (Research report: Gas Processors Association, 1978).
- ³ O. Redlich and J. N. S. Kwong, *Chem. Rev.* **44**, 233 (1949).
- ⁴ G. Soave, *Chem. Eng. Sci.* **27**, 1197 (1972).
- ⁵ B. I. Lee and M. G. Kesler, *AIChE J.* **21**, 510 (1975).
- ⁶ U. Plöcker, H. Knapp, and J. M. Prausnitz, *Ind. Eng. Chem. Proc. Des. Dev.* **17**, 324 (1978).
- ⁷ R. Klimeck, R. Span, R. Kleinrahm, and W. Wagner, *Fundamental Equation for Calorific Properties. Collecting of Data and Test of Existing Equations*. (Final report to GERG WG 1.3; Bochum, Germany, 1996).
- ⁸ F. Dauber and R. Span, *Appl. Energy* **97**, 822 (2012).
- ⁹ D. George, *Development of Accurate Methods for Predicting Hydrocarbon Dew Points* (Final report to United States Minerals Management Service; San Antonio, Texas, USA, 2007).
- ¹⁰ AGA Transmission Measurement Committee, *Thermodynamic Properties of Natural Gas and Related Gases: DETAIL and GROSS Equations of State* (AGA Report No. 8, Part I, 3rd ed.; Washington, D.C., 2017).
- ¹¹ O. Kunz and W. Wagner, *J. Chem. Eng. Data* **57**, 3032 (2012).
- ¹² AGA Transmission Measurement Committee, *Thermodynamic Properties of Natural Gas and Related Gases: GERG-2008 Equation of State* (AGA Report No. 8, Part II, 3rd ed.; Washington, D.C., 2017).
- ¹³ E. W. Lemmon, *Better Defining the Uncertainties for the AGA 8 Equation* (Catalog No. PR-381-12604-R01, 2013).
- ¹⁴ AGA Transmission Measurement Committee <https://pages.nist.gov/AGA8/>, *Computer Code in Fortran, C++, and Visual Basic along with a Spreadsheet for Quick Calculations of Properties for Both Models*.
- ¹⁵ G. H. Thomson, K. R. Brobst, and R. W. Hankinson, *AIChE J.* **28**, 671 (1982).
- ¹⁶ Groupe International des Importateurs de Gaz Naturel Liquéfié (GIIGNL), *LNG Custody Transfer Handbook*; Paris, 2017).
- ¹⁷ R. D. McCarty, *J. Chem. Thermodyn.* **14**, 837 (1982).

- ¹⁸ C. Tietz, M. Richter, R. Kleinrahm, and R. Span, *Fuel Process. Technol.* **165**, 19 (2017).
- ¹⁹ R. Lentner, M. Richter, R. Kleinrahm, and R. Span, *J. Chem. Thermodyn.* **112**, 68 (2017).
- ²⁰ R. Lentner, M. Richter, R. Kleinrahm, P. Eckmann, and R. Span, *J. Chem. Thermodyn.*, to be submitted (2019).
- ²¹ E. W. Lemmon, Dissertation, University of Idaho, 1996.
- ²² R. Klimeck, Dissertation, Ruhr-Universität Bochum, 2000.
- ²³ O. Kunz, R. Klimeck, W. Wagner, and M. Jaeschke, *The GERG-2004 Wide-Range Equation of State for Natural Gases and Other Mixtures* (GERG Technical Monograph No. 15; Düsseldorf, Germany, 2007).
- ²⁴ I. H. Bell and E. W. Lemmon, *J. Chem. Eng. Data* **61**, 3752 (2016).
- ²⁵ E. W. Lemmon and M. O. McLinden, *Method for Estimating Mixture Equation of State Parameters in Conference on Thermophysical Properties of New Refrigerants*, edited by International Institute of Refrigeration, Commission B1, 2001, pp. 23–30.
- ²⁶ E. W. Lemmon and R. Tillner-Roth, *Fluid Phase Equilib.* **165**, 1 (1999).
- ²⁷ R. Span, *Multiparameter Equations of State: An Accurate Source of Thermodynamic Property Data* (Springer, Berlin, 2000).
- ²⁸ E. W. Lemmon and R. T. Jacobsen, *Int. J. Thermophys.* **20**, 825 (1999).
- ²⁹ L. Haar, J. S. Gallagher, and G. S. Kell, *Proc. 8th Symp. Thermophys. Prop.* **8**, 298 (1982).
- ³⁰ U. Setzmann and W. Wagner, *J. Phys. Chem. Ref. Data* **20**, 1061 (1991).
- ³¹ I. H. Bell, K. Gao, and E. W. Lemmon, *J. Phys. Chem. Ref. Data*, to be published (2019).
- ³² L. F. S. Souza, S. Herrig, R. Span, and J. P. M. Trusler, *Applied Energy*, to be published (2019).
- ³³ T. Neumann, M. Thol, I. H. Bell, E. W. Lemmon, and R. Span, *Fluid Phase Equilib.*, to be published (2019).
- ³⁴ G. M. Kontogeorgis, E. C. Voutsas, I. V. Yakoumis, and D. P. Tassios, *Ind. Eng. Chem. Res.* **35**, 4310 (1996).
- ³⁵ W. G. Chapman, K. E. Gubbins, G. Jackson, and M. Radosz, *Fluid Phase Equilib.* **52**, 31 (1989).
- ³⁶ W. G. Chapman, K. E. Gubbins, G. Jackson, and M. Radosz, *Ind. Eng. Chem. Res.* **29**, 1709 (1990).
- ³⁷ S. H. Huang and M. Radosz, *Ind. Eng. Chem. Res.* **29**, 2284 (1990).
- ³⁸ S. H. Huang and M. Radosz, *Ind. Eng. Chem. Res.* **30**, 1994 (1991).
- ³⁹ A. Jäger, I. H. Bell, and C. Breitkopf, *Fluid Phase Equilib.* **469**, 56 (2018).

- ⁴⁰ A. Jäger, E. Mickoleit, and C. Bretkopf, *Fluid Phase Equilib.* **476**, 147 (2018).
- ⁴¹ J. G. Gernert and R. Span, *J. Chem. Thermodyn.* **93**, 274 (2016).
- ⁴² R. Span, H.-J. Collmann, and W. Wagner, *Int. J. Thermophys.* **19**, 491 (1998).
- ⁴³ E. W. Lemmon and R. T. Jacobsen, *J. Phys. Chem. Ref. Data* **34**, 69 (2005).
- ⁴⁴ E. W. Lemmon, M. O. McLinden, and W. Wagner, *J. Chem. Eng. Data* **54**, 3141 (2009).
- ⁴⁵ M. Thol, G. Rutkai, A. Köster, R. Span, J. Vrabec, and R. Lustig, *J. Phys. Chem. Ref. Data* **45**, 023101 (2016).
- ⁴⁶ M. Thol and E. W. Lemmon, *Int. J. Thermophys.* **37**, 28 (2016).
- ⁴⁷ K. Gao, J. Wu, P. Zhang, and E. W. Lemmon, *J. Chem. Eng. Data* **61**, 2859 (2016).
- ⁴⁸ V. D. Arp, J. M. Persichetti, and G.-b. Chen, *J. Fluids Eng.* **106**, 193 (1984).
- ⁴⁹ M. Richter, R. Kleinrahm, R. Lentner, and R. Span, *J. Chem. Thermodyn.* **93**, 205 (2016).
- ⁵⁰ B. H. Sage and W. N. Lacey, *Trans. Am. Inst. Mining, Metall. Pet. Eng.* **136**, 136 (1940).
- ⁵¹ B. H. Sage, R. A. Budenholzer, and W. N. Lacey, *Ind. Eng. Chem.* **32**, 1262 (1940).
- ⁵² R. H. Olds, B. H. Sage, and W. N. Lacey, *Ind. Eng. Chem.* **34**, 1008 (1942).
- ⁵³ B. H. Sage, D. C. Webster, and W. N. Lacey, *Ind. Eng. Chem.* **28**, 1045 (1936).
- ⁵⁴ B. H. Sage, H. H. Reamer, R. H. Olds, and W. N. Lacey, *Ind. Eng. Chem.* **34**, 1108 (1942).
- ⁵⁵ H. H. Reamer, B. H. Sage, and W. N. Lacey, *J. Chem. Eng. Data* **5**, 44 (1960).
- ⁵⁶ B. H. Sage and W. N. Lacey, *Ind. Eng. Chem.* **32**, 992 (1940).
- ⁵⁷ B. H. Sage and W. N. Lacey, *Ind. Eng. Chem.* **31**, 1497 (1939).
- ⁵⁸ W. Blanke and R. Weiss, *Int. J. Thermophys.* **16**, 643 (1995).
- ⁵⁹ A. E. Hoover, Dissertation, Rice University, 1965.
- ⁶⁰ H. Hou, J. C. Holste, K. R. Hall, K. N. Marsh, and B. E. Gammon, *J. Chem. Eng. Data* **41**, 344 (1996).
- ⁶¹ M. Jaeschke, H.-M. Hinze, and A. E. Humphreys, *Supplement to the GERG Databank of High-Accuracy Compression Factor Measurements* (GERG Technical Monograph No. 7; Düsseldorf, Germany, 1996).
- ⁶² M. Jaeschke and A. E. Humphreys, *The GERG Databank of High Accuracy Compressibility Factor Measurements* (Fortschr.-Ber. Reihe 6: Energieerzeugung No. 251; Düsseldorf, Germany, 1991).
- ⁶³ O. Wöll and T. El Hawary, personal communication to Oliver Kunz (2003).
- ⁶⁴ A. Karimi, T. J. Hughes, M. Richter, and E. F. May, *J. Chem. Eng. Data* **61**, 2782 (2016).
- ⁶⁵ H. H. Reamer, B. H. Sage, and W. N. Lacey, *Ind. Eng. Chem.* **42**, 534 (1950).

- ⁶⁶ E. T. S. Huang, G. W. Swift, and F. Kurata, *AIChE J.* **13**, 846 (1967).
- ⁶⁷ K. Arai and R. Kobayashi, *Adv. Cryog. Eng.* **25**, 640 (1980).
- ⁶⁸ W. Wagner, R. Kleinrahm, H. W. Lösch, J.T.R. Watson, V. Majer, A.A.H. Pádua, L. A. Woolf, J. C. Holste, A. M. de Figueiredo Palavra, K. Fujii, and J. W. Stansfeld, *Density in Experimental Thermodynamics*, edited by A. R. H. Goodwin, K. N. Marsh, W. A. Wakeham (Elsevier, Amsterdam, Boston), 2003, Vol. 6, pp. 125–235.
- ⁶⁹ B. H. Sage, W. N. Lacey, and J. G. Schaafsma, *Ind. Eng. Chem.* **26**, 214 (1934).
- ⁷⁰ E. F. May, J. Y. Guo, J. H. Oakley, T. J. Hughes, B. F. Graham, K. N. Marsh, and S. H. Huang, *J. Chem. Eng. Data* **60**, 3606 (2015).
- ⁷¹ T. H. Syed, T. J. Hughes, K. N. Marsh, and E. F. May, *J. Chem. Eng. Data* **59**, 968 (2014).
- ⁷² R. Lentner, Dissertation, Ruhr-Universität Bochum, 2018.
- ⁷³ D. Rowland, T. J. Hughes, and E. F. May, *J. Chem. Thermodyn.* **97**, 206 (2016).
- ⁷⁴ J. A. Beattie, W. H. Stockmayer, and H. G. Ingersoll, *J. Chem. Phys.* **9**, 871 (1941).
- ⁷⁵ R. T. Ellington, personal communication to Jaeschke et al. reported in Ref. 50 (1986).
- ⁷⁶ A. Fenghour, J. P. M. Trusler, and W.A. Wakeham, *Fluid Phase Equilib.* **163**, 139 (1999).
- ⁷⁷ W. M. Haynes, *J. Chem. Thermodyn.* **15**, 903 (1983).
- ⁷⁸ M. J. Hiza, W. M. Haynes, and W. R. Parrish, *J. Chem. Thermodyn.* **9**, 873 (1977).
- ⁷⁹ J. Kestin and J. Yata, *J. Chem. Phys.* **49**, 4780 (1968).
- ⁸⁰ W. P. Pan, M. H. Mady, and R. C. Miller, *AIChE J.* **21**, 283 (1975).
- ⁸¹ H. H. Reamer, K. J. Korpl, B. H. Sage, and W. N. Lacey, *Ind. Eng. Chem.* **39**, 206 (1947).
- ⁸² J. R. Tomlinson, *NGPA Techn. Publ.*, 1 (1985).
- ⁸³ F. Plantier, A. Danesh, M. Sohrabi, J.-L. Daridon, F. Gozalpour, and A. C. Todd, *J. Chem. Eng. Data* **50**, 673 (2005).
- ⁸⁴ D. J. Hutchings, E. J. Lewis, and C. J. Wormald, *J. Chem. Thermodyn.* **10**, 559 (1978).
- ⁸⁵ R. H. Sage, B. L. Hicks, and W. N. Lacey, *Ind. Eng. Chem.* **32**, 1085 (1940).
- ⁸⁶ W. Wagner and R. Kleinrahm, *Metrologia* **41**, S24-S39 (2004).
- ⁸⁷ M. O. McLinden, *Chapter 2. Experimental Techniques 1: Direct Methods in Volume Properties*, edited by E. Wilhelm and T. Letcher (Royal Society of Chemistry, Cambridge), 2014, pp. 73–99.
- ⁸⁸ M. O. McLinden, *Meas. Sci. Technol.* **17**, 2597 (2006).
- ⁸⁹ R. J. J. Chen, P. S. Chapplelear, and R. Kobayashi, *J. Chem. Eng. Data* **19**, 53 (1974).
- ⁹⁰ D. G. Elliot, R. J. J. Chen, P. S. Chapplelear, and R. Kobayashi, *J. Chem. Eng. Data* **19**, 71 (1974).

- ⁹¹ L. C. Kahre, J. Chem. Eng. Data **19**, 67 (1974).
- ⁹² G. W. Nederbragt, Ind. Eng. Chem. **30**, 587 (1938).
- ⁹³ T. J. Rigas, D. F. Mason, and G. Thodos, Ind. Eng. Chem. **50**, 1297 (1958).
- ⁹⁴ L. R. Roberts, R. H. Wang, A. Azarnoosh, and J. J. McKetta, J. Chem. Eng. Data **7**, 484 (1962).
- ⁹⁵ R. H. Wang and J. J. McKetta, J. Chem. Eng. Data **9**, 30 (1964).
- ⁹⁶ H. C. Wiese, J. Jacobs, and B. H. Sage, J. Chem. Eng. Data **15**, 82 (1970).
- ⁹⁷ J. B. Rodosevich and R. C. Miller, AIChE J. **19**, 729 (1973).
- ⁹⁸ S. D. Barsuk, V. G. Skripka, and O. A. Benyaminovich, Gazov. Promst. **15**, 38 (1970).
- ⁹⁹ M. E. Kandil, E. F. May, B. F. Graham, K. N. Marsh, M. A. Trebble, R. D. Trengove, and S. H. Huang, J. Chem. Eng. Data **55**, 2725 (2010).
- ¹⁰⁰ X. Zhang, L. Gao, Z. Liu, J. He, J. Zhang, and B. Han, J. Supercrit. Fluids **23**, 233 (2002).
- ¹⁰¹ R. J. J. Chen, P. S. Chapplelear, and R. Kobayashi, J. Chem. Eng. Data **19**, 58 (1974).
- ¹⁰² T.-C. Chu, R. J. J. Chen, P. S. Chapplelear, and R. Kobayashi, J. Chem. Eng. Data **21**, 41 (1976).
- ¹⁰³ L. C. Kahre, J. Chem. Eng. Data **20**, 363 (1975).
- ¹⁰⁴ M. E. Kandil, M. J. Thoma, T. Syed, J. Y. Guo, B. F. Graham, K. N. Marsh, S. H. Huang, and E. F. May, J. Chem. Eng. Data **56**, 4301 (2011).
- ¹⁰⁵ N. W. Prodany and B. Williams, J. Chem. Eng. Data **16**, 1 (1971).
- ¹⁰⁶ U. K. Deiters and T. Kraska, *High-Pressure Fluid Phase Equilibria: Phenomenology and Computation* (Elsevier, Amsterdam, Netherlands, 2012).
- ¹⁰⁷ E. H. Amick, W. B. Johnson, and B. F. Dodge, Chem. Eng. Prog. Symp. Ser. **48**, 65 (1952).
- ¹⁰⁸ W. B. Kay, Ind. Eng. Chem. **28**, 1014 (1936).
- ¹⁰⁹ H. L. Chang, L. J. Hurt, and R. Kobayashi, AIChE J. **12**, 1212 (1966).
- ¹¹⁰ I. H. Bell and U. K. Deiters, AIChE J. **64**, 2745 (2018).
- ¹¹¹ G. Soave, S. Gamba, and L. A. Pellegrini, Fluid Phase Equilib. **299**, 285 (2010).
- ¹¹² T. J. Hughes, J. Y. Guo, C. J. Baker, D. Rowland, B. F. Graham, K. N. Marsh, S. H. Huang, and E. F. May, J. Chem. Thermodyn. **113**, 81 (2017).
- ¹¹³ M. Jaeschke and P. Schley, *Compression Factor Measurements on Rich Natural Gases* (Final Report to Gas Research Institute, Contract No. 5095-260-3557; Chicago, 1998).
- ¹¹⁴ J. T. R. Watson and B. Millington, *The Density of Rich Natural Gas Mixtures. A Joint Industrial Project*. (NEL, Project No. DRG001 Report No. 110/97, 1998).

- ¹¹⁵ M. J. Hiza and W. M. Haynes, *J. Chem. Thermodyn.* **12**, 1 (1980).
- ¹¹⁶ W. M. Haynes, *J. Chem. Thermodyn.* **14**, 603 (1982).
- ¹¹⁷ R. Span, R. Beckmüller, T. Eckermann, S. Herrig, S. Hielscher, A. Jäger, T. Neumann, S. Pohl, B. Semrau, and M. Thol, *TREND. Thermodynamic Reference and Engineering Data 4.0* (Lehrstuhl für Thermodynamik, Ruhr-Universität Bochum, Bochum, Germany, 2019).
- ¹¹⁸ E. W. Lemmon, I. H. Bell, M. L. Huber, and M. O. McLinden, *NIST Standard Reference Database 23: Reference Fluid Thermodynamic and Transport Properties-REFPROP, Version 10.0* (National Institute of Standards and Technology, Gaithersburg, USA, 2018).
- ¹¹⁹ I. H. Bell, J. Wronski, S. Quoilin, and V. Lemort, *Ind. Eng. Chem. Res.* **53**, 2498 (2014).

APPENDIX - A

In Tables A1 and A2, numerical results for the AARD are presented for the multicomponent data in the pipeline region, which were used for the validation of the GERG-2008.¹¹ Comparisons are made with both the GERG-2008¹¹ and EOS-LNG models.

Table A1. Average absolute relative deviations (AARD / %) of the experimental multicomponent data in the homogeneous state that were available for the development of the GERG-2008¹¹ and which contain butanes or pentanes. The AARD was calculated with EOS-LNG and GERG-2008¹¹ for comparison. The listed mole fractions indicate only the fractions of the components studied in this work (methane: x_{C1} , *n*-butane: x_{C4} , isobutane: x_{C4i} , *n*-pentane: x_{C5} , isopentane: x_{C5i}). For information on the complete composition and the designation of the mixtures, see the GERG Technical Monograph No. 15.²³

Author/Designation	N	$T_{\min} - T_{\max}$	$\frac{p_{\min} - p_{\max}}{p_{\max}}$	x_{C1}	x_{C4}	x_{C4i}	x_{C5}	x_{C5i}	AARD (EOS-LNG)	AARD (GERG-2008)
		K	MPa	mol-%	mol-%	mol-%	mol-%	mol-%	%	%
			Density	$\rho\rho T x$						
D16(BUR)	49	273 - 314	0.4 - 31	84.7831	1.2374	-	-	-	0.034	0.053
D17(OPT)	168	273 - 314	0.4 - 29	84.7831	1.2374	-	-	-	0.027	0.026
D19(OPT)	284	275 - 350	0.3 - 29	88.602	0.3	0.194	0.005	0.021	0.067	0.061
D20(OPT)	153	290 - 350	0.4 - 28	88.652	0.3	0.194	0.005	0.021	0.044	0.041
D22(OPT), GU1	279	275 - 350	0.4 - 28	81.441	0.104	0.1	-	-	0.012	0.013
D23(GDM), GU1	13	299.99	0.5 - 5.0	81.441	0.104	0.1	-	-	0.007	0.007
D24(BUR), GU1	78	250 - 325	0.1 - 11	81.299	0.1	0.101	-	-	0.012	0.013
D25(PYC), GU1	91	225 - 350	3.4 - 60	81.299	0.1	0.101	-	-	0.074	0.075
D26(BUR), GU1	65	226 - 350	1.9 - 35	81.299	0.1	0.101	-	-	0.021	0.023
D27(BUR), GU1	155	273 - 324	0.1 - 34	81.441	0.104	0.1	-	-	0.045	0.046
D28(IBU), GU1	64	242 - 274	0.6 - 4.1	81.441	0.104	0.1	-	-	0.019	0.019
D29(OPT), GU2	269	275 - 350	0.4 - 28	81.212	0.152	0.151	-	-	0.019	0.019
D30(GDM), GU2	13	299.99	0.5 - 8.0	81.212	0.152	0.151	-	-	0.012	0.011
D31(BUR), GU2	85	250 - 325	0.1 - 12	81.202	0.155	0.148	-	-	0.018	0.018
D32(PYC), GU2	89	225 - 350	3.3 - 60	81.202	0.155	0.148	-	-	0.089	0.089
D33(BUR), GU2	70	225 - 350	1.7 - 34	81.202	0.155	0.148	-	-	0.025	0.025
D34(BUR), GU2	119	273 - 324	0.3 - 36	81.212	0.152	0.151	-	-	0.037	0.037
D35(BUR), RG2	18	299.99	0.2 - 23	85.9063	0.3506	0.3486	0.048	0.0509	0.012	0.011
D36(OPT), RG2	275	275 - 350	0.4 - 28	85.9063	0.3506	0.3486	0.048	0.0509	0.034	0.023
D37(GDM), RG2	9	299.99	0.5 - 6.1	85.9063	0.3506	0.3486	0.048	0.0509	0.013	0.009
D38(BUR), RG2	61	274 - 325	0.1 - 11	85.898	0.347	0.351	0.053	0.051	0.019	0.017
D39(PYC), RG2	87	225 - 350	2.7 - 60	85.898	0.347	0.351	0.053	0.051	0.265	0.216
D40(BUR), RG2	65	225 - 350	1.9 - 33	85.898	0.347	0.351	0.053	0.051	0.088	0.065
D41(OPT), NIST1	280	275 - 350	0.4 - 28	96.5222	0.1007	0.0977	0.0324	0.0473	0.016	0.026
D42(GDM), NIST1	15	299.99	0.5 - 8.1	96.5222	0.1007	0.0977	0.0324	0.0473	0.005	0.006
D43(BUR), NIST1	77	250 - 325	0.1 - 11	96.579	0.102	0.099	0.032	0.047	0.012	0.013
D44(PYC), NIST1	82	225 - 350	3.4 - 57	96.579	0.102	0.099	0.032	0.047	0.135	0.107
D45(BUR), NIST1	66	225 - 350	1.9 - 35	96.579	0.102	0.099	0.032	0.047	0.022	0.022
D46(IBU), NIST1	64	242 - 274	0.5 - 4.2	96.5222	0.1007	0.0977	0.0324	0.0473	0.035	0.036
D47(OPT), NIST2	278	274 - 350	0.4 - 28	90.6724	0.1563	0.1037	0.0443	0.0321	0.014	0.015
D48(GDM), NIST2	11	299.99	0.5 - 3.8	90.6724	0.1563	0.1037	0.0443	0.0321	0.008	0.007

Author/Designation	N	$T_{\min} - T_{\max}$	$p_{\min} - p_{\max}$	x_{C1}	x_{C4}	x_{C4i}	x_{C5}	x_{C5i}	AARD (EOS- LNG)	AARD (GERG- 2008)
		K	MPa	mol-%	mol-%	mol-%	mol-%	mol-%	%	%
D49(BUR), NIST2	78	250 - 325	0.1 - 9.6	90.643	0.156	0.1	0.045	0.03	0.020	0.021
D50(PYC), NIST2	66	225 - 350	3.3 - 59	90.643	0.156	0.1	0.045	0.03	0.167	0.146
D51(BUR), NIST2	67	225 - 350	1.9 - 35	90.643	0.156	0.1	0.045	0.03	0.031	0.028
D52(BUR), NIST2	135	273 - 324	0.1 - 39	90.6724	0.1563	0.1037	0.0443	0.0321	0.081	0.077
D53(IBU), NIST2	40	242 - 274	1.1 - 4.2	90.6724	0.1563	0.1037	0.0443	0.0321	0.049	0.051
D54(BUR)	33	298 - 324	0.1 - 16	88.269	0.989	-	-	-	0.026	0.023
D55(BUR)	35	290 - 324	0.1 - 17	80.079	1.75	-	-	-	0.108	0.088
D58(DEH)	13	299.84	1.1 - 5.3	96.5	0.1	0.1	0.1	0.1	0.013	0.012
D59(DEH)	32	288 - 300	1.1 - 6.3	90.66	0.14	0.1	0.02	0.03	0.026	0.028
N1 (DEH)	18	273 - 294	1.9 - 7.0	84.3346	0.6463	0.3381	0.0903	0.0922	0.066	0.058
N2 (DEH)	18	273 - 294	2.0 - 7.0	95.534	0.0892	0.0619	0.0276	0.0311	0.024	0.024
N3 (DEH)	18	273 - 294	2.0 - 7.0	85.1473	0.3232	0.1841	0.0801	0.0648	0.055	0.05
N4 (DEH)	18	273 - 294	2.0 - 7.0	85.4814	0.5668	0.3027	0.0986	0.0905	0.039	0.045
N5 (DEH)	24	273 - 304	2.0 - 7.0	80.1984	0.3454	0.2003	0.0618	0.0539	0.035	0.033
N6 (DEH)	24	273 - 304	2.0 - 7.0	82.1692	0.3586	0.2081	0.0621	0.0554	0.018	0.019
N7 (DEH)	24	273 - 304	2.0 - 7.0	73.6405	0.1482	0.0974	0.0451	0.0293	0.039	0.04
N8 (DEH)	23	273 - 304	2.0 - 7.0	78.7092	0.1631	0.1073	0.0464	0.0315	0.045	0.045
N9 (BUR)	67	273 - 294	0.1 - 8.6	95.5192	0.0896	0.0622	0.0283	0.0308	0.030	0.030
N10 (BUR)	68	273 - 294	0.1 - 8.7	84.4678	0.6304	0.3364	0.1005	0.0994	0.016	0.021
N11 (BUR)	69	273 - 294	0.1 - 8.6	85.1666	0.3216	0.1845	0.0804	0.0647	0.016	0.019
N12 (BUR)	69	273 - 294	0.1 - 8.7	85.4915	0.5683	0.3026	0.0995	0.0907	0.024	0.032
N13 (OPT)	74	273 - 294	0.1 - 7.8	95.5192	0.0896	0.0622	0.0283	0.0308	0.021	0.022
N14 (OPT)	74	273 - 294	0.1 - 7.8	84.4678	0.6304	0.3364	0.1005	0.0994	0.059	0.072
N15 (OPT)	73	273 - 294	0.1 - 7.8	85.1666	0.3216	0.1845	0.0804	0.0647	0.053	0.052
N16 (OPT)	74	273 - 294	0.1 - 7.8	85.4915	0.5683	0.3026	0.0995	0.0907	0.047	0.053
N17 (OPT)	76	273 - 294	0.09 - 7.8	95.548	0.0885	0.0612	0.0269	0.0308	0.044	0.045
N18 (OPT)	68	273 - 294	0.1 - 8.0	84.4333	0.6311	0.3386	0.1015	0.0996	0.039	0.041
N19 (OPT)	73	273 - 294	0.1 - 7.7	85.1784	0.3226	0.1845	0.0804	0.0647	0.042	0.04
N20 (OPT)	77	273 - 294	0.1 - 7.9	85.462	0.5688	0.3024	0.099	0.0912	0.037	0.042
N21 (BUR)	12	273 - 292	0.3 - 7.1	92.2794	0.2498	0.1863	0.0792	0.0691	0.127	0.124
N22 (BUR)	15	273 - 295	0.2 - 11	93.0357	0.1468	0.1348	0.0729	0.0426	0.080	0.078
N23 (DEH)	18	278 - 299	2.0 - 7.0	81.2125	0.067	0.0622	0.0321	0.0233	0.068	0.068
N24 (DEH)	12	278 - 299	2.0 - 7.0	90.8251	0.061	0.0519	0.0027	0.0204	0.061	0.06
N25 (DEH)	10	288 - 294	1.0 - 4.5	83.952	0.627	0.362	0.105	0.104	0.053	0.058
N26 (DEH)	5	283 - 284	1.0 - 4.5	83.8681	0.619	0.357	0.1029	0.102	0.103	0.101
N27 (DEH)	5	278 - 279	1.0 - 4.5	83.75	0.613	0.355	0.0996	0.1	0.122	0.119
N28 (DEH)	64	279 - 300	3.7 - 6.5	88.965	0.33	0.183	0.105	0.058	0.024	0.026
N29 (DEH)	53	280 - 300	3.7 - 6.5	75.72	0.085	0.058	0.047	0.026	0.023	0.022
N30 (DEH)	52	281 - 300	3.7 - 6.5	87.981	0.17	0.144	0.103	0.052	0.021	0.02
N31 (DEH)	53	279 - 300	3.7 - 6.5	92.722	0.056	0.047	0.086	0.021	0.038	0.037
N32 (DEH)	54	280 - 300	3.7 - 6.5	88.802	0.169	0.13	0.072	0.05	0.026	0.024
N33 (DEH)	64	279 - 300	3.7 - 6.5	68.714	0.117	0.085	0.056	0.043	0.03	0.034

Author/Designation	N	$T_{\min} - T_{\max}$	$p_{\min} - p_{\max}$	x_{C1}	x_{C4}	x_{C4i}	x_{C5}	x_{C5i}	AARD (EOS- LNG)	AARD (GERG- 2008)
		K	MPa	mol-%	mol-%	mol-%	mol-%	mol-%	%	%
N34 (DEH)	52	280 - 300	3.7 - 6.5	80.876	0.145	0.094	0.073	0.048	0.038	0.04
N35 (DEH)	55	280 - 300	3.7 - 6.5	65.686	0.115	0.086	0.057	0.045	0.075	0.08
N36 (DEH)	55	280 - 300	3.7 - 6.5	86.646	0.245	0.158	0.09	0.054	0.021	0.02
N37 (DEH)	64	279 - 301	3.7 - 6.5	84.005	0.703	0.376	0.147	0.132	0.049	0.044
N38 (DEH)	65	279 - 300	3.7 - 6.6	79.318	0.077	0.051	0.026	0.028	0.069	0.069
N39 (DEH)	55	280 - 300	3.7 - 6.5	87.97	0.306	0.186	0.102	0.062	0.04	0.047
N40 (DEH)	54	281 - 301	3.7 - 6.5	79.615	0.137	0.096	0.065	0.039	0.060	0.060
N41 (DEH)	16	279 - 294	3.7 - 5.5	81.592	0.08	0.07	0.044	0.027	0.077	0.077
N42 (DEH)	44	279 - 300	3.7 - 6.5	81.478	0.079	0.069	0.04	0.028	0.085	0.085
N43 (DEH)	66	279 - 301	3.7 - 6.6	86.445	0.179	0.152	0.089	0.054	0.042	0.045
N44 (DEH)	66	279 - 300	3.7 - 6.5	92.321	0.113	0.072	0.066	0.034	0.036	0.036
N45 (DEH)	66	279 - 301	3.7 - 6.5	90.44	0.158	0.126	0.068	0.051	0.046	0.048
N46 (DEH)	65	279 - 301	3.7 - 6.5	75.105	0.014	0.005	0.003	0.009	0.093	0.093
N47 (DEH)	65	279 - 301	3.7 - 6.5	70.317	0.014	0.005	0.003	0.008	0.083	0.083
N48 (DEH)	65	279 - 301	3.7 - 6.6	45.236	0.011	0.002	0.001	0.007	0.055	0.055
N49 (DEH)	33	279 - 287	3.8 - 6.4	88.048	0.3	0.313	0.076	0.076	0.103	0.113
N50 (DEH)	22	279 - 284	3.7 - 6.5	81.55	0.072	0.072	0.0325	0.0325	0.071	0.070
N51 (BUR)	31	273 - 314	0.5 - 31	85.4915	0.5683	0.3026	0.0995	0.0907	0.059	0.084
N52 (OPT)	54	313.14	0.3 - 28	85.4915	0.5683	0.3026	0.0995	0.0907	0.031	0.065
N53 (BUR)	47	273 - 354	0.4 - 31	85.462	0.5688	0.3024	0.099	0.0912	0.025	0.042
N54 (OPT)	113	273 - 354	0.3 - 29	85.462	0.5688	0.3024	0.099	0.0912	0.024	0.036
N55 (BUR)	98	275 - 330	0.3 - 28	85.3453	0.5864	0.3111	0.0902	0.0843	0.022	0.035
N56 (OPT)	175	270 - 330	0.3 - 30	85.3453	0.5864	0.3111	0.0902	0.0843	0.023	0.054
N57 (BUR)	30	290.00	0.4 - 26	94.6077	0.0422	0.034	0.0122	0.0122	0.009	0.01
N58 (OPT)	116	280 - 290	0.5 - 29	94.6077	0.0422	0.034	0.0122	0.0122	0.025	0.028
N59 (BUR)	34	309.99	0.3 - 27	82.5198	0.1543	0.0996	0.0413	0.0333	0.024	0.025
N60 (OPT)	342	270 - 350	0.4 - 30	82.5198	0.1543	0.0996	0.0413	0.0333	0.039	0.044
N61 (BUR)	36	309 - 310	0.2 - 27	98.2722	0.0334	0.0258	0.0068	0.0089	0.009	0.010
N62 (OPT)	311	270 - 350	0.3 - 29	98.2722	0.0334	0.0258	0.0068	0.0089	0.023	0.025
N63 (BUR)	62	309 - 330	0.2 - 27	89.4525	0.0043	0.0021	0.0011	0.0009	0.012	0.012
N64 (OPT)	336	270 - 350	0.5 - 29	89.4525	0.0043	0.0021	0.0011	0.0009	0.020	0.020
N65 (BUR)	60	275 - 280	0.3 - 27	85.4541	0.5947	0.3004	0.0848	0.0825	0.028	0.041
N66 (OPT)	333	270 - 350	0.3 - 29	85.4541	0.5947	0.3004	0.0848	0.0825	0.042	0.035
N67 (BUR)	68	273 -304	0.4 - 9.2	82.1692	0.3586	0.2081	0.0621	0.0554	0.043	0.046
N68 (BUR)	69	273 -304	0.4 - 9.2	80.1984	0.3454	0.2003	0.0618	0.0539	0.018	0.019
N69 (BUR)	70	273 -304	0.3 - 9.3	73.6405	0.1482	0.0974	0.0451	0.0293	0.010	0.010
N70 (BUR)	68	273 -304	0.4 - 9.2	82.2373	0.353	0.2067	0.062	0.0554	0.042	0.045
N71 (BUR)	70	273 -304	0.3 - 9.3	80.1543	0.3468	0.2012	0.0613	0.0538	0.016	0.016
N72 (BUR)	67	273 -304	0.4 - 9.3	73.5015	0.1483	0.0975	0.0447	0.0293	0.013	0.012
N73 (BUR)	31	309.99	0.4 - 27	73.5015	0.1483	0.0975	0.0447	0.0293	0.012	0.011
N74 (OPT)	341	270 - 350	0.4 - 29	73.5015	0.1483	0.0975	0.0447	0.0293	0.023	0.023
N75 (OPT)	331	270 - 350	0.4 - 29	85.9284	0.4604	0.2381	0.063	0.0588	0.057	0.040

Author/Designation	N	$T_{\min} - T_{\max}$	$p_{\min} - p_{\max}$	x_{C1}	x_{C4}	x_{C4i}	x_{C5}	x_{C5i}	AARD (EOS- LNG)	AARD (GERG- 2008)
		K	MPa	mol-%	mol-%	mol-%	mol-%	mol-%	%	%
N76 (DMA)	135	273 - 324	0.1 - 8.1	84.3769	0.6574	0.3448	0.0896	0.0916	0.01	0.022
N77 (DEH)	11	296 - 297	3.7 - 7.2	81.314	0.075	0.065	0.038	0.024	0.059	0.059
N78 (DEH)	19	295 - 298	3.6 - 6.6	88.221	0.377	0.212	0.034	0.059	0.074	0.082
N79 (DEH)	21	296 - 297	3.0 - 5.5	83.4177	0.6588	0.3777	0.0895	0.0933	0.045	0.036
N80 (DEH)	44	280 - 294	3.7 - 6.5	65.6961	0.1185	0.086	0.0571	0.0424	0.078	0.083
N81 (DEH)	42	280 - 294	3.8 - 6.5	80.8753	0.1457	0.0943	0.0733	0.0488	0.055	0.059
N82 (BUR)	57	309 - 330	0.5 - 27	84.4872	0.3287	0.1802	0.0555	0.0502	0.013	0.012
N83 (OPT)	353	270 - 350	0.3 - 29	84.4872	0.3287	0.1802	0.0555	0.0502	0.028	0.022
N84 (DEH)	37	283 - 314	1.0 - 8.1	57.693	0.072	0.073	0.018	0.024	0.057	0.059
N85 (DEH)	48	280 - 299	2.8 - 7.5	85.961	-	0.668	-	0.122	0.037	0.044
N86 (EXP)	10	303.11	1.0 - 16	82.71	-	0.12	-	0.01	0.080	0.079
N87 (DEH)	7	288.71	4.9 - 5.3	96.5016	-	0.1999	-	0.2	0.031	0.036
N88 (DEH)	40	283 - 314	1.0 - 6.0	95.022	-	0.19	-	0.092	0.049	0.047
N89 (DEH)	42	283 - 313	1.5 - 6.6	87.432	-	0.05	-	0.028	0.022	0.022
N90 (DEH)	35	283 - 314	1.5 - 5.6	93.62	-	0.21	-	0.095	0.045	0.043
N91 (DEH)	32	282 - 314	1.0 - 5.1	85.297	-	0.5	-	0.172	0.045	0.042
N92 (DEH)	26	283 - 313	1.0 - 4.0	95.616	-	0.014	-	0.006	0.025	0.025
N94 (DEH)	26	286 - 287	2.9 - 7.9	85.923	-	0.664	-	0.121	0.009	0.015
N95 (DEH)	44	280 - 299	2.9 - 7.2	85.903	-	0.669	-	0.122	0.037	0.040
N96 (DEH)	48	280 - 299	2.8 - 7.7	75.203	-	0.018	-	0.013	0.063	0.063
N97 (BUR)	33	309.99	0.3 - 26	64.8023	0.3716	0.1885	0.0541	0.0501	0.021	0.016
N98 (OPT)	306	270 - 350	0.4 - 29	64.8023	0.3716	0.1885	0.0541	0.0501	0.052	0.055
N99 (BUR)	15	290	0.6 - 27	59.0265	0.1229	0.0768	0.0346	0.0266	0.018	0.019
N100 (OPT)	285	270 - 350	0.3 - 28	59.0265	0.1229	0.0768	0.0346	0.0266	0.043	0.043
N101 (OPT)	338	270 - 350	0.4 - 29	47.2554	0.098	0.0612	0.0262	0.0203	0.019	0.019
N102 (BUR)	33	290	0.4 - 27	82.4733	0.5448	0.2775	0.0772	0.0752	0.019	0.023
N103 (OPT)	336	270 - 350	0.4 - 29	82.4733	0.5448	0.2775	0.0772	0.0752	0.046	0.055
N104 (OPT)	223	270 - 350	0.5 - 28	76.337	0.3974	0.2033	0.0486	0.0472	0.106	0.084
N105 (BUR)	33	329.99	0.3 - 27	65.847	0.171	0.107	0.0442	0.0318	0.055	0.059
N106 (OPT)	220	270 - 350	0.4 - 29	65.847	0.171	0.107	0.0442	0.0318	0.105	0.113
N107 (OPT)	460	265 - 350	0.5 - 30	79.3693	0.0179	0.0135	0.0104	0.0062	0.031	0.031
N108 (OPT)	187	270 - 350	0.5 - 20	79.95	0.2598	0.1345	0.0348	0.0324	0.020	0.024
N109 (OPT)	322	265 - 350	0.5 - 31	80.042	0.0564	0.0356	0.014	0.011	0.054	0.056
N110 (OPT)	360	270 - 350	0.5 - 31	27.9285	0.015	0.002	0.0073	0.0007	0.067	0.067
N111 (OPT)	90	270 - 350	0.4 - 4.9	70.7555	0.1034	0.132	0.0078	0.0083	0.042	0.043
N112 (OPT)	100	270 - 350	0.4 - 6.9	81.0253	3.0997	0.0866	0.0367	0.0289	0.049	0.047
N113 (OPT)	173	270 - 350	0.4 - 15	79.5699	0.1202	0.0849	0.0357	0.0293	0.015	0.015
N114 (OPT)	125	270 - 350	0.4 - 8.5	76.845	0.104	0.077	0.0333	0.0267	0.041	0.042
N115 (OPT)	342	270 - 350	0.5 - 29	81.5264	0.208	0.0001	0.072	0.0004	0.018	0.018
N116 (OPT)	345	270 - 350	0.5 - 29	28.8898	0.071	-	0.0271	0.0003	0.024	0.024
Capla <i>et al.</i> (2002), M1	28	253 - 324	0.9 - 16	98.352	0.031	0.021	0.011	0.008	0.023	0.023
Capla <i>et al.</i> (2002),	28	253 - 324	1.0 - 16	90.362	0.169	0.301	0.029	0.059	0.096	0.092

Author/Designation	N	$T_{\min} - T_{\max}$	$\frac{p_{\min}}{p_{\max}}$	x_{C1}	x_{C4}	x_{C4i}	x_{C5}	x_{C5i}	AARD (EOS- LNG)	AARD (GERG- 2008)
		K	MPa	mol-%	mol-%	mol-%	mol-%	mol-%	%	%
M2										
Capla <i>et al.</i> (2002), M3	28	253 - 324	1.0 - 16	92.436	0.046	0.041	0.014	0.015	0.020	0.020
Dushek <i>et al.</i> (1989)	135	273 - 324	0.1 - 8.1	84.382	0.6589	0.3466	0.091	0.0897	0.010	0.023
Guo <i>et al.</i> (1990a), M1	8	299.99	0.5 - 3.8	90.672	0.26	-	0.076	-	0.008	0.008
Guo <i>et al.</i> (1990a), M2	40	273 - 294	0.1 - 12	85.8933	0.4483	0.23	0.0531	0.0519	0.043	0.033
Guo <i>et al.</i> (1990a), M3	14	299.99	0.5 - 8.0	81.212	0.303	-	-	-	0.014	0.013
Guo <i>et al.</i> (1990a), M4	15	299.99	0.5 - 8.1	96.5222	0.1984	-	0.0797	-	0.005	0.005
Guo <i>et al.</i> (1990a), M5	57	273 - 294	0.1 - 13	82.1255	0.1434	0.0968	0.0354	0.0307	0.088	0.087
Guo <i>et al.</i> (1990b), M1	10	299.99	0.5 - 5.0	81.441	0.204	-	-	-	0.006	0.006
Guo <i>et al.</i> (1990b), M2	9	299.99	0.5 - 6.1	85.8988	0.7119	-	0.096	-	0.015	0.011
Guo <i>et al.</i> (1993), M1	8	283.15	2.7 - 9.6	81.7329	0.183	0.097	0.0286	0.026	0.026	0.026
Guo <i>et al.</i> (1993), M2	8	283.15	2.2 - 7.8	83.3243	0.146	0.087	0.0285	0.0245	0.081	0.085
Guo <i>et al.</i> (1993), M3	17	273 - 294	2.3 - 11	83.1821	0.1092	0.0804	0.0339	0.0282	0.088	0.089
Guo <i>et al.</i> (1993), M4	16	273 - 294	2.2 - 8.3	85.4917	0.4817	0.241	0.07	0.0638	0.024	0.010
Guo <i>et al.</i> (1993), M5	17	273 - 294	2.3 - 10	88.0605	0.2515	0.1568	0.0636	0.0479	0.192	0.199
Guo <i>et al.</i> (1993), M6	8	283.15	2.7 - 9.5	98.4435	0.0358	0.0281	0.0046	0.0064	0.016	0.017
Kleinrahm <i>et al.</i> (1996), M1	31	273 - 294	0.6 - 8.2	84.8802	0.4632	0.2342	0.0636	0.0604	0.038	0.052
Kleinrahm <i>et al.</i> (1996), M2	14	283.15	2.4 - 8.6	84.4668	0.1291	0.0868	0.0392	0.0338	0.093	0.094
Jaeschke and Schley (1998), RNG1	268	280 - 350	0.1 - 29	59.0129	5.9958	-	-	-	0.050	0.122
Jaeschke and Schley (1998), RNG2	327	280 - 350	0.1 - 30	58.9863	4.9978	-	-	-	0.065	0.082
Jaeschke and Schley (1998), RNG3	247	280 - 350	0.1 - 28	58.9976	3.2996	-	0.4947	-	0.106	0.038
Jaeschke and Schley (1998), RNG4	249	280 - 350	0.2 - 29	60.0063	4.2898	-	0.5058	-	0.139	0.047
Jaeschke and Schley (1998), RNG5	256	280 - 350	0.2 - 29	63.9757	3.3144	-	0.5074	-	0.072	0.063
Jaeschke and Schley (1998), RNG6	251	280 - 350	0.1 - 29	57.9945	3.2983	-	0.4994	-	0.070	0.181
Jaeschke and Schley (1998), RNG7	250	280 - 350	0.1 - 29	51.981	3.3027	-	0.4948	-	0.151	0.261
Watson and Millington (1998), RNG1	39	318 - 354	10 - 18	59.0013	5.9822	-	-	-	0.041	0.154
Watson and	48	314 - 354	7.8 - 18	59.0055	4.979	-	-	-	0.044	0.094

Author/Designation	N	$T_{\min} - T_{\max}$	$p_{\min} - p_{\max}$	x_{C1}	x_{C4}	x_{C4i}	x_{C5}	x_{C5i}	AARD (EOS- LNG)	AARD (GERG- 2008)
		K	MPa	mol-%	mol-%	mol-%	mol-%	mol-%	%	%
Millington (1998), RNG2 Watson and Millington (1998), RNG3 Watson and Millington (1998), RNG4 Watson and Millington (1998), RNG5 Watson and Millington (1998), RNG6 Watson and Millington (1998), RNG7-A Watson and Millington (1998), RNG7-B	48	313 - 349	7.8 - 18	58.9899	3.2963	-	0.4919	-	0.120	0.024
	48	313 - 349	7.8 - 18	59.9917	4.3049	-	0.5018	-	0.114	0.056
	48	313 - 349	7.8 - 18	64.0068	3.3037	-	0.5065	-	0.067	0.086
	48	313 - 349	7.8 - 18	57.9937	3.2971	-	0.5057	-	0.065	0.211
	48	313 - 349	7.8 - 18	51.9924	3.3033	-	0.5016	-	0.128	0.262
	48	313 - 349	7.9 - 19	52.0035	3.3053	-	0.498	-	0.177	0.326
Haynes (1982), M1	4	110 - 126	$p_{\text{sat,liq}}$	89.071	4.998	-	-	-	0.079	0.356
Haynes (1982), M2	5	115 - 136	$p_{\text{sat,liq}}$	85.133	4.3	-	-	-	0.042	0.305
Haynes (1982), M3	4	115 - 131	$p_{\text{sat,liq}}$	84.566	2.45	-	-	-	0.043	0.207
Haynes (1982), M4	5	115 - 136	$p_{\text{sat,liq}}$	86.04	-	4.57	-	-	0.043	0.024
Haynes (1982), M5	4	115 - 131	$p_{\text{sat,liq}}$	85.378	-	4.741	-	-	0.062	0.006
Haynes (1982), M6	4	115 - 131	$p_{\text{sat,liq}}$	85.892	0.705	0.53	-	-	0.026	0.089
Haynes (1982), M7	4	115 - 131	$p_{\text{sat,liq}}$	84.558	1.252	1.259	-	-	0.048	0.164
Haynes (1982), M8	4	115 - 131	$p_{\text{sat,liq}}$	81.249	2.708	-	-	-	0.021	0.164
Haynes (1982), M9	4	115 - 131	$p_{\text{sat,liq}}$	80.94	-	4.667	-	-	0.053	0.012
Haynes (1982), M10	4	115 - 131	$p_{\text{sat,liq}}$	90.613	0.306	0.3	-	-	0.104	0.134
Haynes (1982), M11	3	115 - 126	$p_{\text{sat,liq}}$	88.225	0.492	0.49	-	-	0.092	0.137
Haynes (1982), M12	4	115 - 131	$p_{\text{sat,liq}}$	85.934	0.707	0.519	-	-	0.160	0.224
Haynes (1982), M13	5	110 - 131	$p_{\text{sat,liq}}$	85.341	0.992	0.854	0.089	0.097	0.011	0.231
Haynes (1982), M14	4	110 - 126	$p_{\text{sat,liq}}$	75.442	1.057	0.978	0.083	0.089	0.050	0.142
Haynes (1982), M15	5	110 - 131	$p_{\text{sat,liq}}$	75.713	1.326	1.336	0.216	0.223	0.023	0.363
Haynes (1982), M16	4	110 - 126	$p_{\text{sat,liq}}$	74.275	0.893	0.843	0.067	0.069	0.066	0.088
Haynes (1982), M17	4	115 - 131	$p_{\text{sat,liq}}$	90.068	0.284	0.291	0.011	0.01	0.099	0.142
Hiza and Haynes (1980), M7	4	105 - 121	$p_{\text{sat,liq}}$	85.442	2.901	2.577	-	-	0.069	0.285
Hiza and Haynes (1980), M8	2	105 - 111	$p_{\text{sat,liq}}$	79.09	4.77	-	-	-	0.056	0.267
Hiza and Haynes (1980), M9	4	105 - 121	$p_{\text{sat,liq}}$	80.6	-	5	-	-	0.026	0.034
Hiza and Haynes	4	105 - 121	$p_{\text{sat,liq}}$	81.3	2.42	2.41	-	-	0.032	0.208

Author/Designation	N	$T_{\min} - T_{\max}$	$p_{\min} - p_{\max}$	x_{C1}	x_{C4}	x_{C4i}	x_{C5}	x_{C5i}	AARD (EOS- LNG)	AARD (GERG- 2008)
		K	MPa	mol-%	mol-%	mol-%	mol-%	mol-%	%	%
(1980), M10										
Speed of sound w										
Blanke and Weiß (1986), M1	24	273 - 304	<0.01 - 6.0	89.6788	0.2849	0.141	0.0527	0.0466	0.195	0.194
Blanke and Weiß (1986), M2	24	273 - 304	<0.01 - 6.0	84.5038	0.0118	0.0129	0.0073	0.0038	0.152	0.152
Blanke and Weiß (1986), M3	24	273 - 304	<0.01 - 6.0	86.416	0.0981	0.059	0.0296	0.0228	0.504	0.504
Blanke and Weiß (1986), M4	24	273 - 304	<0.01 - 6.0	81.2158	0.0075	0.0087	0.0055	0.0024	0.025	0.025
Blanke and Weiß (1986), M5	24	273 - 304	<0.01 - 6.0	82.6909	0.2522	-	0.0516	-	0.097	0.096
Blanke and Weiß (1986), M6	24	273 - 304	<0.01 - 6.0	85.4207	0.4812	-	0.0909	-	0.262	0.260
Blanke and Weiß (1986), M7	24	273 - 304	<0.01 - 6.0	81.8371	0.1898	0.1156	0.0353	0.0304	0.043	0.044
Blanke and Weiß (1986), M8	24	273 - 304	<0.01 - 6.0	83.8939	0.5624	-	0.1023	-	0.197	0.195
Blanke and Weiß (1986), M9	24	273 - 304	<0.01 - 6.0	83.3283	0.599	0.2795	0.2596	-	0.325	0.324
Blanke and Weiß (1986), M10	24	273 - 304	<0.01 - 6.0	80.088	0.9019	0.4349	0.127	0.125	0.679	0.677
Ewing and Goodwin (1993)	11	255.00	0.06 - 6.1	93.961	0.024	0.017	0.001	0.006	0.047	0.047
Fawcett (1995)	42	293 - 304	0.3 - 11	87.645	0.484	0.297	0.003	0.011	0.031	0.031
Ingrain <i>et al.</i> (1993), M1	58	212 - 347	0.1 - 18	88.405	0.226	0.149	0.049	0.056	0.317	0.306
Ingrain <i>et al.</i> (1993), M2	75	213 - 346	0.2 - 18	89.569	0.226	0.149	-	0.015	0.209	0.191
Labes <i>et al.</i> (1994), M1	240	262 - 355	12 - 70	88.405	0.226	0.149	0.049	0.056	0.374	0.358
Labes <i>et al.</i> (1994), M2	286	272 - 414	20 - 70	89.569	0.226	0.149	-	0.015	0.535	0.532
Younglove <i>et al.</i> (1993), M1	83	250 - 350	0.4 - 11	96.561	0.098	0.098	0.032	0.046	0.027	0.027
Younglove <i>et al.</i> (1993), M2	82	250 - 350	0.5 - 24	90.708	0.141	0.106	0.065	0.027	0.021	0.021
Younglove <i>et al.</i> (1993), M3	91	250 - 350	0.4 - 11	83.98	0.067	0.04	0.008	0.013	0.037	0.036
Younglove <i>et al.</i> (1993), M4	44	299 - 350	0.4 - 11	74.348	3.026	-	0.575	-	0.084	0.065
Isobaric heat capacity c_p										
van Kasteren and Zeldenrust (1979), M1	11	115 - 265	5.07	89.94	0.63	0.74	0.03	0.01	0.850	0.803

Table A2. Average absolute relative deviations (AARD) of the experimental bubble-point pressure data, which were available for the development of the GERG-2008¹¹ and which contain butanes or pentanes. The AARD was calculated with EOS-LNG and GERG-2008¹¹ for comparison. The listed mole fractions indicate only the fractions of the components studied in this work (methane: x_{C1} , *n*-butane: x_{C4} , isobutane: x_{C4i} , *n*-pentane: x_{C5} , isopentane: x_{C5i}). For information on the complete composition and the designation of the mixtures, see the GERG Technical Monograph No. 15.²³

Author/Designation	N	$T_{\min} - T_{\max}$	$p_{\min} - p_{\max}$	x_{C1}	x_{C4}	x_{C4i}	x_{C5}	x_{C5i}	AARD _{pliq} (EOS-LNG)	AARD _{pliq} (GERG-2008)
		K	MPa	mol-%	mol-%	mol-%	mol-%	mol-%	%	%
Haynes (1982), M1	4	110 - 126	0.24 - 0.52	89.071	4.998	-	-	-	2.4	0.50
Haynes (1982), M2	5	115 - 136	0.12 - 0.43	85.133	4.3	-	-	-	0.37	0.15
Haynes (1982), M3	4	115 - 131	0.12 - 0.32	84.566	2.45	-	-	-	0.11	0.38
Haynes (1982), M4	5	115 - 136	0.12 - 0.43	86.04	-	4.57	-	-	0.37	0.29
Haynes (1982), M5	4	115 - 131	0.12 - 0.32	85.378	-	4.741	-	-	0.33	0.78
Haynes (1982), M6	4	115 - 131	0.12 - 0.32	85.892	0.705	0.53	-	-	1.5	1.7
Haynes (1982), M7	4	115 - 131	0.12 - 0.32	84.558	1.252	1.259	-	-	0.16	0.37
Haynes (1982), M8	4	115 - 131	0.22 - 0.48	81.249	2.708	-	-	-	2.3	0.86
Haynes (1982), M9	4	115 - 131	0.30 - 0.61	80.94	-	4.667	-	-	3.4	2.1
Haynes (1982), M10	4	115 - 131	0.15 - 0.37	90.613	0.306	0.3	-	-	1.8	1.9
Haynes (1982), M11	3	115 - 126	0.16 - 0.30	88.225	0.492	0.49	-	-	4.7	5.0
Haynes (1982), M12	4	115 - 131	0.18 - 0.42	85.934	0.707	0.519	-	-	4.9	5.3
Haynes (1982), M13	5	110 - 131	0.08 - 0.32	85.341	0.992	0.854	0.089	0.097	0.33	0.48
Haynes (1982), M14	4	110 - 126	0.07 - 0.22	75.442	1.057	0.978	0.083	0.089	0.31	0.54
Haynes (1982), M15	5	110 - 131	0.12 - 0.37	75.713	1.326	1.336	0.216	0.223	3.7	5.4
Haynes (1982), M16	4	110 - 126	0.12 - 0.29	74.275	0.893	0.843	0.067	0.069	7.1	8.0
Haynes (1982), M17	4	115 - 131	0.15 - 0.37	90.068	0.284	0.291	0.011	0.01	1.3	1.4
Hiza & Haynes (1980), M7	4	105 - 121	0.05 - 0.17	85.442	2.901	2.577	-	-	1.2	1.7
Hiza & Haynes (1980), M8	2	105 - 111	0.19 - 0.25	79.09	4.77	-	-	-	7.1	1.6
Hiza & Haynes (1980), M9	4	105 - 121	0.20 - 0.38	80.6	-	5.0	-	-	5.9	6.5
Hiza & Haynes (1980), M10	4	105 - 121	0.18 - 0.44	81.3	2.42	2.41	-	-	14	17

APPENDIX - B

In Tables B1 and B2, test values for computer implementation of the pure fluids and mixture models are provided.

Table B1. Test values for computer implementation of the pure-fluid equations. For the calculation of these numbers, the pure-fluid equations of GERG-2008¹¹ have to be used.

T / K	$\rho / (\text{mol m}^{-3})$	p / MPa	$c_p / (\text{J mol}^{-1} \text{K}^{-1})$	$w / (\text{m s}^{-1})$	$h / (\text{J mol}^{-1})$	$s / (\text{J mol}^{-1} \text{K}^{-1})$	$a / (\text{J mol}^{-1})$
methane							
100	27406.610	1	54.868319	1464.5158	-15236.349	-113.32123	-3940.7137
120	0	0	33.282635	287.93074	-6041.2613	-	-
140	28000	86.944725	49.940566	1717.1465	-10929.814	-103.18433	410.82371
<i>n</i> -butane							
300	9843.1324	1	142.63587	900.91307	-21373.441	-78.648099	2119.3951
350	0	0	111.86921	232.56836	5451.6508	-	-
400	9000	30.067445	159.96336	821.38364	-5167.3813	-41.042991	7908.9879
isobutane							
310	9240.7816	1	145.53721	757.31587	-18230.312	-71.028634	3680.3490
370	0	0	116.36648	238.75073	7651.7986	-	-
420	8000	21.886007	167.02059	625.65914	-687.40298	-29.460374	8950.2030
<i>n</i> -pentane							
320	8315.8811	1	174.34854	917.11174	-22939.139	-74.192342	682.15867
380	0	0	146.14923	215.48326	10885.768	-	-
490	8000	81.238484	209.67109	1070.5936	14531.654	-5.6882702	7164.0963
isopentane							
350	7750.9465	1	185.36233	723.97364	-16198.681	-55.939712	3251.2021
410	0	0	156.07505	223.39951	15395.183	-	-
495	7000	35.733998	215.14793	719.56797	13984.485	4.5579997	6623.4179

Table B2. Test values for computer implementation for the molar composition of methane $x_{C1} = 0.6$. For the calculation of these numbers, the pure-fluid equations of GERG-2008¹¹ have to be used.

T / K	$\rho / (\text{mol m}^{-3})$	p / MPa	$c_p / (\text{J mol}^{-1} \text{K}^{-1})$	$w / (\text{m s}^{-1})$	$h / (\text{J mol}^{-1})$	$s / (\text{J mol}^{-1} \text{K}^{-1})$	$a / (\text{J mol}^{-1})$
methane + <i>n</i> -butane							
150	18.002169	10	77.267071	1403.3993	-22943.229	-116.52476	-6020.0044
200	0	0	50.685467	245.98640	-5437.2169	-	-
300	30	0.074343218	61.334843	294.99437	61.371614	8.4300240	-4945.7429
methane + isobutane							
160	17241.868	5	74.785284	1331.9880	-21294.389	-107.68110	-4355.4044
210	0	0	49.836159	252.48358	-4824.3458	-	-
350	100	0.28707693	67.807492	314.72845	3166.9980	6.8573366	-2103.8391
methane + <i>n</i> -pentane							
130	17089.860	8	79.265640	1625.1808	-28032.170	-137.18563	-10666.152
280	0	0	66.877640	262.83238	-1236.8530	-	-
400	500	1.5482355	90.379908	293.73614	7003.4459	3.9203586	2338.8314
methane + isopentane							
170	16073.699	5	73.858626	1124.0030	-23615.595	-109.92284	-5239.7800
220	0	0	57.100707	235.86043	-4921.2983	-	-
380	450	1.3276094	84.553729	285.77896	5619.9888	1.5214116	2091.6092

Supporting information available:

Four text files containing the parameters of the equations are available. For the use in TREND¹¹⁷, they have to be renamed into methane-butane.mix, methane-isobutan.mix, methane-pentane.mix, and methane-ipentane.mix.